This work was supported by the US Department of Energy, Division of Operational and Environmental Safety.

Prepared by Group N-6 word processing

LA-11158-M
Manual

UC-32 and UC-34
Issued: December 1987

NF85: A Three-Dimensional, Air-Dynamics Computer Code for Analyzing Explosions in Structures

R. G. Steinke

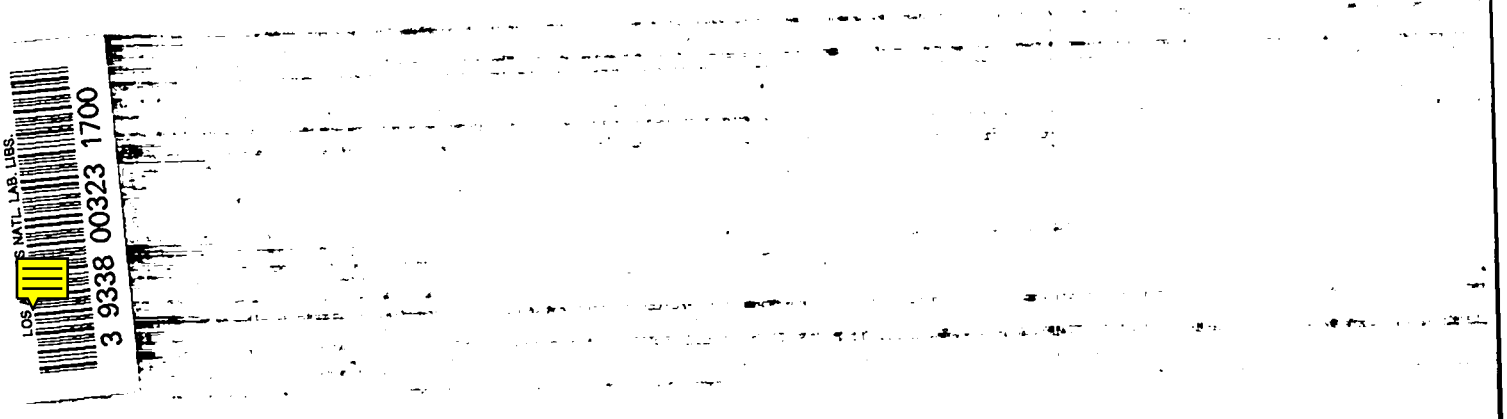

Los Alamos National Laboratory
Los Alamos, New Mexico 87545

CONTENTS

CONTENTS (CONT)

COMPUTER PROGRAM OUTLINE

Program Name:	NF85 (Near-Field 85)
Computers:	Programmed for efficient execution on a large-memory, vector-arithmetic computing machine such as a Cray. Small problems can be evaluated on a limited-memory, scalar-arithmetic computer.
Problem or Function Description:	NF85 provides a three-dimensional (cartesian or cylindrical geometry) numerical model for analyzing the effect of explosions on the dynamics of air in structures. The effects of shock and expansion wave interactions and reflections from structure surfaces can be modeled correctly in three dimensions. The effects of vent ducts, passageways, and openings to adjacent rooms on the dynamics of air in the room(s) where the explosion(s) occur can be modeled efficiently by attaching one-dimensional, boundary-condition regions to the external boundary of the three-dimensional domain. NF85 can edit interface conditions as tabular functions of time to be used as boundary conditions for the EVENT84 computer code, which evaluates gas dynamic transients in one-dimensional flow networks.
Solution Method:	The governing partial-differential equations are solved in their finite-difference form using a semi-implicit differencing method. An internal procedure automatically adjusts the time-step size based on the rate of change of the transient solution. The time-step size can be increased beyond the sonic limit to the material-Courant limit using the semi-implicit method. For time steps exceeding 80% of the material-Courant limit, the stability-enhancing two-step (SETS) method is applied in addition to the semi-implicit method to allow the use of time steps that exceed the material-Courant limit to be used. Attaching one-dimensional regions to the three-dimensional region's external boundary is modeled by one-dimensional gas dynamics equations having full semi-implicit (and SETS) coupling to the three-dimensional equations.
Problem Complexity Restrictions:	All array storage is assigned to common-block areas in computer memory and is fixed-dimensioned using parameter-statement variables. An update/compile/load procedure is used with the parameter-statement variables assigned dimension values appropriate for the problems to be evaluated. No overlaying of program or variable storage is done. Thus, a computer with more than a quarter-million words of memory is required for most problems. The three-dimensional region variables generally require 98% to 99% of the array storage.
Typical Running Time:	The running time is highly problem dependent and is a function of the number of mesh cells in the three-dimensional region and the dynamic nature of the transient. Typical times for a Cray-1 computer range from 1 to 2 ms per time step per

	three-dimensional region mesh cell. The evaluation times for one-dimensional region mesh cells are generally 5% to 10% of the above times.
Unusual Program Features:	The effect of the surrounding region on the domain of the explosion can be modeled efficiently with one-dimensional regions attached to the external boundary of the three-dimensional domain. There is no numerical-stability restriction on time-step size because the semi-implicit and SETS methods are used to solve the gas dynamics equations.
Related and Auxiliary Programs:	The EXCON/TRAP computer programs can be used to postprocess file GRFDAT data (generated by NF85) into a versatile selection of graphic plots of the parameters determined by NF85.
Status:	NF85 is operational on the Cray-1 computers at the Los Alamos National Laboratory.
References:	References are provided in the NF85 User's Manual.
Machine Requirement:	A computer with more than a quarter-million words of fast-core memory is required to evaluate most problems.
Programming Language:	The programming language is FORTRAN-IV.
Operating Systems or Monitors:	NF85 is updated using HISTORIAN and compiled/loaded using the Cray FORTRAN (CFT) compiler/loader. Access to the Cray-1 computers at Los Alamos is through the Cray Time-Sharing System (CTSS).
Other Programming, Operating Information, or Restrictions:	Subroutines from the Cray FORTRAN mathematics libraries are required to perform vectorized matrix-inversion operations.
Available Materials:	A source listing, the NF85 User's Manual, and sample problems are available.

NF85: A THREE-DIMENSIONAL, AIR-DYNAMICS COMPUTER CODE FOR ANALYZING EXPLOSIONS IN STRUCTURES

by

R. G. Steinke

ABSTRACT

The NF85 (Near-Field 85) computer program analyzes the effect of explosions on the dynamic behavior of air in structures. The explosion is modeled as a time- and space-dependent source of equivalent air mass and energy. Chemical reactions can be modeled directly with a combustion-model option, and tracer particles may be used to monitor combustion-products convection by the air. The near-field region of the explosion is modeled in three-dimensional cartesian or cylindrical geometry. Internal structures can be defined in the region to reflect shock waves and obstruct airflow. A convenient dump/restart capability allows the movement or removal of internal structures during the transient solution. The effects of the surrounding far-field region are modeled at the three-dimensional region's external boundary by a wall surface, time- and space-dependent pressure or velocity boundary conditions, and/or one-dimensional cartesian-geometry regions attached to openings in the external boundary. Ventilation ducts, passageways, and adjacent rooms can be modeled directly with one-dimensional regions, and the presence of blowers and filters can be modeled as well. One-dimensional regions in NF85 cannot be interconnected, thus requiring the approximation of complex flow-network geometry in the far field. An approximate far-field representation only needs to model its feedback effect on the near-field region accurately to obtain an accurate near-field solution. From its solution, NF85 can optionally edit the time-dependent solution-state condition at any location in its region of solution. This then may be used as an accurate boundary condition for the EVENT84 one-dimensional flow-network computer program to enable it to efficiently evaluate the air-dynamics behavior in a complex flow-network geometry of the far field.

---

1. INTRODUCTION

The NF85 (Near-Field 85) computer code is a three-dimensional, gas dynamic, numerical model for analyzing explosions within structures. An explosion is modeled as a time- and space-dependent source of gas mass and energy, and energy from chemical reactions can be modeled directly. The region of solution is a multi- (one-, two-, or three-) dimensional domain in cartesian or cylindrical geometry that models a room or several interconnected rooms encompassing the explosion.

We will refer to the room containing the explosions as the "near field;" space outside the near field is termed the "far field." The near field, and possibly a portion of the far field, are modeled by NF85's multidimensional region. Additional portions of the far field can be modeled by connecting separate one-dimensional regions to the outer surface of the multidimensional region. This special feature of NF85, that of defining one-dimensional boundary-condition regions, can be used to model ducts, passageways, or adjacent interconnecting rooms.

NF85 evaluates the behavior of gas (air) in the near-field region. A portion of the far field can be modeled with the multidimensional region and/or one-dimensional, boundary-condition regions to account for the far field's feedback effect on the near-field solution. The larger the openings on the near-field boundary and the smaller the volume of ducts, passageways, and rooms in the far field that connect to the near field, the further one must model into the far field. The distance also increases with the magnitude of the explosion, the presence of reflecting surfaces in the adjacent far field, and the amount of time to be simulated following the explosion.

Although the far field's feedback effect on the near-field solution is important, a correct modeling of the near-field geometry is generally more important. Shock waves propagate from an explosion and reflect from interior and boundary surfaces numerous times. Without symmetry, this behavior has three-dimensional spatial dependence. The locations of an explosion in a room and of interior and boundary surfaces that reflect shock waves and obstruct gas flow have a dramatic effect on the gas dynamic solutions. The shock front's overpressure can be amplified by as much as a factor of 8 in air[1] each time it is reflected from a solid surface. Shock-wave-front interactions compress and heat the air. The rarefaction (expansion) wave, which propagates in the opposite direction from the shock wave, reduces the overpressure and cools the air that it

passes through. Surface reflections and the interactions of these wave fronts produce a complicated space- and time-dependent gas behavior in the field.

After evaluating the near field's gas dynamic solution, NF85 can edit the explosion (chemical, nuclear, or physical) energy and the volumetric (pressure and temperature) or interface-flow (energy and mass) condition as a tabular function of time at the far-field interface. This information can be used directly as input data for the EVENT84 computer code.[2] EVENT84 analyzes explosion-induced, gas dynamic transients in complicated far-field flow networks and has an efficient, lumped-parameter model with one-dimensional spatial dependence appropriate for analyzing the extensive domain of the far field. Using NF85 to analyze the entire region of interest in the far field could result in a large computational cost; however, using EVENT84 to model the near field could result in an inaccurate analysis. Using them in combination (oy using NF85 to model the near field and then interfacing its solution as a boundary condition to EVENT84 for analyzing the far field) can provide both accuracy and reduced computational cost.

Sections II and III provide users with a description of the numerical models and program structure of NF85. The input-data parameters and format are defined in Sec. IV, and a representative problem executed in combination with EVENT84 is described in Sec. V. Samples of the input/output files are shown along with a graphic presentation of the results. From this, users should be able to gain a sufficient understanding of the capabilities of NF85 to enable them to model and prepare input data for their own problems.

II. NUMERICAL MODELS

A. Finite-Differencing of Space and Time

NF85 simulates the behavior of an explosion in a room using a numerical model of the structure and the physical state of the air in the room by partitioning the room's volume into subvolumes called mesh cells using an imaginary grid. The physical state of the air within each mesh-cell volume is modeled by mass, momentum, and energy conservation equations. This behavior varies over time and is evaluated consecutively over discrete time intervals called time steps.

Determining the air's physical state involves modeling both time and space dependence. Although these dependencies in the actual phenomena are continuous,

NF85 models the air properties as constant over the discrete intervals of mesh cells and time steps with step changes at interval interfaces. As the sizes of mesh cells and time steps are decreased (resulting in more to evaluate), the numerical model's discrete solution approaches the physical phenomena's continuous behavior. To model time and space dependence accurately, the model's intervals need to be made small. On the other hand, the calculative effort and cost are somewhat proportional to the number of such intervals in the model. When defining the model, a compromise on interval size must be made to keep the calculative effort and cost within reason and yet evaluate time and space dependence accurately.

1. Spatial Mesh. The number of mesh cells in the region of solution is a user decision. The mesh cells must be regular; that is, the imaginary-grid interface between mesh cells is a straight line in two dimensions and a flat plane in three dimensions. The interfaces are parallel or orthogonal to each other. The user has the option of modeling cartesian or cylindrical geometry in the multidimensional region. However, only cartesian geometry is used in the one-dimensional boundary-condition regions. In cartesian geometry, the multidimensional region's direction having the most mesh cells should be defined as the z-direction. This enables NF85 to execute more efficiently on a vector machine because the innermost DO loops (which the compiler vectorizes) are over mesh cells in the z-direction.

Mesh-cell interval lengths are defined through the input data and can vary from mesh cell to mesh cell in a given direction. Smaller mesh-cell lengths should be defined in locations where larger variation in the air's physical behavior is anticipated. Generally, this is difficult because spatial variations migrate around the region of solution as problem time advances, whereas the mesh-cell grid is fixed in space (an Eulerian spatial mesh). This situation probably is modeled best with a constant mesh-size grid.

2. Time Steps. NF85 determines the appropriate time-step size at the beginning of each time step based on the rate of change of the air parameters in the previous time step. The user controls the time-step size only through the input-data-defined initial time-step size, DELT, and the minimum and maximum time-step size constraints, DTMIN and DTMAX, for each time domain. The internal criteria that NF85 uses to adjust the time-step size are the following.

- DELFMX = 10 times the material Courant-limit time-step size = min(10*DELVMX, 9.9999999), where DELVMX = 1/max(VMAXT,

2*VMAXT-VMAX, 0.1), where VMAXT = max($|\underline{V}_{n+½}|/\Delta x_{n+½}$) for all n = (i,j,k) and n = i mesh cells, and where VMAX = previous time-step value of VMAXT.

- DELIMX = The estimated time-step size that would result in five pressure iterations being required to converge the next time step's gas dynamic solution = $\Delta t*(5/ITNO)$, where Δt is the previous time-step size and ITNO is the number of pressure iterations required to converge the previous time-step solution.
- DELCMX = The estimated time-step size that would result in a maximum 5% change in any mesh cell's air temperature or pressure during the next time step = min($\Delta t*0.05$/max(DTVMX, DPRMX), 9.999999), where DTVMX = max [$|T_n(t)-T_n(t-\Delta t)|/T_n(t-\Delta t)$] and DPRMX = max [$|P_n(t)-P_n(t-\Delta t)|/P_n(t-\Delta t)$] for all n = (i,j,k) and n = i mesh cells. $T_n(t)$ and $P_n(t)$ are the air temperature and pressure in mesh cell n at the start of the present time step.
- DELRMX = A time step that is 5% larger than the previous time step = $1.05*\Delta t$.

The next DELT time-step size is taken to be the minimum value among these four criteria and the maximum time-step size, DTMAX:

$$DELT = \min(DELFMX, DELIMX, DELCMX, DELRMX, DTMAX). \quad (1)$$

If DELT is less than the minimum time-step size (DTMIN), NF85 generates a full edit (short, long, graphics, dump/restart, and EVENT interface) and ends the calculation. A smaller minimum time-step size would be required to restart the calculation.

B. Gas Dynamics Equations

The behavior of air within the region of solution over time is governed by the following partial-differential equations for

mass, $$\frac{\partial \rho}{\partial t} + \underline{\nabla} \cdot \rho \underline{V} = m_s \quad ; \quad (2)$$

motion, $$\frac{\partial \underline{V}}{\partial t} + \underline{V} \cdot \underline{\nabla} \underline{V} = - \frac{1}{\rho} \underline{\nabla} P - K |\underline{V}| \underline{V} + \underline{g} \quad ; \text{ and} \tag{3}$$

and energy, $$\frac{\partial \rho e}{\partial t} + \underline{\nabla} \cdot \rho e \underline{V} = -P \underline{\nabla} \cdot \underline{V} + m_s e_s \quad , \tag{4}$$

where

t is time,
ρ is air density,
m_s is the explosion's source of equivalent-air mass per unit time per unit volume,
$\underline{V}$ is air velocity (a vector),
P is air pressure
K is the friction-factor coefficient for air drag on structure surfaces,
$\underline{g}$ is the acceleration of gravity (a vector),
e is the air internal energy per unit mass, and
e_s is the internal plus combustion energy per unit mass of the explosion's mass source.

The air total energy per unit mass is $e+\frac{1}{2}|\underline{V}|^2$, and the air temperature is e/c_v, where (in NF85) c_v = 717.890403 J/kg/K is the specific heat of air at constant volume. The air-parameter variables (ρ, $\underline{V}$, e, and P) are functions of time and space. In the above differential equations, spatial dependence is determined by the gradient $\underline{\nabla}$ and divergence $\underline{\nabla} \cdot$ operators.

In these equations, we first define the parameters ρ, e, and P to have their values volume-averaged over the mesh cell and defined at the mesh-cell center. The air-velocity vector's component that is normal to a mesh-cell side had its value area-averaged over the mesh-cell side and defined on the mesh-cell side. Only the normal component of the velocity vector was defined. This commonly is referred to as a staggered spatial mesh on each mesh-cell side.

Using this notation, the mass, motion, and energy differential equations were integrated over a time-step interval and a spatial volume. The mass and energy equations' spatial volume is a mesh-cell volume. For the motion equation, we first took its dot product with a unit vector in each orthogonal direction to obtain a velocity-component differential equation for each direction.

Then, each velocity-component equation was integrated over the spatial volume of the adjacent halves of the two mesh cells on whose common side the velocity component is defined.

This procedure is detailed and involves a number of difference-scheme approximations. Appendix A contains a description of this procedure; the resulting finite-difference equations that are programmed in and solved by NF85 also are presented in Appendix A.

Many of the terms in the equations derived in Appendix A were defined to have implicit (rather than explicit) spatial coupling; that is, the equations for all mesh cells were coupled, and they need to be solved as a matrix equation rather than as individual equations. The derived equations are based on a semi-implicit, finite-difference scheme that provides a stable solution using time steps larger than the sonic limit. The sonic limit is the minimum time required for a pressure wave traveling at the speed of sound ($c = \sqrt{\partial P/\partial \rho}$) to cross any mesh cell. For an ideal gas (discussed in the next section),

$$c = \sqrt{\gamma P/\rho} = \sqrt{\gamma(\gamma-1)e} \quad , \tag{5}$$

where $\gamma = c_p/c_v$ = the ratio of specific heats at constant pressure and constant volume = 1.39986953 for air in NF85. An expansion-wave front travels at the speed of sound. A shock-wave front travels at the speed of sound times a Mach number M_s (where $M_s \geq 1$), where for an ideal gas,

$$M_s = \sqrt{\frac{(\gamma-1)}{2\gamma}\left[1 + \frac{P_-}{P_+}\left(\frac{\gamma+1}{\gamma-1}\right)\right]} \tag{6}$$

and $P_{\pm}$ = the gas pressure ahead of (+) and behind (−) the shock-wave front.

After an explosion, the shock and expansion waves produced are propagating throughout the region of solution, reflecting from structure surfaces, and interacting. A large change can occur in the air temperature and pressure when these waves cross a mesh cell. This results in the time-step size probably being limited to a fraction of the sonic limit by DELCMX's 5% maximum change in temperature or pressure during a time step or by DELIMX's desired five pressure

iterations per time step (Sec. II.A.2). During the initial 0.1 s after an explosion, evaluating the multiple reflections and interactions of shock waves and rarefaction waves with the semi-implicit equations requires several times the calculative effort that would be required to evaluate the explicit equations. However, the implicit method will allow the time step to increase an order of magnitude beyond the sonic limit after the rapid transient of wave motion has dissipated throughout the region of solution. If the explicit method equations had been used, the time-step size would be constrained to the sonic limit, and the calculative requirement would be almost an order of magnitude more for transients of 0.5 s or longer. The EVENT84 analysis of the far field usually spans a time interval of 1 or 2 s after the explosion. NF85 needs to be evaluated over that time interval to provide a far-field interface boundary condition for EVENT84.

NF85 goes one step further by superimposing the stability-enhancing, two-step (SETS) method[3,4] on the semi-implicit method. The method's stabilizer equations are defined in Appendix B. By evaluating the stabilizer equations of motion before the pressure iteration (which evaluates the semi-implicit method's mass, motion, and energy equations) and then completing the time step by evaluating the stabilizer mass and energy equations, the SETS method provides numerical stability when the semi-implicit method's material-Courant limit on time-step size is exceeded. The material-Courant limit time-step size is the minimum time required for the gas (air) to cross any mesh cell based on its material velocity ($\underline{V}$). This time-step size limit on the semi-implicit method solution is generally an order of magnitude larger than the explicit method's sonic limit. The rate of change of the near-field transient a few tenths of a second after the explosion may decrease to the point where the time-step size becomes constrained by the material-Courant limit. With the SETS method (which increases the calculative effort per time step by about 20%), larger time steps can be used to reduce the overall calculative effort. NF85 currently allows the time step to increase with the SETS method to 10 times the material-Courant limit before DELFMX limits the time-step size.

Until the time-step size reaches the material-Courant limit, the SETS method's stabilizer equations do not need to be evaluated to maintain the numerical stability of the solution. NF85 is programmed to start evaluating the SETS method equations when the time step exceeds 80% of the material-Courant limit and to continue evaluating them until the time step decreases to below 75% of

the material-Courant limit. The SETS method is used only when a larger time step can be used based on the rate of change of the transient solution. The criterion for applying the SETS method has a 5% historesis to reduce back-and-forth switching, which could result in the method being applied on alternate time steps.

C. Equation of State

Air is assumed to behave as an ideal gas defined by the following equation of state (EOS):

$$P = (\gamma-1)\ \rho\ e, \tag{7}$$

where

P is air pressure,
γ is the c_p/c_v ratio of specific heats at constant pressure and constant volume (equals 1.39986953 for air in NF85),
ρ is air density, and
e is air internal energy per unit mass.

Other gases introduced into the room from the explosion are represented by their equivalent moles of air. This approximation is valid as long as the explosion gases represent no more than a few per cent of the moles of air in the room.

From statistical mechanics, the value of $\gamma = (n+2)/n$ depends on the internal degrees of freedom (n) of the gas. For a noble gas, $n = 3$ and $\gamma = 5/3 = 1.67$; for a diatomic gas such as air, $n = 5$ and $\gamma = 7/5 = 1.4$. For more complicated gas molecules, n increases and γ decreases and approaches unity. At large energies, n and γ can be time-dependent. For a short time after an explosion, the gas formed from the detonation can behave as though $\gamma = 3$.[5] Therefore, assuming the explosion gases behave as air can be a poor approximation. The error can be kept small only by having a relatively small amount of explosion gases in the air of the room.

D. Internal Structure

Mesh cells within the multidimensional region can contain air, structure (solid material), or both. Structure is assigned to each mesh cell through

input data as the fraction of its volume that is not air. The volume fraction of structure in a mesh cell is constant throughout a calculation. The only way to modify it is to change the structure volume fraction in a dump/restart data edit from a previous calculation and perform a restart calculation using that dump/restart edit as input data. In this way, doors, walls, ceilings, ducts, and so on can be moved within or removed from the region of solution.

The presence of structure in a mesh cell is defined through the volume fraction it occupies; its obstruction to airflow is modeled by the fraction of a mesh cell's side area that is not available for flow. A mesh cell that is entirely structure must have zero flow-area fractions defined to all of its sides.

E. Wall Friction

The presence of an internal structure or an external boundary implies the presence of a solid surface (wall) applying friction drag to air flowing past it. Wall friction is modeled by the $K|\underline{V}|\underline{V}$ term in the motion equation [Eq. (3)]. Using the Fanning equation,[6] the friction coefficient is defined by

$$K = 2f/D_h, \tag{8}$$

where

f = Fanning friction factor and
D_h = hydraulic diameter for airflow through the mesh-cell side area that is open to flow.

For laminar flow,

$$f = 16/Re \text{ for } Re \leq 2100 \tag{9}$$

from the Hagen-Poiseille equation. NF85 constrains f in Eq. (9) to be less than or equal to unity. For turbulent flow,

$$f = 0.0791 * Re^{-0.25} \text{ for } Re > 2100 \quad (10)$$

from the Blasius equation. Re is the Reynolds number equal to $D_h|\underline{V}|\rho/\mu$. NF85 uses Re = 1187.4 rather than 2100 as the transition point between these two definitions so that f is continuous. The air viscosity μ is dependent on the air temperature T and is approximated by the following second-order polynomial approximation.[7]

$$\mu = 1.708 \times 10^{-5} + 5.927 \times 10^{-8}(T-273.15) + 8.14 \times 10^{-11}(T-273.15)^2 \text{ for } T \leq 502.15 \text{ K, and}$$
$$\mu = 2.4748 \times 10^{-5} + 4.193 \times 10^{-8}(T-273.15) + 1.09 \times 10^{-11}(T-273.15)^2 \text{ for } T > 502.15 \text{ K.} \quad (11)$$

The zeroth-order coefficient value, 2.4748×10^{-5}, has been increased from the 1.735×10^{-5} value in Ref. 7 to provide continuity at T = 502.15 K. For noncircular-flow areas, the input-data-specified hydraulic diameter D_h should be approximated by 4 times the cross-sectional flow area divided by the wetted-surface perimeter.

In NF85, the friction coefficient K defined by Eq. (8) has an input-data-specified, friction-adjustment factor, CFZV, applied to it at each mesh-cell interface,

$$K = |CFZV|\ 2\ f/D_h \quad . \quad (12)$$

Inputting CFZV = 0 or $|D_h| \leq 10^{-5}$ m turns off the air/wall friction model at the mesh-cell interface. Inputting a value for |CFZV| different from the nominal value of unity allows the user to incorporate effects such as surface roughness or arbitrary adjustment of air/wall friction. Applying a negative sign to the value for CFZV acts as a flag to constrain the definition of the Fanning friction factor (f) to the 16/Re laminar-flow functional form for all values of the Reynolds number (Re). This provides an approximate flow-resistance model for a filter component. Inputting a hydraulic diameter $D_h < -10^{-5}$ m will result in

NF85 modeling an orifice plate at the mesh-cell interface. NF85 does this by replacing $|\underline{V}|$ in the K $|\underline{V}|\underline{V}$ term with $n \cdot \underline{V}$, that is, the velocity component normal to the mesh-cell interface rather than the total velocity. No cross-flow is assumed to occur along a mesh-cell side having an orifice plate. The absolute value of D_h defines the hydraulic diameter.

F. Boundary Conditions

The external boundary of the multidimensional region is a solid external-wall surface by default. The mesh-cell sides on the external boundary are defined internally to have a zero flow area and a zero normal-velocity component. Gas-state properties are reflected across the external boundary to define a zero-gradient boundary condition.

The user can modify this boundary condition locally through the input data. Applying a different boundary condition locally involves defining its rectangular subarea on the external boundary. The rectangular subarea spans a distance of one or more mesh cells in each of the rectangle's two directions. One of the following boundary conditions then is defined in that subarea on the external boundary.

NBC = 0 for a time-independent (constant) air velocity normal to and on the external boundary.

NBC = ±1 for a time-independent (constant) air pressure located a half-mesh-cell distance outside the external boundary. (The numerical sign ± defines how momentum in-flow to the external-boundary velocity cell is to be modeled, that is, how the normal velocity a mesh-cell distance outside the external boundary is to be defined. Inputting -1 defines that velocity to be the same as the calculated normal velocity on the external boundary such that $\underline{V} \cdot \nabla \underline{V} = 0$ on the velocity cell's external boundary; inputting +1 defines that velocity to be the input-data-specified normal velocity on the external boundary held constant throughout the calculation such that $\underline{V} \cdot \nabla \underline{V} \neq 0$ on the velocity cell's external boundary.)

NBC $\geq$ 2 for a one-dimensional, boundary-condition region of NBC mesh cells with its gas dynamics equations coupled implicitly to the gas dynamics equations of the multidimensional region.

The first two of these boundary conditions can be defined to vary spatially over its rectangular subarea of mesh-cell sides on the external boundary. Any number of these boundary conditions can be defined through input and applied locally on any of the six external-boundary faces of the multidimensional region.

G. One-Dimensional, Boundary-Condition Regions

Ventilation ducts, passageways, and adjacent rooms connected to the near-field room's multidimensional region by areas open to airflow can be modeled by one-dimensional, boundary-condition regions. This generally is more accurate than modeling them indirectly using time-independent velocity or pressure boundary conditions. They could be modeled more accurately by expanding the multidimensional region to include them, but the cost of the calculation and the computer-memory requirement can become excessive.

The gas dynamic, finite-difference equations for the one-dimensional, boundary-condition regions are presented in Appendix C. They are the multidimensional, gas dynamics equations reduced to one-dimensional, spatial dependence in cartesian geometry. Their solution is coupled implicitly to the multidimensional region's equations. The one-dimensional region's first mesh cell is coupled directly by convection to all the mesh cells of the multidimensional region that contact the boundary condition's rectangular subarea. Solving the one-dimensional region equations involves defining them to be a function of the gas-state parameters in the contacting mesh cells of the multidimensional region. These equations for the one-dimensional region's mesh cells are directly inverted. The resulting equation for the first mesh cell is applied as the boundary-condition requirement for the multidimensional region. After the multidimensional region's solution is determined, its gas-state parameter values in the mesh cells that contact the boundary condition's rectangular subarea are back-substituted into the one-dimensional region's inverted equations to solve for their gas-state solution. This solution procedure is performed on the semi-implicit equations evaluated during the pressure iteration as well as on the stabilizer equations of the SETS method.

The user has more latitude in modeling physical geometry with a one-dimensional, boundary-condition region than with the multidimensional region. The multidimensional region's orientation and volume are limited by its regular mesh-grid overlay. On the other hand, the one-dimensional, boundary-condition region can change direction and volume from mesh cell to mesh cell. Directional

orientation is defined by the gravity component specified through input for each mesh-cell interface. A mesh-cell volume can range from being a portion of a duct to being an entire room. Each mesh cell's volume is input as the actual volume occupied by air, not as a volume fraction. Each mesh cell's length also is input. The mesh cell's volume divided by its length defines the mesh cell's cross-sectional area. The flow area between mesh cells also is input and may differ from the cross-sectional area of either of its adjacent mesh cells.

The outer-end interface of the last mesh cell (NBC) has a +1 type pressure boundary condition (Sec. II.F) applied to it. The boundary condition's time-independent pressure and temperature are the input-specified values for fictitious mesh cell NBC+1. Specifying a zero flow area on the outer-end interface yields a zero-velocity boundary condition at the end of the one-dimensional region. A major restriction on defining a one-dimensional, boundary-condition region is that mesh cell NBC only couples to mesh cell NBC-1. It cannot be coupled to any mesh cell of any one-dimensional region or to any rectangular subarea of mesh cells on the multidimensional region's external boundary. Doing this would form a flow loop that would complicate the numerics of the one-dimensional region's solution.

H. Blower/Fan Model

The presence of a blower/fan in a vent duct is modeled by the pressure change it effects across its component. This is done with a blower curve of tabular data based on actual experimental measurements, including backflow and outrunning-flow conditions. The blower curve input to NF85 is its pressure change as a function of the flow velocity through the blower. If the available blower curve is a function of the volumetric flow rate, dividing the volumetric-flow values by the flow area at the one-dimensional region mesh-cell interface where the blower is defined gives the flow velocity through the blower. In the portion of the blower curve where the blower's pressure change is driving airflow, the numerical sign of the pressure change should be the same as that of the velocity. The slope of the blower curve must be negative throughout its defined range. Linear extrapolation is used to evaluate the pressure change outside the curve's defined velocity range.

I. Tracer Particles

The gas in the region of solution is assumed to be air with its behavior modeled by the ideal gas EOS for air (Sec. II.C). Actually, there may be particulate matter or other gases suspended in the air that convect with the air, and it may be of interest to the user to trace the movement of these other materials within the region of solution. For this purpose, up to five different materials, called tracer particles, can have their initial spatial distributions specified through input and then convected with the air during the calculation. The user specifies the fraction of the air velocity by which all tracer particles are to be convected. This allows the reduced velocity of tracer particles relative to the air to be taken into account. The effect of tracer-particle material on pressure is accounted for by its equivalent moles of air included with the air that is present. Tracer particles per se do not affect the gas dynamic solution; however, the gas dynamic solution's air velocity connects the tracer particles. The tracer-particle initial spatial distribution is specified through input and then convected with the air during the calculation.

Explosions that produce external sources of equivalent air mass and energy can be defined to produce a mass source for each tracer particle. The mass-generation rate for each tracer particle has its own time history specified through input, but its spatial distribution is the same as for the air-mass source. If the explosion source uses the combustion model described in Sec. II.K, array storage for four of the five tracer particles is reserved for the combustion model's chemical reactants. This results in the user being limited to one tracer particle when using the combustion model.

J. External Sources

Any number of external sources can be specified through input data. Each source defines a time-dependent mass-generation rate and energy per unit mass having spatial dependence within a subvolume of the multidimensional region. The mass source is the explosive-material mass-generation rate in units of kilograms per second or pounds-mass per second. Any portion of that mass can be assigned to each of the one to five tracer particles defined. A factor is input or defined internally to convert the explosive-material mass to its decomposed gas-mole equivalent mass of air. The energy per unit mass can be the total energy addition, or it can be the internal energy associated with the mass source.

In the latter case, the combustion model is used to evaluate the additional energy yield from chemical combustion.

K. Chemical Combustion

The chemical-combustion model evaluates the energy yield from the chemical reactions of hydrogen gas (H_2), carbon solid (C), and carbon monoxide gas (CO) with oxygen gas (O_2). At the start of each time step in each mesh cell, the following reactions take place until either all of the H_2, C, and CO or all of the O_2 has reacted.

$$H_2 + \tfrac{1}{2}\, O_2 \longrightarrow H_2O + \text{energy}$$

$$C + \tfrac{1}{2}\, O_2 \longrightarrow CO + \text{energy}$$

$$CO + \tfrac{1}{2}\, O_2 \longrightarrow CO_2 + \text{energy}$$

It is assumed that all of the H_2 first reacts with O_2 before C reacts with O_2. Then all C reacts with O_2 before CO reacts with O_2. When generated, the reaction products (H_2O and CO_2 gases) are modeled as equivalent moles of air. The reaction product CO gas is the source of the next reactant. For the reactions to take place, it is assumed that only the presence of H_2, C, or CO and O_2 in a mesh cell is necessary.

When using the combustion model, NF85 internally reserves four of the five possible tracer particles to store the spatial distributions of H_2, C, CO, and O_2. Initially, the 21% mole fraction (23.29% weight fraction) of air throughout the region of solution is defined to be O_2. During the calculation, one or more external sources can be defined to generate H_2, C, CO, and/or O_2. The amount of each reactant is the time- and space-dependent source of explosive-material mass multiplied by FRM_n and RAMEM. FRM_n is the reactant-to-air mass ratio for the n^{th} reactant, where n = 1 for H_2, n = 2 for C, n = 3 for CO, and n = 4 for O_2. RAMEM is the air-to-explosive-material mass ratio for an equivalent number of moles of air and decomposed-explosive component gases. For example, when decomposed, TNT ($C_7H_5N_3O_6$) has 2.5 moles H_2, 1.5 moles N_2, and 3.0 moles O_2 for a total of 7.0 moles of component gases in a unit molecular weight of TNT. Thus, in this case, RAMEM = [7.0 * (0.21 * 2.0 * 16.0 + 0.79 * 2.0 * 14.008)]/(7.0 * 12.011 + 5.0 * 1.008 + 3.0 * 14.008 + 6.0 * 16.0) = 0.889177.

For each external source that specifies internal energy and uses the combustion model to evaluate chemical-combustion energy, FRM_n can be specified through input or defined internally by NF85 from Table I for n = 1 to 4.

The three chemical reactions of H_2, C, and CO with O_2 are the default reactions modeled by NF85. Other reactants reacting with oxygen are possible replacements if in addition to FRM_n and RAMEN, the user specifies input values for the following combustion-model parameters.

1. The ratio of reactant n mass to oxygen mass combining in the nth priority chemical reaction, WTR(N). [The internally defined values are WTR(1) = 0.126, WTR(2) = -0.750687, and WTR(3) = 1.750687; the value's numerical sign defines the reactant to be a gas (+) or solid (-)]

2. The ratio of a mole of air mass to a mole of the n^{th} chemical-reaction product mass, PDR(N). [The internally defined values are PDR(1) = 1.601501, PDR(2) = -1.030047, and PDR(3) = 0.655578; the value's numerical sign defines the reaction product to be stable and represented by equivalent air (+) or to be the next reactant (-).]

3. The energy released from the chemical reaction per unit mass of reaction product, ECB(N). [The internally defined values are ECB(1) = 1.58661×10^7 J/kg, ECB(2) = 3.94575 x 106 J/kg, and ECB(3) = 6.43010×10^6 J/kg (obtained from Ref. 8).]

An important capability of the combustion model is its ability to evaluate the condition where there is insufficient oxygen in a mesh cell to react with all the H_2, C, and CO that is present. To react them with O_2 requires that they be convected into adjacent mesh cells where oxygen is present and/or that oxygen be convected into their mesh cell. This results in a delayed release of chemical-combustion energy with a spatial distribution extending beyond the reactant's mass-source spatial distribution.

L. EVENT84 Interface-Condition Edit

One or more interface conditions can be edited by NF85 for use as an input-data boundary condition for the EVENT84 computer program. Each interface condition can be located anywhere within the multidimensional region or within the

TABLE I

REACTANT TO GAS-MOLES-OF-EQUIVALENT-AIR-MASS RATIOS (FRM_n)
AND RAMEN FOR EXPLOSIVE MATERIALS

Reactants	n	Trinitrotoluene (TNT)	Tributyl Phosphate (TBP) or "red oil"	Hydrogen Gas	Acetylene Gas
Hydrogen gas	1	0.024954	0.060856	0.069872	0.069872
Carbon solid	2	0.416288	0.322287	0.0	0.832575
Carbon monoxide	3	0.0	0.0	0.0	0.0
Oxygen gas	4	0.475322	0.143108	0.0	0.0
RAMEN		0.889177	1.679230	14.311825	1.108097

one-dimensional, boundary-condition regions. The interface condition can be either the average volumetric state (gas temperature, gas pressure, and tracer-particle densities) next to user-defined filled rectangular area or the average flow state (gas-mass, gas-energy, and tracer-particle-mass flow rates) through a user-defined filled rectangular area. In the multidimensional region, the rectangular area is the combined interfaces in a plane on the positive-direction side of a range of input-specified mesh cells. In a one-dimensional region, the rectangular area is the positive-direction interface of a mesh cell. The interface condition is averaged over either the volume of all mesh cells whose positive-direction faces lie within the rectangular area or the surface area of all mesh-cell interfaces within the rectangular area. These spatially averaged parameters are evaluated and edited to file EVIDAT beginning at a starting time and with a frequency specified through input data. The maximum number of tabular time points of interface-condition parameter data is the fixed dimension defined to parameter-statement variable NTPEV in NF85 (Sec. III.A).

III. PROGRAM DESCRIPTION

A. Program Structure

NF85 is programmed in FORTRAN IV for execution on a large-memory computer without program or variable-storage overlays. The programming was done in a

manner that enhances compiler vectorization on a vector machine. Array variables are stored in a common area of memory with fixed dimensions defined by parameter statements. The parameters defining those array dimensions are shown in Table II.

The program's array-storage requirement needs to be specified for a given problem by defining the problem's actual size values using the parameters in Table II. This is done with an update file named UPNF85 that defines values to these parameters in the first four parameter statements of *COMDECK PARSET1 in program-library file PLNF85. File UPNF85 has the following lines of update information.

```
*IDENT DIMSIZ
*DELETE PARSET1.3,6
      PARAMETER (NXRMX = ###, NYTMX = ###, NZMX = ###, NXYZMN = ###, NRTZ = #)
      PARAMETER (NTBC = ###, NTCBC = ###, NBT = ###, NBPT = ###)
      PARAMETER (NES = ###, NTPES = ###, NXYZES = ###)
      PARAMETER (NEV = ###, NTPEV = ###)
```

The characters ### stand for the user-specified, dimension-size value for each variable name. With program-library file PLNF85, binary-executable file BNF85, update file UPNF85, and controller file CNF85 in your local file space on a Cray computer, execute the following command:

```
XEQ CNF85 / 1 1.2
```

The CNF85 controller updates, compiles, and loads the NF85 program to generate an appropriately dimensioned, executable file called GONF85 for evaluating a problem. For access to the above files, contact the NF85 computer-program custodian to obtain the central file system (CFS) path name where these files are stored permanently. File UPNF85 can be obtained from CFS storage, and a text editor can be used to redefine its parameter values for a specific problem size.

The array-storage requirement for the three-dimensional region can be very large. The total words of array-storage requirement can be estimated by evaluating the following expression.

TABLE II

ARRAY-DIMENSION PARAMETERS

Variable Name	Description
NXRMX	Number of mesh cells in the x or r direction
NYTMX	Number of mesh cells in the y or t direction
NZMX	Number of mesh cells in the z direction
NXYZMN	The minimum value among the values of NXRMX, NYTMX, and NZMX
NRTZ	Geometry-type number [0 = cartesian, 1 = cylindrical]
NTBC	Number of one-dimensional, boundary-condition regions
NTCBC	Maximum number of mesh cells in a one-dimensional, boundary-condition region
NBT	Maximum number of blower curves defined to interfaces in all one-dimensional, boundary-condition regions
NBPT	Maximum number of data pairs in any one of the blower curves
NES	Number of external sources in the three-dimensional region
NTPES	Maximum number of time points in an external-source history table
NXYZES	Maximum number of mesh cells in an external-source spatial-shape distribution
NEV	Number of interface conditions to be edited for EVENT84
NTPEV	Maximum number of time points in an interface-condition history table

$$116 * (NXRMX+3) * (NYTMX+3) * (NZMX+3) + [(3+(1-NRTZ)/NXYZN) * NXRMX * NYTMX + 1] * NXRMX * NYTMX * NZMX * INT ((NXYZN+1)/NXYZN) + 63 + 8 * NTBC (4 + 49 * NTBC) * (NTCBC + 2) + 2 * NBT * (NBPT + 1) + NES * (13 + 8 * NTPES + 2 * NXYZES) + NEV * (9 + 8 * NTPEV),$$

where NXYZN = NXYZMN + NRTZ * (NZMX - NXYZMN).

For a representative problem where NXRMX = 10, NYTMX = 5, NZMX = 20, NTBC = 2, NTCBC = 50, NBT = 1, NBPT = 10, NES = 2, NTPES = 20, NXYZMN = 5, NRTZ = 0, NXYZES = 18, NEV = 3, and NTPEV = 100, and NRTZ = 0, the array-storage estimate from the above expression is 466 922 words. Data for the three-dimensional region (dimensioned by NXRMX, NYTMX, NZMX, NXYZMN, and NRTZ) represents 98.2% of the total storage requirement.

B. Input/Output Files

When executing NF85, up to seven input/output data channels may be required. Table III lists the unit number, assigned file name, and type of data transferred through these data channels.

Unit 5 is the only input-data channel. File INPUT contains problem-defining parameter values specified by the user. The format for file INPUT is described in the next section. During execution of GONF85, NF85 reads in data from file INPUT and echoes it back to file OUTPUT. As the calculation proceeds, calculative results are sent to file OUTPUT at a frequency and in an amount specified in the input data. Messages describing the progress of the calculation and the occurrence of any execution errors are sent to files OUTPUT and MSGDAT and to the terminal display.

The gas-state solution also is edited by NF85 to the GRFDAT file at an input-data-defined frequency. GRFDAT is a binary data file formatted to be read by the EXCON/TRAP computer programs[9] for graphics postprocessing. EXCON (**EX**ecute data **CON**version) and TRAP (**TRAc P**lot) are a pair of computer programs developed independently as a graphics postprocessor package for the **T**ransient **R**eactor **A**nalysis **C**ode (TRAC).[7] The convenience and versatility of this graphics-generating package are the reasons for using it for graphic presentation of NF85 results. The data from NF85 or TRAC is ordered in blocks associated with spatial subregions within edits at successive problem times. EXCON reads these data and rearranges them into blocks of spatial-subregion data for all problem time edits. These blocks of data are written to binary files named COMP##, where ## is the spatial-subregion number. TRAP then reads the COMP## files for

TABLE III

NF85 INPUT/OUTPUT DATA CHANNELS

Unit Number		
5	INPUT	ASCII
6	OUTPUT	ASCII
7	MSGDAT	ASCII
11	GRFDAT	Binary
12	RESDAT	ASCII
13	EVIDAT	ASCII
59	Terminal Display	ASCII

the spatial-subregions whose data are to be plotted. For NF85, the three-dimensional region data are in file COMP01, and the N^{th} one-dimensional, boundary-condition region data are in file COMP## where ## = N+1. User-defined input data for EXCON and TRAP can be specified interactively at the terminal or specified through an input-data file. Refer to the TRAP User's Manuals for further information about the features of these computer programs and how to use them. TRAP is highly dependent on the unique graphics-hardware and -software capability provide by the Los Alamos National Laboratory's Computing Center Facility. Converting TRAP for use at another computing facility may require extensive changes.

File RESDAT is a dump/restart data file containing gas-state time edits in the input-data format. The frequency of these edits is defined by the time-step domain input data. After evaluating a problem, any one of these edits can be copied with a text editor from file RESDAT to a new file named INPUT. If the time edit copied is the last one and no changes are made to the data, executing GONF85 represents a restart continuation of the calculation that generated the RESDAT file. If another one of the time edits is chosen and the data are changed, executing GONF85 represents a restart-branch calculation. When restarting a calculation, care must be taken to rename the output files from the previous calculation to save them in your local file space. Not renaming them will result in the next calculation overwriting them.

File EVIDAT is used by NF85 to edit the interface-condition parameter data for EVENT84 in EVENT84's required input-data format. The interface condition is either the volume-averaged air pressure, air temperature, and tracer-particle densities or the area-averaged air energy flow, air mass flow, and tracer-particle mass flow at a specified interface location. The parameter data are defined as a tabular function of problem time. File EVIDAT is written by NF85 only when the interface-condition edit is requested in the NF85 input data.

IV. INPUT-DATA PREPARATION

A. Input-Data File Organization

The problem-defining parameters required by NF85 are user-specified through an input-data file named INPUT. Table IV outlines the data categories in file INPUT and the parameter-defining cards within each category. The first four categories (title, general parameters, three-dimensional geometry parameters,

TABLE IV

INPUT-DATA FILE ORGANIZATION

Category Description	Card Description
Title	Number of title cards
	Title card(s)
General parameters	Number of mesh cells in each of the three directions
	Geometry type, I/O parameter units, number of edit levels
	Number of boundary-condition regions, external sources, interface conditions, and tracer particles, and the initial time-step number
	Initial problem time, convergence criterion, atmospheric pressure, and tracer-particle-to-air-velocity ratio
3-D geometry parameters	Gravity components in each of the three directions
	Mesh cell lengths in the x or r direction
	Mesh cell lengths in the y or t direction
	Mesh cell lengths in the z direction
Fluid-state parameters for each 2-D level in the z direction	Level number (or repeat a previous level)
	Air temperatures
	Air pressures
	Air volume fractions
	Flow-area fraction of mesh cell interfaces in x or r direction
	Flow-area fraction of mesh cell interfaces in y or t direction
	Flow-area fraction of mesh cell interfaces in z direction
	Hydraulic diameter at mesh cell interfaces in x or r direction
	Hydraulic diameter at mesh cell interfaces in y or t direction
	Hydraulic diameter at mesh cell interfaces in z direction
	Friction-adjustment factor at interfaces in x or r direction
	Friction-adjustment factor at interfaces in y or t direction
	Friction-adjustment factor at interfaces in z direction
	Air velocity at mesh cell interface in x or r direction
	Air velocity at mesh cell interfaces in y or t direction
	Air velocity at mesh cell interfaces in z direction
	Tracer-particle 1 to tracer-particle NTRHO densities
	Level numbers whose parameters are to be edited

TABLE IV (CONT)

Category Description	Card Description
Fluid-state parameters for each 1-D boundary-condition region	Number of mesh cells in the 1-D region, x or r and y or t mesh-cell range defining interface to 3-D region z mesh-cell range defining interface to 3-D region Flow-area fraction of each 3-D region mesh cell at interface to 3-D region Hydraulic diameter of each 3-D region mesh cell at interface to 3-D region Air velocity of each 3-D region mesh cell at interface to 3-D region Gravity component at each mesh-cell interface Air temperature Air pressure Air volumes Mesh-cell lengths Mesh-cell interface flow areas Hydraulic diameters Friction-adjustment factors Air velocities Tracer-particle 1 to tracer-particle NTRHO densities
Mass generation-rate and energy tables for each external source	Number of time points in the table, x or r and y or t mesh-cell range defining source spatial location z mesh cell range defining source spatial location Air-mass-to-explosive-material-mass ratio Air-mass generation-rate source history table Tracer-particle 1 to tracer-particle NTRHO mass generation-rate source history table Air-mass source spatial distribution Air-energy per unit mass history table Air-energy spatial distribution Nondefault values of combustion-model parameters
Definition of each EVENT84 interface condition to be editted	Parameter-type option, x or r and y or t mesh-cell range z mesh-cell range defining interface, number of time points in history table Time interval between table entry pairs, time of next entry pair Interface-condition history table (only present in a restart input-data file)
Time-step and edit-control parameters	Minimum and maximum time-step sizes, end time, initial time-step size Edit time intervals for output, graphics, and restart data

and fluid-state parameters for each two-dimensional level in the z direction) and the last category (time-step and edit-control parameters) are required data. The three categories between them (fluid-state parameters for each one-dimensional boundary-condition region, mass generation-rate and energy tables for each external source, and definition of each EVENT84 interface condition to be edited) are optional data. The third card in the general-parameters category defines the number of entries in each of these optional categories. The optional number of tracer-particles to be convected with the air also is specified on this card.

Defining the fluid state in a three-dimensional geometry can require an enormous amount of data. To aid the user in specifying these data compactly, file INPUT is defined with a free format using an optional repeat (R##) or fill (F) modifier for each value. Free format means that values do not have to be located in specific columns on a record line. Up to five data values can be entered anywhere on each 80-column record line with values separated by one or more blanks. When successive values are the same, they can be specified with the value to be repeated ## times using the R## repeat modifier before the value. For example, the value 1.7, seven values of 1.5, and 1.4 could be entered as 1.7 R07 1.5 1.4. This example has three data values on the record line. Note that the number of times a value is to be repeated is a two-digit number. When a value is to be repeated 2 to 9 times, a zero digit is needed between the R and the single digit. A value can be repeated up to 99 times when input as a single value with a repeat modifier. When all the values to be specified on a parameter-defining card are the same, the value proceeded by the fill modifier F and a blank specifies that all the parameter's array-elements be assigned that value.

When preparing an input-data file, interspersing comments with the data can help in recognizing and understanding the data at a later time. To enter a comment on any record line, type a * character followed by the comment. All data values on a record line must appear before the * character. A record line can be devoted entirely to a comment without any data values. A blank record line (to set off blocks of input data) can have a * character or can be left entirely blank. When NF85 reads data from file INPUT, it reads as many record lines as necessary to obtain the number of values required by the parameter array. Any remaining values on the last record line that is read are lost.

B. Input-Data Description

This section describes the data format for the parameter cards in each of the eight categories of file INPUT. Each parameter value has a defined "Data Type" that is either A for alphanumeric data (any combination of letters and numbers), F for floating-point data (fixed-point value ±###.### with a fixed decimal point or exponential-notation value ±#.###E±##, where # represents digits 0 to 9), or I for integer data (±###).

The F and I "Data Type" values can be entered individually, as a repeated number of a value with the R## (repeat) modifier, or as a value with the F (fill-modifier to fill the entire parameter array. A value must be specified for each parameter and parameter-array element. Under free-format input, blanks do not default to the input value 0 or 0.0. A blank is recognized only as a delimiter between values. Each record line can have from 0 to 5 values, with or without the R## or F modifiers applied. A parameter card requires one or more record lines to supply the necessary number of values.

1. Title. The title provides a description of the problem to be evaluated. The title is written to the beginning of file OUTPUT and to each edit on the dump/restart file RESDAT.

	Value Position	Parameter Description	Data Type	Variable Name
Card 1		Number of record lines of title information ($0 \leq$ NUMTCR ≤ 20)	I	NUMTCR
Card 2		Title describing the problem to be evaluated is defined on NUMTCR record lines of 80 columns each	A	JTITLE(N), where N = 1 to 10*NUMTCR

2. General Parameters. General parameters define the size of the problem, user-selected options, and scalar-parameter values. The number of one-dimensional boundary-condition regions, external sources, EVENT85 interface conditions to be edited, and tracer particles convected by the air is specified on Card 3. Defining their number to be greater than zero provides for their optional implementation in the calculation.

	Value Position	Parameter Description	Data Type	Variable Name
Card 1	1st	Number of mesh cells in the x or r direction ($1 \leq NXR \leq NXRMX$)	I	NXR
	2nd	Number of mesh cells in the y or t direction ($1 \leq NYT \leq NYTMX$)	I	NYT
	3rd	Number of mesh cells in the z direction ($1 \leq NZ \leq NZMX$)	I	NZ

	Value Position	Parameter Description	Data Type	Variable Name
Card 2	1st	Three-dimensional geometry-type option 0 = x-y-z cartesian 1 = r-t-z cylindrical	I	NGEOM
	2nd	Input-parameter units option -2 = English gage (s, ft, lbm, Btu, F, psig) -1 = English absolute (s, ft, lbm, Btu, R, psia) 1 = SI absolute (s, m, kg, J, K, Pa) 2 = SI gage (s, m, kg, J, C, Pag)	I	NIUN
	3rd	Output-parameter units option -2 = English gage -1 = English absolute 1 = SI absolute 2 = SI gage) All parameters edited by NF85 (except the EVENT84 interface-condition parameters) will be in these units	I	NOUN
	4th	Number of z-direction levels whose parameters are to be included in each large edit ($0 \leq NLEVED \leq NZ$)	I	NLEVED

	Value Position	Parameter Description	Data Type	Variable Name
Card 2 (cont)	5th	Printout-control option parameter for backup calculations and reverse-flow occurrences [NBURF = 0 for no printout, NBURF = 1 for printout of all backup calculations (when the time step is reevaluated with a reduced time-step size because of numerical difficulty), NBURF = 2 for printout of all backup and flow-reversal occurrences; note: this printout is to the message file MSGDAT only.]	I	NBURF

	Value Position	Parameter Description	Data Type	Variable Name
	1st	Number of velocity, pressure, and one-dimensional boundary-condition region boundary conditions to be defined on the outer boundary of the three-dimensional region ($0 \leq$ NXYZBC $\leq$ NTBC + number of velocity and pressure boundary conditions)	I	NXYZBC
	2nd	Number of external sources to be defined in the three-dimensional region ($0 \leq$ NEST $\leq$ NES)	I	NEST
Card 3	3rd	Number of EVENT84 interface conditions to be edited ($0 \leq$ NEVENT $\leq$ NEV)	I	NEVENT
	4th	Number of tracer-particle densities to be convected with the air ($0 \leq$ NTRHO ≤ 5 or 1 if combustion model is used)	I	NTRHO
	5th	Initial time-step number for the calculation (define NSTEP = 0 initially; restart input-data files will have NSTEP > 0.)	I	NSTEP

	Value Position	Parameter Description	Data Type	Variable Name
Card 4	1st	Initial problem time(s) for the calculation (ETIME can be positive or negative.)	F	ETIME
	2nd	Pressure-iteration convergence criterion (The maximum fractional change in the local pressure during the last iteration is less than EPSO for pressure-solution convergence to be satisfied; convergence to at least four significant digits of accuracy with EPSO = 0.0001 is recommended.)	F	EPSO
	3rd	Atmospheric pressure in units of psia or Pa based on the sign of NIUN	F	PATM
	4th	The ratio of tracer-particle velocity to air velocity (If $0.0 < TRVFR \leq 1.0$ is not satisfied, TRVFR = 1.0 is defined internally.)	F	TRVFR

3. Three-Dimensional Geometry Parameters. The component lengths of the gravity unit-vector and the three-dimensional region's mesh-cell lengths in each coordinate direction are defined by four cards in this category. For the radial and theta directions in cylindrical geometry, the gravity unit vector component lengths are input only for the interface associated with mesh cell 1. The gravity unit-vector component lengths at all other mesh-cell interfaces in the r and t directions are evaluated internally by NF85.

	Value Position	Parameter Description	Data Type	Variable Name
Card 1	1st	The gravity unit-vector component length in the x-cartesian or r-cylindrical geometry direction (defined at the radial-direction interface of theta mesh cell 1 for cylindrical geometry). The component length is the cosine of the angle between the gravity vector and the x-cartesian or r-cylindrical direction vector.	F	GCXR
	2nd	The gravity unit-vector component length in the y-cartesian or t-cylindrical geometry direction (defined at the theta-direction interface between theta mesh cells 1 and 2 for cylindrical geometry). The component length is the cosine of the angle between the gravity vector and the y-cartesian or t-cylindrical direction vector.	F	GCYT
	3rd	The gravity unit-vector component length in the z-direction. The component length is the cosine of the angle between the gravity vector and the z-direction vector.	F	GCZ
	4th	Acceleration-of-gravity constant [g_c = 9.80665 m/s^2 = 32.1740 ft/s^2; the effect of gravity can be turned off by inputting g_c = 0.0.]	F	GC
Card 2		Mesh-cell length in the x-cartesian or r-cylindrical direction for each of the NXR mesh cells	F	DXR(N), where N = 1 to NXR

	Value Position	Parameter Description	Data Type	Variable Name
Card 3		Mesh-cell length in the y-cartesian or t-cylindrical direction for each of the NYT mesh cells [The t-cylindrical DYT (N) is the mesh-cell sector angle in units of radians.]	F	DYT(N) where N = 1 to NYT
Card 4		Mesh-cell length in the z direction for each of the NZ mesh cells	F	DZ(N) where N = 1 to NZ

4. Fluid-State Parameters for Each x-y or r-t Level in the z Direction.

The input-data parameters in this category define the fluid-state condition in the three-dimensional region of solution. All parameter data are defined in two-dimensional (x-y or r-t) region blocks of data for each z-direction mesh-cell level. When the parameter data in a given level are identical to the data in a previously defined level, the following fixed-format, level-repeat card can be entered instead of the block of data.

```
Columns (fixed format)
                    1 1 1 1 1 1 1 1 1 1 2 2 2 2 2 2 2 2
1 2 3 4 5 6 7 8 9 0 1 2 3 4 5 6 7 8 9 0 1 2 3 4 5 6 7 ...
L E V E L   # # #   R E P E A T S   L E V E L   # # #
```

The first ### is the z-direction mesh-cell level number whose parameters are to be defined by the second ### level's parameter values specified earlier in file INPUT. The levels can be defined in any order. All NZ levels must have their parameter data defined either by the following block of data defining the parameter data for the level or by the above level-repeat card.

	Value Position	Parameter Description	Data Type	Variable Name
Card 1		Columns (fixed format) 1 1 1 1 1 1 2 3 4 5 6 7 8 9 0 1 2 3 4 ... L E V E L # # #	A	
Card 2		Air temperature in units of degrees F (NIUN = -2), R (NIUN = -1), K (NIUN = 1), or C (NIUN = 2) in each of the NXR*NYT mesh cells of level K (K = ### from Card 1)	F	TN (I,J,K), where I = 1 to NXR, J = 1 to NYT
Card 3		Air pressure in units of psig (NIUN = -2) psia (NIUN = -1), Pa (NIUN = 1), or Pag (NIUN = 2) in each of the NXR*NYT mesh cells of level K	F	PN(I,J,K), where I = 1 to NXR, J = 1 to NYT
Card 4		Volume fraction of air in each of the NXR*NYT mesh cells of level K; the remaining 1.0-VOL(I,J,K) volume fraction is structure (solid material fixed in the mesh cell)	F	VOL(I,J,K), where I = 1 to NXR, J = 1 to NYT
Card 5		Fraction of the interface area between mesh cells (I,J,K) and (I+1,J,K) that is open to airflow in the x or r direction for each of the NXR*NYT mesh cells of level K	F	FAXR(I,J,K) where I = 1 to NXR, J - I to NYT

	Value Position	Parameter Description	Data Type	Variable Name
Card 6		Fraction of the interface area between mesh cells (I,J,K) and (I,J+1,K) that is open to airflow in the y or t direction for each of the NXR*NYT mesh cells of level K	F	FAYT(I,J,K), where I = 1 to NXR, J = 1 to NYT
Card 7		Fraction of the interface area between mesh cells (I,J,K) and (I,J,K+1) that is open to airflow in the z direction for each of the NXR*NYT mesh cells of level K	F	FAZ(I,J,K), where I = 1 to NXR, J - 1 to NYT
Card 8		Hydraulic diameter in units of ft (NIUN < 0) or m (NIUN > 0) for airflow through the interface between mesh cells (I,J,K) and (I+1,J,K) for each of the NXR*NYT mesh cells of level K	F	HDXR(I,J,K), where I = 1 to NXR, J = 1 to NYT
Card 9		Hydraulic diameter in units of ft (NIUN < 0) or m (NIUN > 0) for airflow through the interface between mesh cells (I,J,K) and (I,J+1,K) for each of the NXR*NYT mesh cells of level K	F	HDYT(I,J,K), where I = 1 to NXR, J = 1 to NYT
Card 10		Hydraulic diameter in units of ft (NIUN < 0) or m (NIUN > 0) for airflow through the interface between mesh cells (I,J,K) and (I,J,K+1) for each of the NXR*NYT mesh cells of level K	F	HDZ(I,J,K), where I = 1 to NXR, J = 1 to NYT

	Value Position	Parameter Description	Data Type	Variable Name
Card 11		Wall-friction adjustment factor for airflow between mesh cells (I,J,K) and (I+1,J,K) for each of the NXR*NYT mesh cells of level K	F	CFZVXR(I,J,K), where I = 1 to NXR, J = 1 to NYT
Card 12		Wall-friction adjustment factor for airflow between mesh cells (I,J,K) and (I,J+1,K) for each of the NXR*NYT mesh cells of level K	F	CFZVYT(I,J,K), where I = 1 to NXR, J = 1 to NYT
Card 13		Wall-friction adjustment factor for airflow between mesh cells (I,J,K) and (I,J,K+1) for each of the NXR*NYT mesh cells of level K	F	CFZVZ(I,J,K), where I = 1 to NXR, J = 1 to NYT
Card 14		Air velocity in units of ft/s (NIUN < 0) or m/s (NIUN > 0) across the interface between mesh cells (I,J,K) and (I+1,J,K) for each of the NXR*NYT mesh cells of level K	F	VNXR(I,J,K), where I = 1 to NXR, J = 1 to NYT
Card 15		Air velocity in units of ft/s (NIUN < 0) or m/s (NIUN > 0) across the interface between mesh cells (I,J,K) and (I,J+1,K) for each of the NXR*NYT mesh cells of level K	F	VNYT(I,J,K), where I = 1 to NXR, J = 1 to NYT
Card 16		Air velocity in units of ft/s (NIUN < 0) or m/s (NIUN > 0) across the interface between mesh cells (I,J,K) and (I,J,K+1) for each of the NXR*NYT mesh cells of level K	F	VNZ(I,J,K), where I = 1 to NXR, J = 1 to NYT

	Value Position	Parameter Description	Data Type	Variable Name
Card 17		Tracer-particle 1 density in units of lbm/ft^3 (NIUN < 0) or kg/m^3 (NIUN > 0) in each of the NXR*NYT mesh cells of level K [Note: input this card when NTRHO = 1 to 5.]	F	TRHO1(I,J,K), where I = 1 to NXR, J = 1 to NYT
Card 18		Tracer-particle 2 density in units of lbm/ft^3 (NIUN < 0) or kg/m$_3$ (NIUN > 0) in each of the NXR*NYT mesh cells of level K [Note: input this card when NTRHO = 2 to 5.]	F	TRHO2(I,J,K), where I = 1 to NXR, J = 1 to NYT
Card 19		Tracer-particle 3 density in units of lbm/ft^3 (NIUN < 0) or kg/m$_3$ (NIUN > 0) in each of the NXR*NYT mesh cells of level K [Note: input this card when NTRHO = 3 to 5.]	F	TRHO3(I,J,K), where I = 1 to NXR, J = 1 to NYT
Card 20		Tracer-particle 4 density in units of lbm/ft^3 (NIUN < 0) or kg/m$_3$ (NIUN > 0) in each of the NXR*NYT mesh cells of level K [Note: input this card when NTRHO = 4 to 5.]	F	TRHO4(I,J,K), where I = 1 to NXR, J = 1 to NYT
Card 21		Tracer-particle 5 density in units of lbm/ft^3 NIUN < 0) or kg/m$_3$ (NIUN > 0) in each of the NXR*NYT mesh cells of level K [Note: input this card when NTRHO = 5.]	F	TRHO5(I,J,K), where I = 1 to NXR, J = 1 to NYT

After all NZ levels of parameter data are defined, the following card is entered to specify the NLEVED level numbers whose fluid-state parameters are to be included in the long edit to file OUTPUT.

	Value Position	Parameter Description	Data Type	Variable Name
Card 22		NLEVED level numbers whose fluid-state parameters are to be written to file OUTPUT during each long edit	I	LEVED(N), where N = 1 to NLEVED

5. Boundary Conditions: Time-Independent Velocity or Pressure and One-Dimensional, Boundary-Condition Region. On the external boundary of the multi-dimensional region, the user can define time-independent normal-velocity or external-pressure boundary conditions locally. Cards 1 to 6 that follow define the velocity boundary condition; cards 1 to 7 define the pressure boundary condition. Both can have spatial variation over the portion of the external boundary where they are defined.

A one-dimensional, cartesian-geometry region can be attached to any one of the three-dimensional region's six outer-surface faces as a boundary condition. The attachment is to one or more mesh cells whose combined outer-surface area is a filled rectangle. The fluid-dynamic solution in each one-dimensional, boundary-condition region is coupled fully to the three-dimensional region's solution. The parameters defined for each two-dimensional level also are defined for each of the boundary-condition regions. Each such region has a specified number of mesh cells whose length, volume, interface airflow area, and direction can vary from cell to cell. The following six cards of parameter data are specified for each of the NXYZBC boundary conditions whether they are velocity, pressure, or a one-dimensional, boundary-condition region.

Value Position	Parameter Description	Data Type	Variable Name
Card 6	Air velocity in units of ft/s (NIUN < 0) or m/s (NIUN > 0) normal to the interface of each three-dimensional region mesh cell on the rectangular area of attachment to the one-dimensional boundary-condition region; the sign of the velocity value is based on the three-dimensional region's coordinate system [If IL = 0 or IR = NXR + 1, specify VNXYZ(M,N), where M = JL to JR, N = KL to KR; if JL = 0 or JR = NYT + 1, specify VNXYZ(M,N), where M = IL to IR, N = KL to KR; if KL = 0 or KR = NZ + 1, specify VNXYZ(M,N), where M = IL to IR, N = JL to JR.]	F	VNXYZ(M,N), where M and N define the mesh cells in the rectangular area of attachment

Skip cards 7 to 21 if this is a time-independent, velocity boundary condition; that is, NBC = 0. Skip card 7 and go to card 8 if NBC $\geq$ 2.

Value Position	Parameter Description	Data Type	Variable Name
Card 7	Air pressure in units of psig (NIUN = -2), psia (NIUN = -1), Pa (NIUN = 1), or Pag (NIUN = 2) a half-mesh-cell outside the external boundary and adjacent to each three-dimensional region mesh cell in the rectangular area of attachment to the one-dimensional boundary-condition region [If IL = 0 or IR = NXR + 1, specify PNXYZ(M,N), where M = JL to JR, N = KL to KR; if JL = 0 or JR = NYT + 1, specify PNXYZ(M,N), where M = IL to IR, N = KL to KR; if KL = 0 or KR = NZ + 1, specify PNXYZ(M,N), where M = IL to IR, N = JL to JR.]	F	PNXYZ(M,N), where M and N define the mesh cells in the rectangular area of attachment

	Value Position	Parameter Description	Data Type	Variable Name
Card 2	1st	Lower mesh-cell number in the z direction defining the rectangular area of attachment on the xr or yt normally directed faces of the three-dimensional region; when attached to the z normally directed faces, KL = 0 for the lower face and KL = NZ for the upper face	I	KL
	2nd	Upper-mesh cell number in the z direction defining the rectangular area of attachment on the xr or yt normally directed faces of the three-dimensional region; when attached to the z normally directed faces, KR = 1 for the lower face and KR = NZ + 1 for the upper face	I	KR
	3rd	Number of blower curves to be applied at mesh-cell interfaces in this one-dimensional, boundary-condition region	I	NB
Card 3		Fraction of the mesh-cell interface area that is open to airflow to/from the one-dimensional boundary-condition region for each three-dimensional-region mesh cell in the rectangular area of attachment [If IL = 0 or IR = NXR + 1, specify FAXYZ(M,N), where M = JL to JR, N = KL to KR; if JL = 0 or JR = NYT + 1, specify FAXYZ(M,N) where M = IL to IR, N = KL to KR; if KL = 0 or KR = NZ + 1, specify FAXYZ(M,N), where M = IL to IR, N = JL to JR.]	F	FAXYZ(M,N), where M and N define the mesh cells in the rectangular area of attachment

	Value Position	Parameter Description	Data Type	Variable Name
Card 4		Hydraulic diameter in units of ft (NIUN < 0) or m (NIUN > 0) for airflow through the external-boundary interface of each three-dimensional-region mesh cell the rectangular area of attachment [If IL = 0 or IR = NXR + 1, specify HDXYZ(M,N), where M = JL to JR, N = KL to KR; if JL = 0 or JR = NYT + 1, specify HDXYZ(M,N), where M = IL to IR, N = KL to KR; if KL = 0 or KR = NZ+1, specify HDXYZ(M,N), where M = IL to IR, N = JL to JR.]		HDXYZ(M,N), where M and N define the mesh cells in the rectangular area of attachment
Card 5		Wall-friction adjustment factor for airflow through the external-boundary interface of each three-dimensional-region mesh cell in the rectangular area of attachment [If IL = 0 or IR = NXR+1, specify CFZVXY(M,N), where M = JL to JR, N = KL to KR; if JL = 0 or JR = NYT + 1, specify CFZVXY(M,N) where M = IL to IR, N = KL to KR; if KL = 0 or KR = NZ + 1, specify CFZVXY(M,N) where M = IL to IR, N = JL to JR.]		CFZVXY(M,N) where M and N define the mesh cells in the rectangular area of attachment

	Value Position	Parameter Description	Data Type	Variable Name
Card 1	1st	Boundary-condition-type option [NBC = 0 for a time-independent normal velocity specified on the external boundary; NBC = ±1 for a time-independent external pressure specified a half-mesh-cell length outside the external boundary (-1 for $\underline{V}\cdot\underline{\nabla V} = 0$, +1 for $\underline{V}\cdot\underline{\nabla V} \neq 0$); NBC $\geq$ 2 for the number of mesh cells in a one-dimensional, boundary-condition region.]	I	NBC
	2nd	Lower mesh-cell number in the x or r direction defining the rectangular area of attachment on the yt or z normally directed faces of the three-dimensional region; when attached to the xr normally directed faces, IL = 0 for the lower face and IL = NXR for the upper face	I	IL
	3rd	Upper mesh-cell number in the x or r direction defining the rectangular area of attachment on the yt or z normally directed faces of the three-dimensional region; when attached to the xr normally directed faces, IR = 1 for the lower face and IR = NXR + 1 for the upper face	I	IR
	4th	Lower mesh-cell number in the y or t direction defining the rectangular area of attachment on the xr or z normally directed faces of the three-dimensional region; when attached to the yt normally directed faces, JL = 0 for the lower face and JL = NYT for the upper face	I	JL
	5th	Upper mesh-cell number in the y or t direction defining the rectangular area of attachment of the xr or z normally directed faces of the three-dimensional region; when attached to the yt normally-directed faces, JR = 1 for the lower face and JR = NYT + 1 for the upper face	I	JR

Skip cards 8 to 21 if this is a time-independent, pressure boundary condition; that is, NBC = ±1.

	Value Position	Parameter Description	Data Type	Variable Name
Card 8		The gravity unit vector component length that is normal to the interface between mesh cells N and N + 1; the component length is the cosine of the angle between the gravity vector and a vector normal to the mesh-cell interface	F	GCBC(N), where N = 1 to NBC
Card 9		Air temperature in units of degrees F (NIUN = -2), R (NIUN = -1), K (NIUN = 1), or c (NIUN = 2) in each of the NBC mesh cells	F	TNBC(N), where N = 1 to NBC
Card 10		Air pressure in units of psig (NIUN = 2), psia (NIUN = -1), Pa (NIUN = 1), or Pag (NIUN = 2) in each of the NBC mesh cells	F	PNBC(N), where N = 1 to NBC
Card 11		Volume of the air in units of ft^3 (NIUN < 0) or m^3 (NIUN > 0) in each of the NBC mesh cells	F	VOLBC(N), where N = 1 to NBC
Card 12		Mesh-cell length in units of ft (NIUN < 0) or m (NIUN > 0) for each of the NBC mesh cells; VOLBC(N)/DABC(N) is the cross-sectional area within mesh cell N	F	DABC(N), where N = 1 to NBC
Card 13		Interface area between mesh cells N and N + 1 that is open to air in units of ft^2 (NIUN < 0) of m^2 (NIUN > 0) for each of the NBC mesh cells	F	FABC(N), where N = 1 to NBC

	Value Position	Parameter Description	Data Type	Variable Name
Card 14		Hydraulic diameter in units of ft (NIUN < 0) or m (NIUN > 0) for airflow through the interface between mesh cells N and N + 1 for each of the NBC mesh cells [Wall friction is not modeled when [|HDBC(N)| $\leq$ 1.0 x 10^{-5} m.]	F	HDBC(N), where N = 1 to NBC
Card 15		Friction-adjustment factor for airflow between mesh cells N and N + 1 for each of the NBC mesh cells [Applying a negative sign to the value serves as a flag to constrain friction-factor evaluation to the laminar-flow regime.]	F	CFZVBC(N), where N = 1 to NBC
Card 16		Air velocity in units of ft/s (NIUN < 0) or m/s (NIUN > 0) across the interface between mesh cells N and N + 1 for each of the NBC mesh cells [Flow from mesh cell N to mesh cell N + 1 has a positive velocity value; flow in the opposite direction has a negative velocity value.]	F	VNBC(N), where N = 1 to NBC
Card 17		Tracer-particle 1 density in units of lbm/ft^3 (NIUN < 0) or kg/m^3 (NIUN > 0) for each of the NBC mesh cells [Note: input this card only when NTRHO = 1 to 5.]	F	TR1BC(N), where N = 1 to NBC
Card 18		Tracer-particle 2 density in units of lbm/ft^3 (NIUN < 0) or kg/m^3 (NIUN > 0) for each of the NBC mesh cells [Note: input this card only when NTRHO = 2 to 5.]	F	TR2BC(N), where N = 1 to NBC

	Value Position	Parameter Description	Data Type	Variable Name
Card 19		Tracer-particle 3 density in units of lbm/ft^3 (NIUN < 0) or kg/m^3 (NIUN > 0) for each of the NBC mesh cells [Note: input this card only when NTRHO = 3 to 5.]	F	TR3BC(N), where N = 1 to NBC
Card 20		Tracer-particle 4 density in units of lbm/ft^3 (NIUN < 0) or kg/m^3 (NIUN > 0) for each of the NBC mesh cells [Note: input this card only when NTRHO = 4 to 5.]	F	TR4BC(N), where N = 1 to NBC
Card 21		Tracer-particle 5 density in units of lbm/ft^3 (NIUN < 0) or kg/m^3 (NIUN > 0) for each of the NBC mesh cells [Note: input this card only when NTRHO = 5.]	F	TR5BC(N) where N = 1 to NBC

Input Cards 22, 23, and 24 for <u>each</u> of the NB blower curves to be applied at mesh-cell interfaces of this one-dimensional, boundary-condition region.

	Value Position	Parameter Description	Data Type	Variable Name
Card 22	1st	Number of tabular-data value pairs defining this blower curve	I	NBP
	2nd	The mesh-cell interface number (between mesh cell NBI and mesh cell NBI + 1) where the blower-curve pressure change is to be applied	I	NBI

	Value Position	Parameter Description	Data Type	Variable Name
Card 23		The airflow velocity abscissa-coordinate values in units of ft/s (NIUN < 0) or m/s (NIUN > 0) definging the blower curve [Note: successive values of VBT(N) increase monotoncally, that is, VBT(N)<VBT(N+1).]	F	VBT(N), where N = 1 to NBP
Card 24		The pressure-change ordinate-coordinate values in units of psi (NIUN < 0) or Pa (NIUN > 0) defining the blower curve [Note: VBT(N) and DPBT(N) define the blower curve's Nth pair of values; the pressure change is the pressure in mesh cell NBI whose difference is affected by the action of the blower.]	F	DPBT(N), where N = 1 to NBP

6. Mass-Generation Rate and Energy Tables for Each External Source. An external source can be defined to generate (or extract) mass and energy in a local volume of mesh cells within the three-dimensional region as a function of time. The total mass-generation rate and the total or internal energy per unit mass of that mass-generation rate are specified as a tabular function of time. Time increases with each entry pair in these tables. Mass-generation rate values outside the defined time range of the tables are assumed to be zero. An unnormalized spatial distribution over a local three-dimensional volume of mesh cells is defined separately for mass and energy and is super- imposed upon the time-dependent data. The following block of parameter data Cards 1 to 13 is to be specified for each of the NEST external sources to be defined.

	Value Position	Parameter Description	Data Type	Variable Name
Card 1	1st	Number of entry pairs in the problem time vs mass-generation rate or energy tables ($2 \leq NTP \leq NTPES$)	I	NTP
	2nd	Lower mesh-cell number in the x or r direction defining the local volume of the spatial distribution ($1 \leq IL \leq IR$)	I	IL
	3rd	Upper mesh-cell number in the x or r direction defining the local volume of the spatial distribution ($IL \leq IR \leq NXR$)	I	IR
	4th	Lower mesh-cell number in the y or t direction defining the local volume of the spatial distribution ($1 \leq JL \leq JR$)	I	JL
	5th	Upper mesh-cell number in the y or t direction defining the local volume of the spatial distribution ($JL \leq JR \leq NYT$)	I	JR

	Value Position	Parameter Description	Data Type	Variable Name
Card 2	1st	Lower mesh-cell number in the z direction defining the local volume of the spatial distribution ($1 \leq KL \leq KR$)	I	KL
	2nd	Upper mesh-cell number in the z direction defining the local volume of the spatial distribution ($KL \leq KR \leq NZ$)	I	KR
	3rd	Type of energy source option; for ITYP = 0, the time and spattially dependent total energy table is input on Cards 11 and 12; for ITYP > o, the chemical-combustion energy source is evaluated by NF85 using the combustion model [(ITYP >0) defines the explosive material to be trinitrotoluene (TNT) for ITYP = 1, tributyl phosphate (TBP or "red oil") for ITYP = 2, hydrogen gas for ITYP = 3, or acetylene gas; for ITYP = 4, some or all of the combustion-model parameters may be redefined from their internally defined values by inputting cards 14 to 17; for the above explosive material, add to ITYP the value 10 for card 14. 20 for card 15, 40 for card 16, and 80 for card 17.]	I	ITYP
Card 3		Air-to-explosive-material mass ratio for an equivalent number of moles of air and decomposed-explosive component gases [Note: input a RAMEM value if ITYP = 0 or ITYP has had 10 added to it; that is, ITYP/10 is an odd value and Card 14 is being input; otherwise, the internally defined values are 0.889177 for TNT, 1.679230 for TBP, 14.311825 for H_2, and 1.108097 for C_2H_2]	F	RAMEM

	Value Position	Parameter Description	Data Type	Variable Name
Card 4		Time-point values in units of s for the NTP entry pairs in the problem time vs mass generation-rate or energy tables	F	TP(N), where N = 1 to NTP
Card 5		Total explosive-material mass-generation rate in units of lbm/s (NIUN < 0) or kg/s (NIUN > 0) for the NTP entry pairs in the problem time vs mass-generation rate table	F	SMTP(N), where N = 1 to NTP
Card 6		Tracer-particle 1 mass-generation rate in units of lbm/s (NIUN < 0) or kg/s (NIUN > 0) for the NTP entry pairs in the problem time vs tracer-particle 1 mass-generation rate table [Note: input this card only when NTRHO = 1 to 5]	F	SMT1(N), where N = 1 to NTP
Card 7		Tracer-particle 2 mass-generation rate in units of lbm/s (NIUN < 0) or kg/s (NIUN > 0) for the NTP entry pairs in the problem time vs tracer-particle 2 mass-generation rate table [Note: input this card only when NTRHO = 2 to 5]	F	SMT2(N), where N = 1 to NTP
Card 8		Tracer-particle 3 mass-generation rate in unitsof lbm/s (NIUN < 0) or kg/s (NIUN > 0) for the NTP entry pairs in the problem time vs tracer-particle 3 mass-generation rate table. [Note: input this card only when NTRHO = 3 to 5]	F	SMT3(N), where N = 1 to NTP

	Value Position	Parameter Description	Data Type	Variable Name
Card 9		Tracer-particle 4 mass-generation rate in units of lbm/s (NIUN < 0) or kg/s (NIUN > 0) for the NTP entry pairs in the problem time vs tracer-particle 4 mass-generation rate table. [Note: input this card only when NTRHO = 4 to 5]	F	SMT4(N), where N = 1 to NTP
Card 10		Tracer-particle 5 mass-generation rate in units of lbm/s (NIUN < 0) or kg/s (NIUN > 0) for the NTP entry pairs in the problem time vs tracer-particle 5 mass-generation rate table. [Note: input this card only when NTRHO = 5]	F	SMT5(N), where N = 1 to NTP
Card 11		Unnormalized spatial distribution defining the mass-generation rate spatial dependence	F	SMXYZ (I,J,K), where I = IL to IR, J = JL to JR, K = KL to KR
Card 12		Total or internal energy per unit of explosive-material mass in units of Btu/lbm (NIUN < 0) or J/kg (NIUN > 0) for the NTP entry pairs in the probem time vs total or internal energy table. [Note: input total energy when ITYP = 0 and internal energy when ITYP > 0]	F	SETP(N), where N = 1 to NTP
Card 13		Unnormalized spatial distribution defining the energy per unit mass spatial dependence	F	SEXYZ(I,J,K), where I = IL to IR, J = JL to JR, K = KL to KR,

	Value Position	Parameter Description	Data Type	Variable Name
Card 14 (Input this card when ITYP/10 is odd valued)	1st	Fraction of the air-equivalent mass-generation rate source that is the first oxygen-gas reactant in the combustion model [The internally defined value is 0.024954 for TNT and 0.060856 for TBP, and 0.069872 for H_2 and C_2H_2.]	F	FRM(1)
	2nd	Fraction of the air-equivalent mass-generation rate source that is the second oxygen-gas reactant in the combustion model [the internally defined value is 0.416288 for TNT, 0.322287 for TBP 0.0 for H_2, and 0.832575 for C_2H_2]	F	FRM(2)
	3rd	Fraction of the air-equivalent mass-generation rate source that is the third oxygen-gas reactant in the combustion model [the internally defined value is 0.0 for all reactants.]	F	FRM(3)
	4th	Fraction of the air-equivalent mass-generation rate source that is oxygen gas in the combustion model [The internally defined value is 0.475322 for TNT, 0.143108 for TBP, and 0.0 for H_2 and C_2H_2.]	F	FRM(4)

If any of the NEST external sources defined above have a ITYP value greater than 20, 1 or more of the following cards need to be input to redefine a portion or all of the combustion-model parameters.

	Value Position	Parameter Description	Data Type	Variable Name
Card 15		Ratio of the Nth reactant's mass to the oxygen gas mass that chemically react [The internally defined values are WTR(1) = 0.126 = 2.016/16.0, WTR(2) = -0.750687 = -12.011/16.0, and WTR(3) = 1.750687 = 28.011/16.0]. [Note: input this card when one or more of the ITYP > 20 values input above satisfy 1 = MOD(ITYP/20,2) = ITYP/20-((ITYP/20)/2)*2]	F	WTR(N), where N = 1 to 3
Card 16		Ratio of a mole of air mass to the mole of Nth chemical reaction's stable product mass; define PDR(N)when the Nth reaction product is the (N+1)th reactant [The internally defined values are PDR(1) = 1.601501 = 28.85264/18.016, PDR(2) = -1.030047 = 28.85264/28.011, and PDR(3) = 0.65566578 = 28.85264/44.011).] [Note: input this card when one or more of the ITYP > 40 values input above satisfy 1 = MOD (ITP/40,2) = ITYP/40-((ITYP/40)/2)*2]	F	PDR(N), where N = 1 to 3
Card 17		Nth chemical reaction's energy of combustion per unit mass of its product gas in units of Btu/lbm (NIUN < 0) or J/kg (NIUN > 0) [The internally defined values are ECB(1) = 1.58661×10^7 J/kg, ECB(2) = 3.94575×10^6 J/kg, and ECB(3) = 6.43010×10^6 J/kg.] [Note: input this card when one or more of the ITYP values input above are > 80]	F	ECB(N), where N = 1 to 3

7. EVENT84 Interface Conditions to be Edited. NF85 was developed to analyze the near-field effects of an explosion in a room. A portion of the space external to the room, the far field, may need to be modeled by one-dimensional, boundary-condition regions to account for the feedback effect of the far field on the near-field solution. A separate analysis of the far field may be performed by the EVENT84 computer program, which evaluates gas dynamic transients in flow networks; the near-field explosion that drives the far-field solution may be evaluated by NF85. The fluid-state condition at the far-field interface location may be extracted from the NF85 solution and defined as an interface (boundary) condition for input to EVENT84. That fluid-state condition can be either the average volumetric state (air temperature, air pressure, and tracer-particle densities) in the three- or one-dimensional mesh cells adjacent to the far-field interface or the average flow state (air-mass, air-energy, and tracer-particle-mass flow rates) through the cross-sectional area of the far-field interface. It is the user's option as to which state is edited as a tabular function of time. NEST blocks of the following input-parameter data for each EVENT84 interface condition are to be specified by the NF85 user.

Value Position	Parameter Description	Data Type	Variable Name
1st	Type of parameter state to be edfor input to EVENT84 [ITY = 1, volumetric (SI absolute); -1, volumetric (English absolute 2, volumetric (SI gage); -2, volumetric (English gage); 3, flow rate (SI units): and -3, flow rate (English units) where volumetric = T, P, ρ_{TP} and flow rate = dmass/dt, denergy/dt, $dmass_{TP}/dt$]	I	ITY
2nd	Lower mesh-cell number in the x or r direction defining the EVENT84 interface's three-dimensional region mesh cells; IL is made negative and IR is set equal to IL if the EVENT84 interface lies between mesh cells |IL| and |IL|+1 normal to the x or r direction; if the	I	IL

	Value Position	Parameter Description	Data Type	Variable Name
	2nd	(Continued) EVENT84 interface is between mesh cells in a one-dimensional, boundary-condition region, IL is the one-dimensional, boundary-condition region number with a negative sign		
Card 1	3rd	Upper mesh-cell number in the x or r direction defining the EVENT84 interface's three-dimensional region mesh cells; IR is negative and equal t IL if the EVENT84 interface lies between mesh cells |IR| and |IR|+1 normal to the x or r direction; if the EVENT84 interfere is between mesh cells in a one-dimensional, boundary-condition region, IR is the lower mesh cell number	I	IR
	4th	Lower mesh-cell number in the y or t direction defining the EVENT84 interface's three-dimensional region mesh cells; JL is made negative and JR is set equal to JL if the EVENT84 interface lies between mesh cells |JL| and |JL|+1 normal to the y or t direction; set JL = 0 if the EVENT84 interface is in a one-dimensional, boundary-condition region	I	JL
	5th	Upper mesh-cell number in the y or t direction defining the EVENT84 interface's three-dimensional region mesh cells; JR is negative and equal to JL if the EVENT84 interface lies between mesh cells |JR| and |JR|+1 normal to the y or t direction; set JR = 0 if the EVENT84 interface is in a one-dimensional, boundary-condition region	I	JR

	Value Position	Parameter Description	Data Type	Variable Name
	1st	Lower mesh-cell number in the z direction defining the EVENT84 interface's three-dimensional region mesh cells; KL is made negative and KR is set equal to KL if the EVENT84 interface lies between mesh cells |KL| and |KL|+1 normal to the z direction; set KL = 0 if the EVENT84 interface is in a one-dimensional, boundary-condition region	I	KL
Card 2	2nd	Upper mesh-cell number in the z direction defining the EVENT84 interface's three-dimensional region mesh cells; KR is negative and is equal to KL if the EVENT84 interface lies between mesh cells |KR| and |KR|+1 normal to the z direction; set KR = 0 if the EVENT84 interface is in a one-dimensional, boundary-condition region	1	KR
	3rd	Number of time points in the EVENT84 interface-condition's history table already generated; the user defines LPT = 0 initially and NF85 increments it when evaluating each EVENT84 interface-condition time-point entry	1	LPT

	Value Position	Parameter Description	Data Type	Variable Name
Card 3	1st	Time interval in units of s between EVENT84 interface-condition entries in the history table	F	DPT
	2nd	Problem time in units of s for the next time-point entry in the EVENT84 interface-condition history table; EVENT84 is dimensioned for a maximum of 99 time-point entry pairs in the interface-condition history table; thus, the maximum time range of the table generated by NF85 would be TPT(1) $\leq$ time $\leq$ TPT(1)+NTPEV*DPT, where NTPEV = 99 is the parameter-statement dimension defined in NF85	F	TPT(LPT+1)

Note: No Cards 4 and 5 are defined initially when LPT = 0; there will be LPT>0 Cards 4 and 5 (generated by NF85) defined here when this is a dump/restart input data file.

	Value Position	Parameter Description	Data Type	Variable Name
Card 4	1st	Problem time in units of s for the Nth entry in the EVENT84 interface-condition history table	F	TPT(N)
	2nd	First parameter (air temperature when ITY = ±1, ±2 or air-energy flow rate when when ITY = ±3) value for the Nth entry in the EVENT84 interface-condition history table	F	PAR1(N)
	3rd	Second parameter (air pressure when ITY = ±1, ±2 or air mass flow rate when ITY = ±3) value for the Nth entry in the EVENT84 interface-condition history table	F	PAR2(N)
	4th	Third parameter (tracer-particle 1 density when ITY = ±1, ±2 or mass flow rate when ITY ± 3) value for the Nth entry in the EVENT84 interface-condition history table. [NF85 defines this value only when NTRHO = 1 to 5]	F	PAR3(N)

	Value Position	Parameter Description	Data Type	Variable Name
Card 5	1st	Fourth parameter (tracer-particle 2 density when ITY = ±1, ±2, or mass flow rate when ITY = ±3) value for the Nth entry in the EVENT84 interface-condition history table [NF85 defines this value only when NTRHO = 2 to 5]	F	PAR4(N)
	2nd	Fifth parameter (tracer-particle 3 density when ITY = ±1, ±2, or mass flow rate when ITY = ±3) value for the Nth entry in the EVENT84 interface-condition history table [NF85 defines this value only when NTRHO = 3 to 5]	F	PAR5(N)
	3rd	Sixth parameter (tracer-particle 4 density when ITY = ±1, ±2, or mass flow rate when ITY = ±3) value for the Nth entry in the EVENT84 interface-condition history table [NF85 defines this value only when NTRHO = 4 to 5]	F	PAR6(N)
	4th	Seventh parameter (tracer-particle 5 density when ITY = ±1, ±2, or mass flow rate when ITY = ±3) value for the Nth entry in the EVENT84 interface-condition history table [NF85 defines this value only when NTRHO = 5]	F	PAR7(N)

8. Time-Step and Edit-Control Parameters. This is the last category of input data that controls the calculation's time-step size and parameter-value edits. The problem time simulated is separated into time domains that the user controls individually. Each time domain, controllable by the parameters on the following two cards, has a specified minimum and maximum time-step size, ending time, starting time-step size, and edit frequencies for parameter data. The minimum and maximum time-step sizes provide a range constraint on the time-step size that NF85 automatically adjusts based on the rate of the transient behavior being evaluated. When problem time reaches the time domain's ending time, NF85 reads in the next time domain's two cards of control parameters. The last time domain, which defines the ending time for the problem, is followed by a time-domain Card 1 (only) with a negative minimum time-step size value. Use the fill modifier card, F -1.0 *END OF PROBLEM , after the last time domain's parameter data to provide the above flag to end the problem. The edit frequency parameters define the time interval between long edits to file OUTPUT, graphics-data edits to file GRFDAT, dump/restart- data edits to file RESDAT, and short edits to file OUTPUT. A short edit is generated automatically before each long edit.

	Value Position	Parameter Description	Data Type	Variable Name
Card 1	1st	Minimum time-step size in units of s during this time domain	F	DTMIN
	2nd	Maximum time-step size in units of s during this time domain	F	DTMAX
	3rd	Ending problem time in units of s for this time domain	F	TEND
	4th	Initial time-step size in units of seconds for this time domain [Note: inputing a negative value is a flag that its absolute value is to be multiplied by the previous time-step size to define the initial time-step size for this time domain; the previous time-step size is used when DELT = -1.0 or $\|DELT\| < 1.0 \times 10^{-10}$ is input.]	F	DELT

	Value Position	Parameter Description	Data Type	Variable Name
Card 2	1st	Time interval in units of s between long edits during this time domain [Note: apply a negative sign to this value if a long edit is to be made at the start of this time domain.]	F	EDINT
	2nd	Time interval in units of s between graphics-data edits during this time domain [Note: apply a negative sign to this value if a graphics-data edit is to be made at the start of this time domain.]	F	GFINT
	3rd	Time interval in units of s between dump/restart-data edits during this time domain [Note: apply a negative sign to this value if a dump/restart-data edit is to be made at the start of this time domain.]	F	DMPINT
	4th	Time interval in units of s between short edits during this time domain [Note: apply a negative sign to this value if a short edit is to be made at the start of this time domain.]	F	SEDINT

V. SAMPLE PROBLEM

A. Problem Description.

The EVENT84 user's manual sample problem[2] entitled "Explosion in a Large Room" will be used as the NF85 sample problem. The problem is suitable for demonstrating the ability of NF85 to evaluate the near-field effects of an explosion occurring in a multidimensional room. Interesting variations on this problem also will be considered to show how they affect the behavior of the problem's solution. A comparison will be made between the EVENT84 and NF85 solutions. This comparison will be extended to a further EVENT84 calculation of the sample problem's far-field ventilation systems using the NF85 solution at the room/vent interfaces as a boundary input-specified condition.

Figure 1 shows a diagram of the room and ventilation system for the EVENT84 sample problem. The dampers, filter, and blowers are modeled by interface conditions (numbered in parentheses) between single-node (numbered) volumes. Figure 2 shows a diagram of the same system as modeled for NF85. The primary difference between these two spatial models is the division of single-node volumes into a number of mesh-cell volumes. EVENT84 node volumes 2, 3, 7, 8, and 9 are each 5 ft long and have been divided into three one-dimensional mesh cells that are 1.6667 ft long. The long duct volumes 5 and 6 are each 50 ft long and have been divided into 30 one-dimensional mesh cells that are 1.6667 ft long. The single node, room number 4, that has volume of 1000 ft^3 is modeled for NF85 in three-dimensional (x,y,z) cartesian coordinates with 7 by 5 by 7 mesh cells along the 12.5-ft width, 8-ft height, and 10-ft length, respectively, having mesh-cell lengths of 1.7857 ft, 1.6 ft, and 1.4286 ft.

Even with these additional mesh cells in the NF85 model, the spatial mesh remains "coarse." This is appropriate for demonstration purposes. Using a coarse mesh in this sample problem allows the problem to be evaluated by NF85 with a computer memory requirement of only 194,240 words. For an accurate solution, mesh cell lengths of 0.6 ft or less are needed. This would result in 3 times as many one-dimensional mesh cells and 27 (3^3) times as many three-dimensional mesh cells.

The NF85 input-data file for its sample problem "Explosion in a Room" is presented in Fig. 3. (Refer to Chap. IV for a description of the input-data format.) The time-domain data are set up to evaluate the steady-state solution over the problem-time interval -3.0 to 0.0 s. From 0.0 to 0.001 s, 1 lbm of TNT explosive is added to the (4,3,4) central mesh cell in the room and combusted with the oxygen present in the air. The transient effects of this explosion are evaluatec for 1.0 s.

The parameters in the input-data file are derived from the EVENT84 sample-problem data. Converting the pressure head (inches of water) vs volumetric flow (ft^3/min) blower tables from EVENT84 to pressure change (psig) vs flow velocity (ft/s) blower tables for NF85 requires units conversion and numerical sign definition. For the blower in the ventilation system inlet-flow duct, steady-state positive flow corresponds to a negative velocity for NF85. For this blower table, translating volumetric flow to flow velocity requires adding a negative sign and reversing the order of the data in the blower table so that successive abscissa-coordinate values increase.

The airflow resistance of the dampers and filter is simulated using the wall-friction model (Sec. II.E) in NF85. For steady-state airflow conditions in a horizontal duct, the motion equation [Eq. (3)] reduces to

$$\underline{0} = -\frac{1}{\delta} \underline{\nabla P} - K \, |\underline{V}| \, \underline{V} \quad , \tag{13}$$

where $\underline{0}$ is a null vector.

The drag coefficient, K = CFZV 2 f/D_h [Eq. (12)], has its Fanning friction factor f evaluated for turbulent airflow [Eq. (10)] to model the dampers and for laminar airflow [Eq. (9)] to model the filter. In this problem, the high Reynold's number turbulent airflow is forced to be laminar flow at the filter interface by defining the input-specified CFZV value to be negative (line 105 in Fig. 3). At the mesh-cell interfaces where the dampers and filter are modeled, the steady-state pressure change and airflow conditions are known. The only unknown is the value of the input-specified air/wall-friction adjustment factor CFZV. It is determined for input to NF85 by requiring that Eq. (13) be satisfied at each of the damper/filter mesh-cell interfaces. The CFZV value for all other mesh-cell interfaces (modeling air/wall friction on the 4-ft^2 cross-section ventilation duct) is determined by applying the same procedure to all mesh-cell interfaces along the 100-ft-long duct between the room and the filter. For the input-specified 0.00725-psig (0.2-inches of water) pressure drop along the 100-feet duct, a CFZV value of 48.0 is needed by NF85 to evaluate the same steady-state pressure drop. Such a large value for CFZV over the nominal smooth-walled duct value of 1.0 implies the presence of internal structure within the duct that acts as an additional resistance to airflow.

Figures 4 to 12 show the air pressure, temperature, volume flow, mass flow, and pressure differential across the filter interface that result from the transient portion of the NF85 calculation based on Fig. 3 input data. The parameters plotted are the same as those plotted for the EVENT84 sample problem. To aid in comparing these results with those in the EVENT84 user's manual, the EVENT84 node or branch location corresponding to the NF85 mesh cell or mesh-cell interface location is shown in the plotted-curve index labels of Figs. 4 to 12. The mesh cells are centered geometrically within the much larger node volumes.

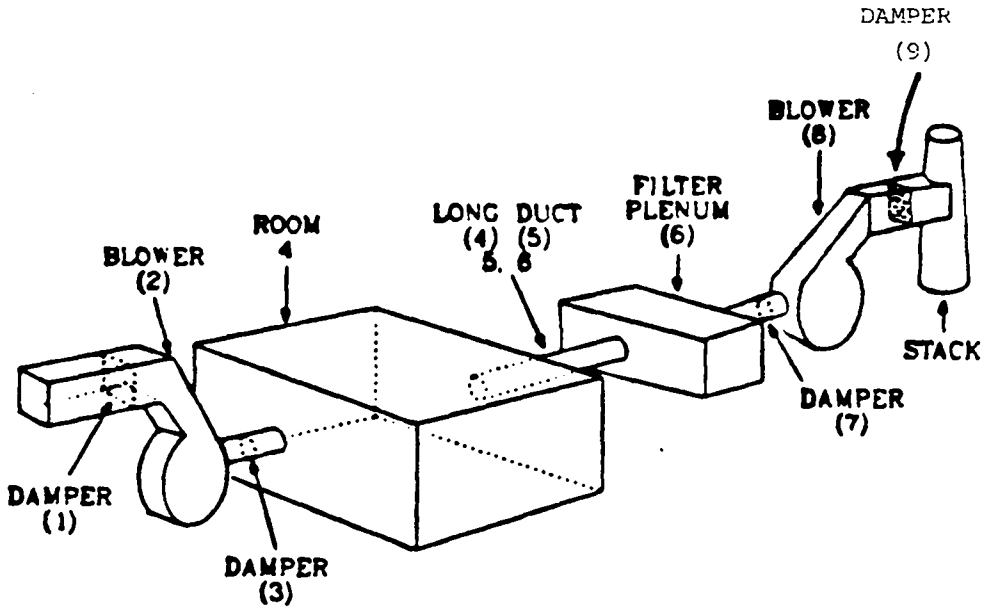

Fig. 1.
Ventilation system used for the EVENT84 sample problem.

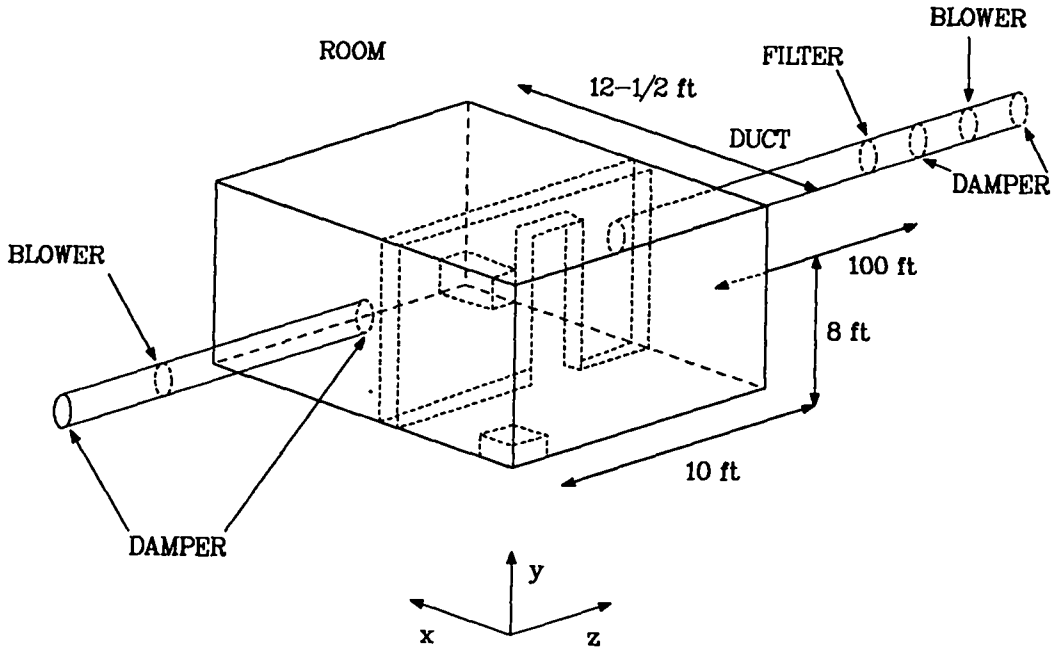

Fig. 2.
Spatial model of the ventilation system used in the NF85 sample problem.

```
 1  10 *NUMTCR
 2 NF85 SAMPLE PROBLEM : AN EXPLOSION IN A ROOM
 3 BASED ON EVENT84 SAMPLE PROBLEM: AN EXPLOSION IN A LARGE ROOM
 4 EXHAUST VENTS MODELED BY TWO 1-D BOUNDARY-CONDITION REGIONS
 5 1 LBM TNT EXPLOSIVE IS LOCATED AT (4,3,4) CENTER OF THE ROOM
 6 EXPLOSIVE INTERNAL ENERGY IS INPUT & COMBUSTION IS CALCULATED
 7 FLOW RESISTANCE OF THE FILTER IS MODELED WITH LAMINAR FLOW
 8 FLOW RESISTANCE OF THE FOUR DAMPERS IS MODELED
 9 PRESSURE CHANGE OF THE TWO BLOWERS IS DEFINED BY TABLES
10 NO INTERNAL WALL IS PRESENT IN THE ROOM
11 TWO VENT-OPENING INTERFACE CONDITIONS FOR EVENT84 ARE EDITED
12 *
13 * GENERAL PARAMETERS
14 *
15  7 5 7          *NXR,NYT,NZ
16  0 -2 -2 3 1 *NGEOM,NIUN,NOUN,NLEVED,NBURF
17  2 1 2 0 0    *NXYZBC,NEST,NEVENT,NTRHO,NSTEP
18  -3.0 1.0E-04 14.7 1.0 *ETIME,EPSO,PATM,TRVFR
19 *
20 * GEOMETRY PARAMETERS
21 *
22  0.0 -1.0 0.0 32.174 *GCXR,GCYT,GCZ,GC
23 F 1.7857 *DXR
24 F 1.6000 *DYT
25 F 1.4286 *DZ
26 *
27 * X-Y-Z REGION PARAMETERS
28 *
29 LEVEL   1
30 F 60.0     *TN
31 F 0.03624 *PN
32 F 1.0       *VOL
33 F 1.0       *FA-XR
34 F 1.0       *FA-YT
35 F 1.0       *FA-Z
36 F 0.0       *HD-XR
37 F 0.0       *HD-YT
38 F 0.0       *HD-Z
39 F 0.0       *CFZV-XR
40 F 0.0       *CFZV-YT
41 F 0.0       *CFZV-Z
42 F 0.0       *VN-XR
43 F 0.0       *VN-YT
44 R17 0.0 4.1667 R17 0.0 *VN-Z
45 LEVEL   2 REPEATS LEVEL   1
46 LEVEL   3 REPEATS LEVEL   1
47 LEVEL   4 REPEATS LEVEL   1
48 LEVEL   5 REPEATS LEVEL   1
49 LEVEL   6 REPEATS LEVEL   1
50 LEVEL   7 REPEATS LEVEL   1
51  1 4 7 *LEVED
52 *
53 * 1ST 1-D BOUNDARY-CONDITION REGION PARAMETERS
54 *
55  6 3 5 3 3    *NBC,IL,IR,JL,JR
56  0 1 1          *KL,KR,NB
57  0.2 1.0 0.2 *FA-Z
58  1.0 3.2 1.0 *HD-Z
59 F 240.0       *CFZV-Z
60 F 4.1667      *VN-Z
61 F 0.0          *GC-BC
62 F 60.0         *TN-BC
63  0.03975 0.03987 0.03999 -.01824 -.01812 *PN-BC
64  -.01800 0.00000                          *PN-BC
65 F 6.6667   *VOL-BC
66 F 1.6667   *DA-BC
67 F 4.0       *FA-BC
68 F 2.0       *HD-BC
69 R05 48.0 7150.0 *CFZV-BC
70 F -4.1667 *VN-BC
71  6 3         *NBP,NBI
72  -5.8333 -5.4167 -4.1667 -3.3333  0.0000 *VBT
```

Fig. 3.
NF85 input-data file for "Explosion in a Room" sample problem.

```
 73   0.4167                                              *VBT
 74  0.00000 -.02899 -.05799 -.06524 -.06886 *DPBT
 75  -.09786                                             *DPBT
 76 *
 77 * 2ND 1-D BOUNDARY-CONDITION REGION PARAMETERS
 78 *
 79  69 3 5 3 3   *NBC,IL,IR,JL,JR
 80  7 8 1        *KL,KR,NB
 81  0.2 1.0 0.2 *FA-Z
 82  1.0 3.2 1.0 *HD-Z
 83 F 48.0        *CFZV-Z
 84 F 4.1667      *VN-Z
 85 F 0.0         *GC-BC
 86 F 60.0        *TN-BC
 87  0.03612 0.03600 0.03588 0.03576 0.03564 *PN-BC
 88  0.03552 0.03540 0.03528 0.03516 0.03503 *PN-BC
 89  0.03491 0.03479 0.03467 0.03455 0.03443 *PN-BC
 90  0.03431 0.03419 0.03407 0.03395 0.03383 *PN-BC
 91  0.03371 0.03358 0.03346 0.03334 0.03322 *PN-BC
 92  0.03310 0.03298 0.03286 0.03274 0.03262 *PN-BC
 93  0.03250 0.03238 0.03226 0.03214 0.03201 *PN-BC
 94  0.03189 0.03177 0.03165 0.03153 0.03141 *PN-BC
 95  0.03129 0.03117 0.03105 0.03093 0.03081 *PN-BC
 96  0.03069 0.03056 0.03044 0.03032 0.03020 *PN-BC
 97  0.03008 0.02996 0.02984 0.02972 0.02960 *PN-BC
 98  0.02948 0.02936 0.02924 0.02911 0.02899 *PN-BC
 99  -.00713 -.00725 -.00737 -.01075 -.01087 *PN-BC
100  -.01099 0.01462 0.01450 0.01438 0.00000 *PN-BC
101 F 6.6667 *VDL-BC
102 F 1.6667 *DA-BC
103 F 4.0    *FA-BC
104 F 2.0    *HD-BC
105 R59 48.0 -249600.0 R02 48.0 1360.0 *CFZV-BC
106 R05 48.0 5730.0                    *CFZV-BC
107 F 4.1667 *VN-BC
108  6 66     *NBP,NEI
109  -0.8333  0.0000  2.9167  4.1667  5.8333 *VBT
110   6.6667                                  *VBT
111  0.05074 0.03624 0.03262 0.02537 0.01450 *DPBT
112  0.00000                                 *DPBT
113 *
114 * EXTERNAL-SOURCE PARAMETERS
115 *
116  2 4 4 3 3    *NTP,IL,IR,JL,JR
117  4 4 1        *KL,KR,ITYP
118  0.0 1.0E-03 *TPT
119 F 1.0E+03     *SMTP
120 F 1.0         *SMXYZ
121 F 1.246E+02   *SETP
122 F 1.0         *SEXYZ
123 *
124 * 1ST EVENT84 INTERFACE-CONDITION EDIT PARAMETERS
125 *
126  -3 3 5 3 3 *ITY,IL,IR,JL,JR
127  -0 -0 0     *KL,KR,LPT
128  0.01 0.0    *DPT,TPT
129 *
130 * 2ND EVENT84 INTERFACE-CONDITION EDIT PARAMETERS
131 *
132  -3 3 5 3 3 *ITY,IL,IR,JL,JR
133  -7 -7 0     *KL,KR,LPT
134  0.01 0.0    *DPT,TPT
135 *
136 * TIME-DOMAIN PARAMETERS
137 *
138    1.0E-06  1.0E-01  0.0E+00  1.0E-03 *DTMIN,DTMAX,TEND,DELT
139    3.0E+00 -1.0E-01  3.0E+00  3.0E+00 *EDINT,GFINT,DMPINT,SEDINT
140    1.0E-08  1.0E-03  2.0E-01  1.0E-06 *DTMIN,DTMAX,TEND,DELT
141    2.0E-01  5.0E-03  2.0E-01  2.0E-01 *EDINT,GFINT,DMPINT,SEDINT
142    1.0E-06  1.0E-02  1.0E+00 -1.0E+00 *DTMIN,DTMAX,TEND,DELT
143    4.0E-01  1.0E-02  8.0E-01  4.0E-01 *EDINT,GFINT,DMPINT,SEDINT
144 F -1.0 *END OF TIME-STEP DATA
```

Fig. 3 (cont).

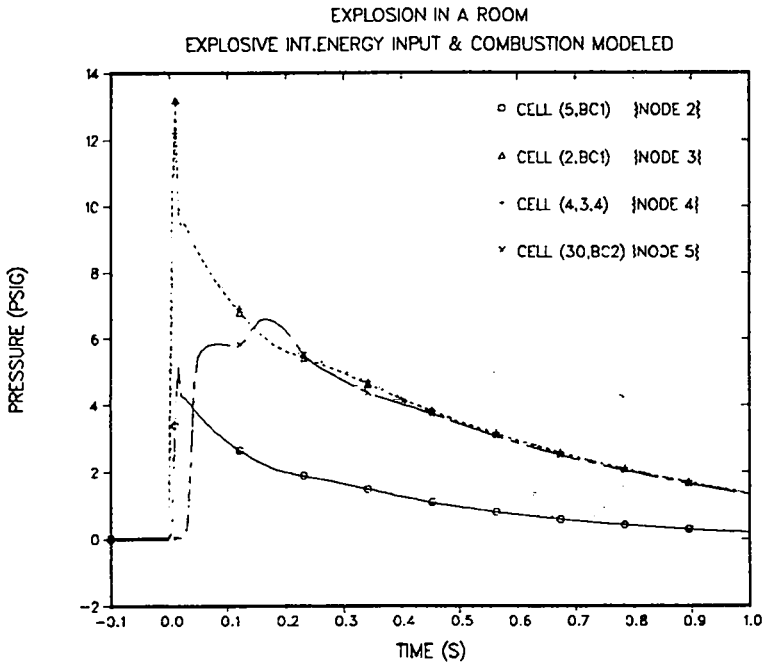

Fig. 4.
Air pressure in the "Explosion in a Room" sample problem (Nodes 2 through 5).

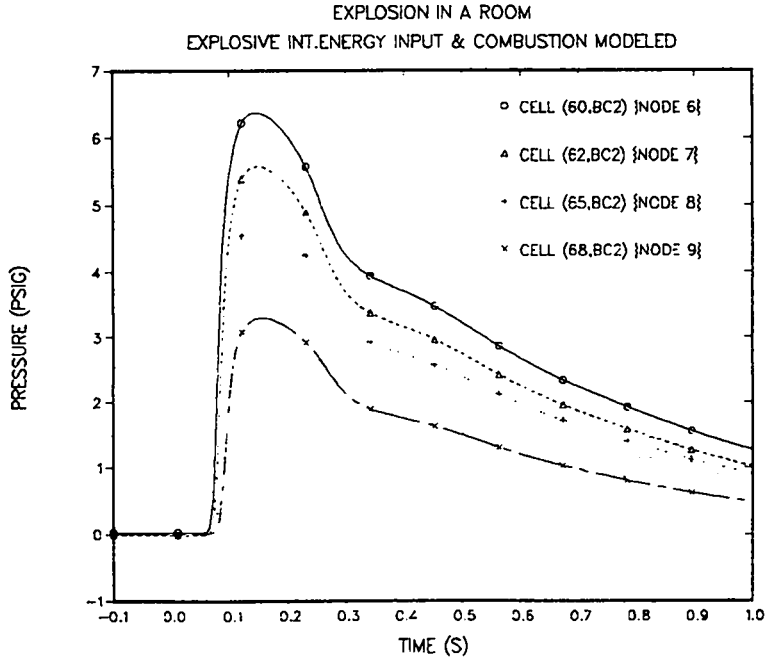

Fig. 5.
Air pressure in the "Explosion in a Room" sample problem (Nodes 6 through 9).

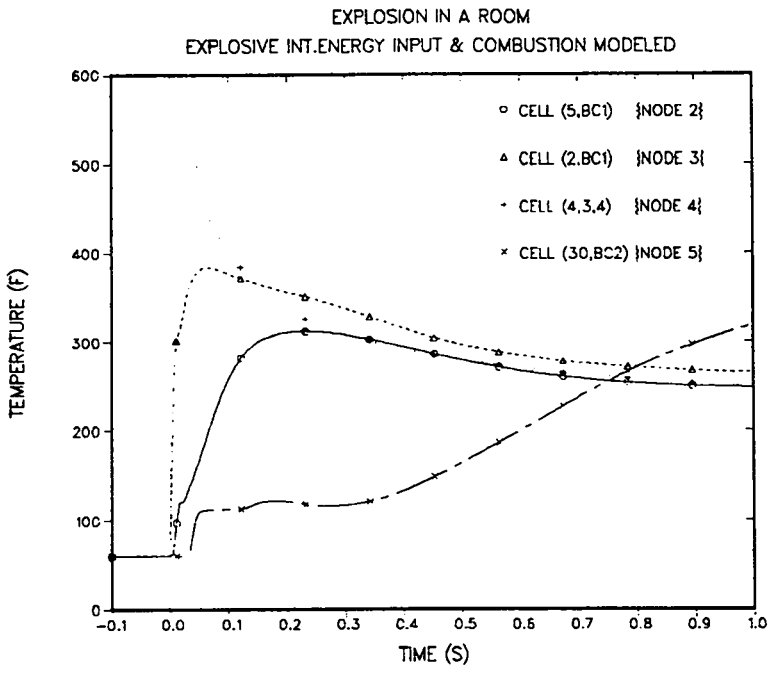

Fig. 6.
Air temperature in the "Explosion in a Room" sample problem (Nodes 2 through 5).

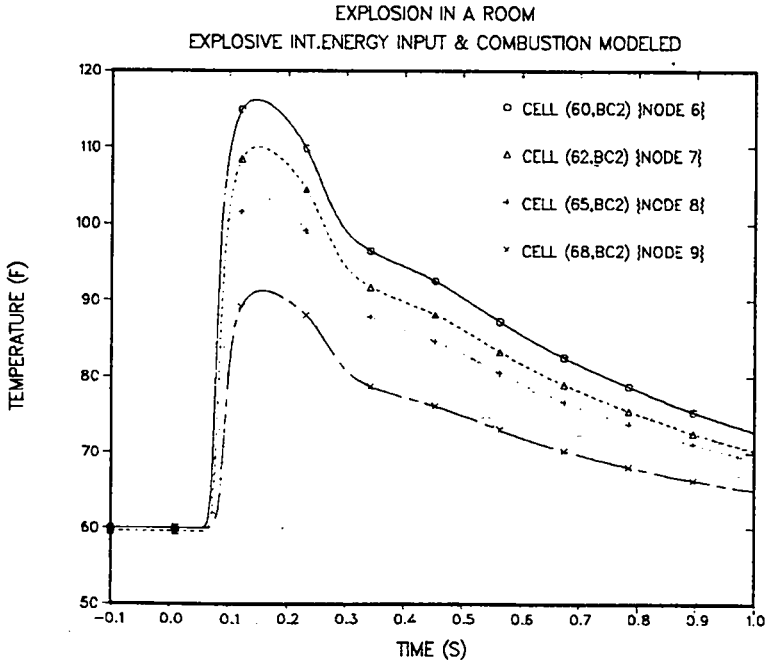

Fig. 7.
Air temperature in the "Explosion in a Room" sample problem (Nodes 6 through 9).

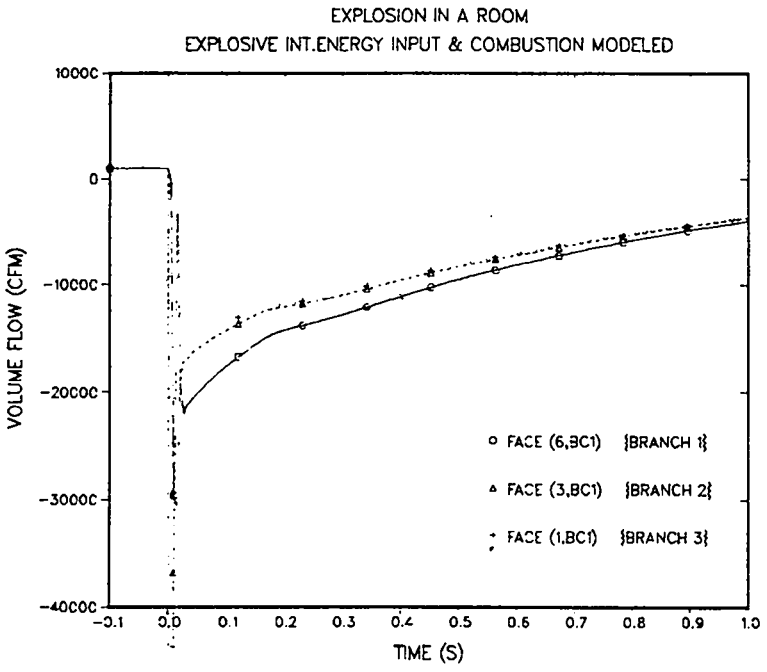

Fig. 8.
Air volume flow in the "Explosion in a Room" sample problem (Nodes 1 through 3).

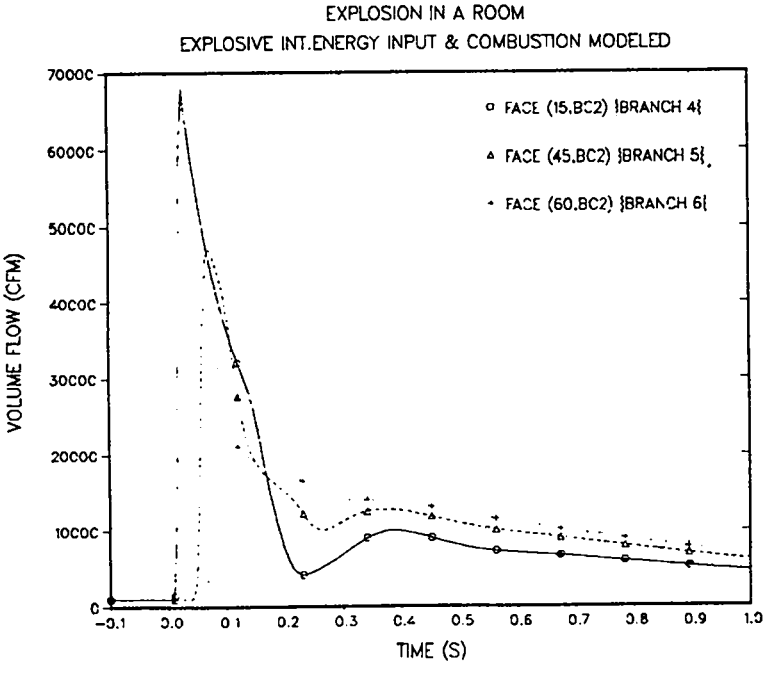

Fig. 9.
Air volume flow in the "Explosion in a Room" sample problem (Nodes 4 through 6).

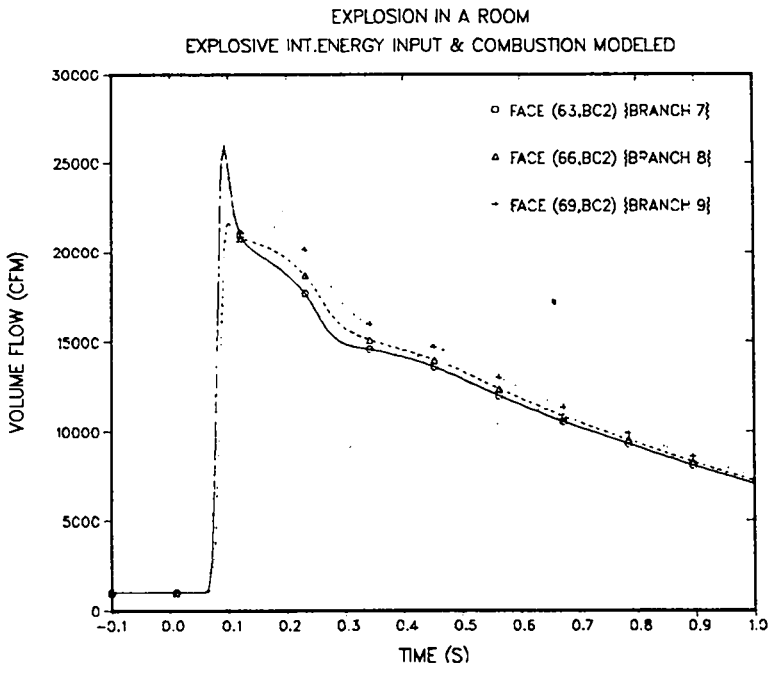

Fig. 10.
Air volume flow in the "Explosion in a Room" sample problem (Nodes 7 through 9).

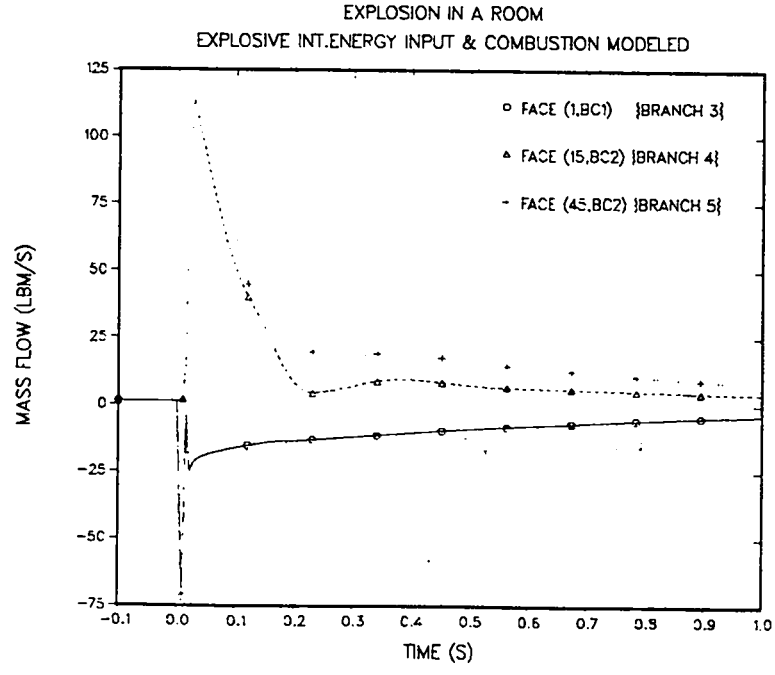

Fig. 11.
Air mass flow in the "Explosion in a Room" sample problem (Nodes 3 through 5).

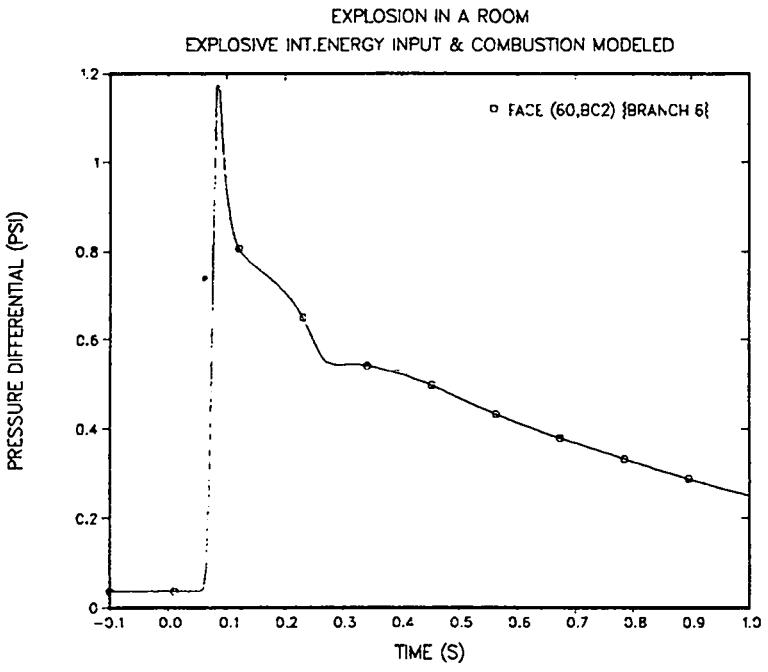

Fig. 12.
Pressure differential across the filter in the "Explosion in a Room" sample problem.

The NF85 results are not averaged over all mesh cells associated with each EVENT84 node. The numerical sign of the NF85-evaluated volume and mass flows in the air-inlet duct has been reversed in Figs. 8 and 11 to correspond to the directional notation of the EVENT84 model in order to compare them. The NF85 results are similar but yet in some ways different from the EVENT84 results; a direct comparison will be made in Sec. V.C.

B. Problem Variations

The room where the explosion occurs in the sample problem is idealized to the modeling limitations of EVENT84. There is no internal structure (the room is empty), and the explosion is located at the center of the room in direct line with the ventilation ducts. On the other hand, NF85 is able to model internal-structure surfaces as well as external-boundary surfaces where pressure (shock and rarefaction/expansion) wave reflection and interaction in a multidimensional environment can be simulated accurately. The explosion can be located anywhere within NF85's multidimensional region. Modeling these effects (which generally are present in actual-problem situations) will produce a different solution.

How much of a difference these effects make will be addressed by a sensitivity study of three problem variations.

1. Inputting the internal plus combustion energy (**TOT**al) of the explosion vs inputting the internal energy of the explosion and having NF85 internally evaluate the combustion energy (**I**nternal + **C**ombustion).

2. Locating the explosion at the center of the room (**CEN**ter) vs at the corner of the room adjacent to the inlet-vent wall (**COR**ner).

3. Not having an internal wall in the room (**NO W**all) vs including an internal wall with an open doorway between the vent openings and the explosion at the corner of the room (**WALl**).

The last variation has its location outlined by dashes in the room in Fig. 2. The first variation uses the EVENT84 approximation that the explosive's internal energy of 124.6 Btu/lbm (line 121, Fig. 3) is equivalent to that of air. The variation occurs by inputting a 6236-Btu/lbm combustion energy for 1 lbm of TNT explosive vs having NF85 evaluate the combustion energy internally to be 6566 Btu/lbm. The input combustion energy is from the time-dependent combustion-energy table in the EVENT84 input file. However, in the EVENT84 calculation, the internal explosion-chamber model is used to evaluate the combustion energy. Unfortunately, the combustion energy evaluated by EVENT84 is not known because is not output.

In addition to the "base-case" problem, **I**nternal + **C**ombustion/**CEN**ter/**NO W**all (I+C/CEN/NOW) discussed in the previous section, three other NF85 calculations were performed with one variation being made each time: TOT/CEN/NOW, I+C/COR/NOW, and I+C/COR/WAL. The last problem is a single variation from the I+C/COR/NOW problem rather than the "base-case" problem because having the explosion in the corner of the room makes adding the internal wall an obstruction to the explosion affecting the ventilation system.

Some of the air pressure, temperature, volume flow, mass flow, and pressure differential results from these four NF85 calculations are shown in Fig. 13 through Fig. 28. Representative results from the air-inlet duct, room, and air-outlet duct are presented at mesh cells and their interfaces corresponding to

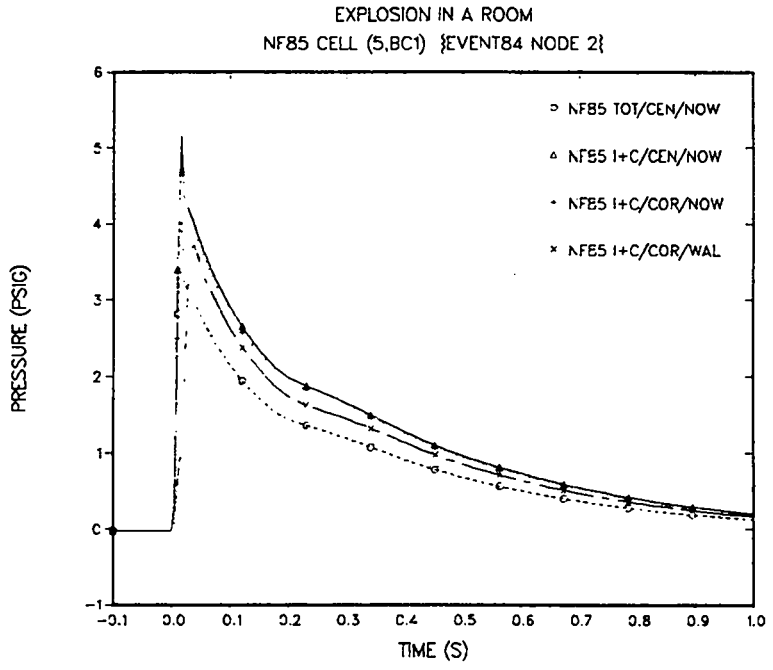

Fig. 13.
Air pressure from variations of the "Explosion in a Room" sample problem (Node 2).

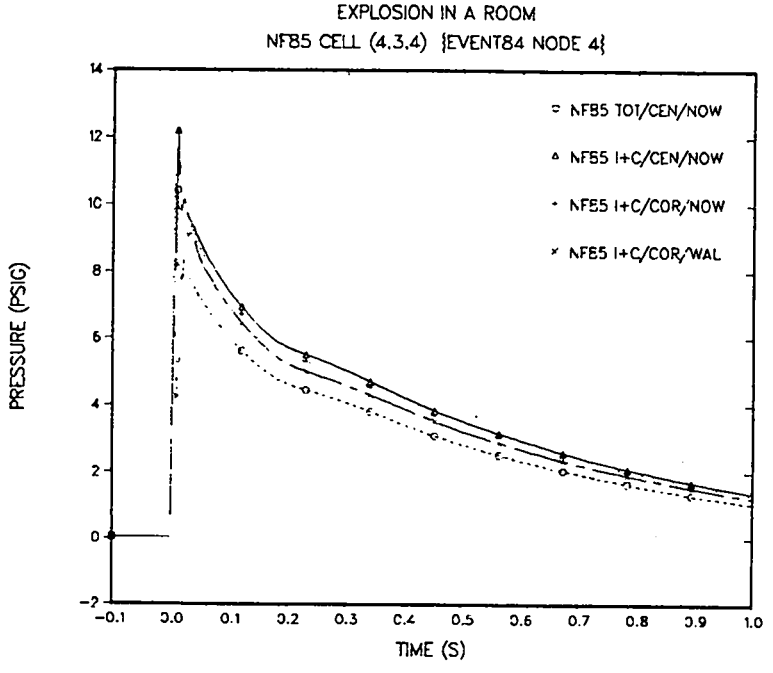

Fig. 14.
Air pressure from variations of the "Explosion in a Room" sample problem (Node 4).

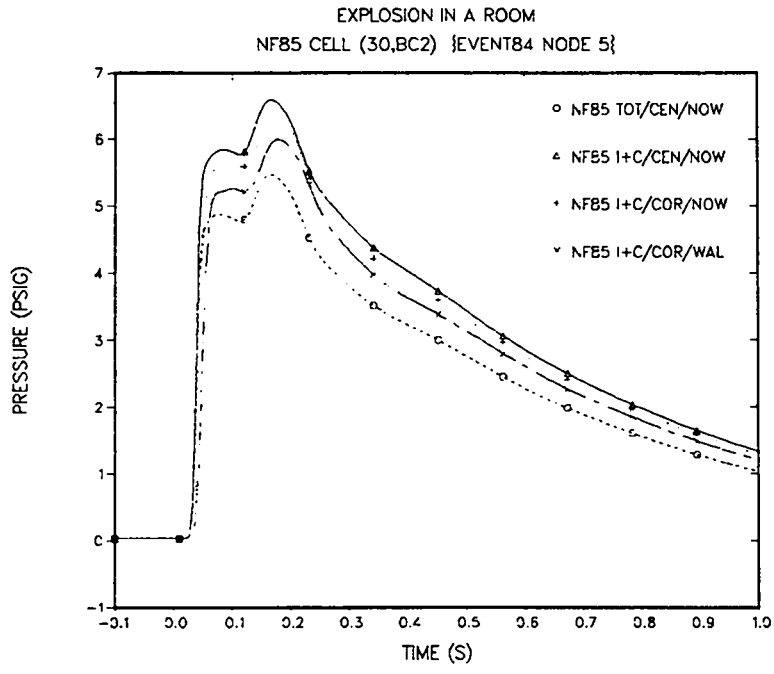

Fig. 15.
Air pressure from variations of the "Explosion in a Room" sample problem (Node 5).

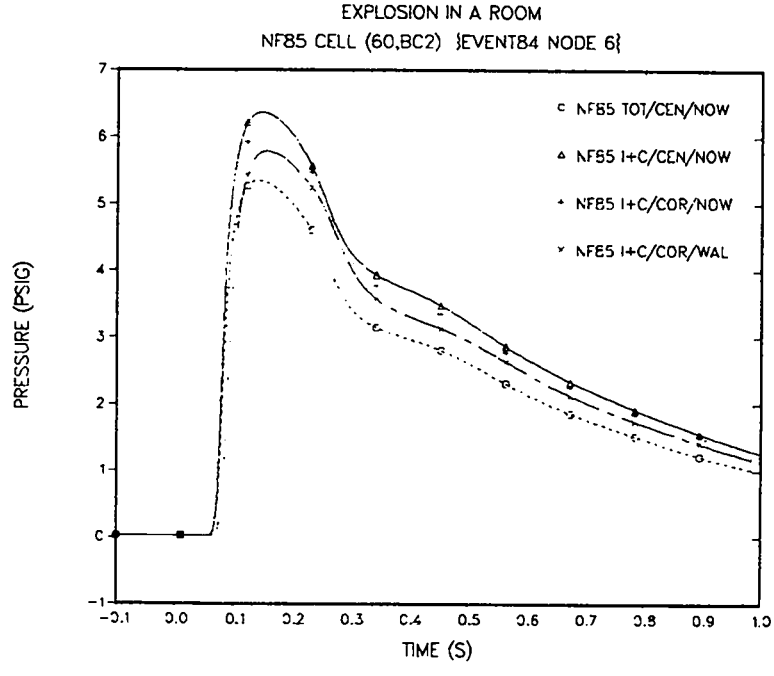

Fig. 16.
Air pressure from variations of the "Explosion in a Room" sample problem (Node 6).

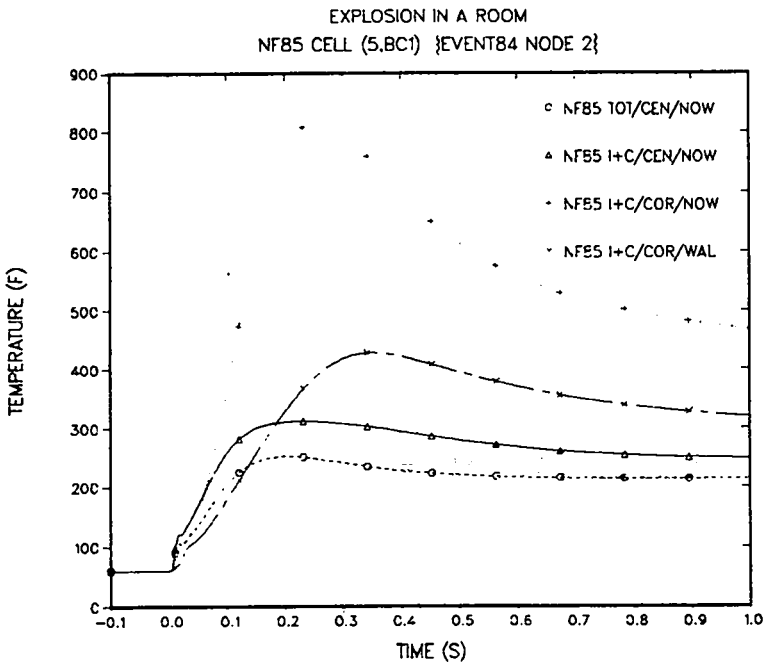

Fig. 17.
Air temperature from variations of the "Explosion in a Room" sample problem (Node 2).

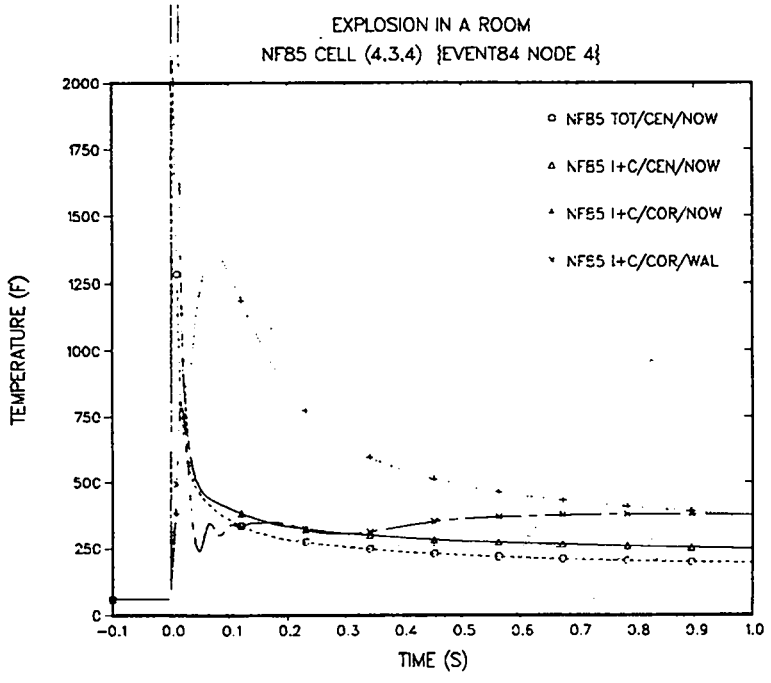

Fig. 18.
Air temperature from variations of the "Explosion in a Room" sample problem (Node 5).

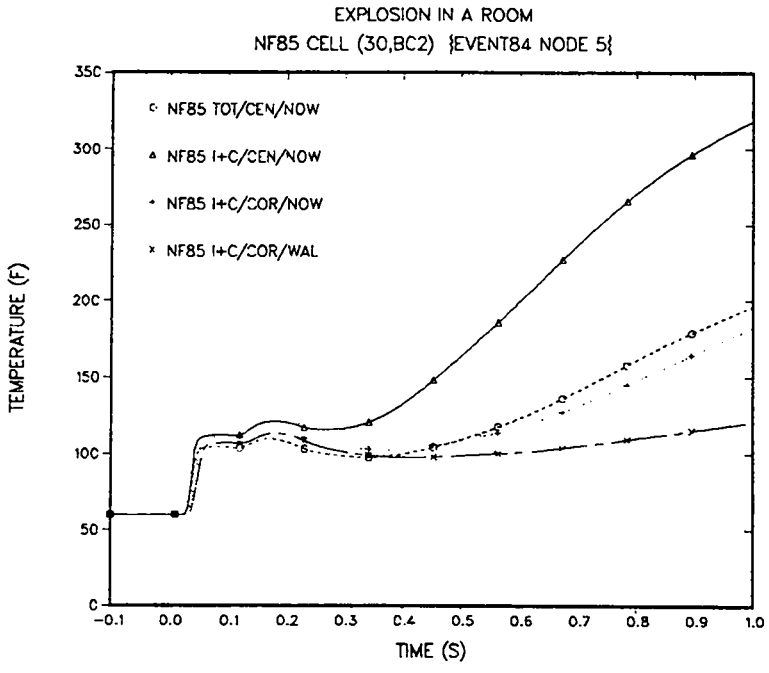

Fig. 19.
Air temperature from variations of the "Explosion in a Room" sample problem (Node 5).

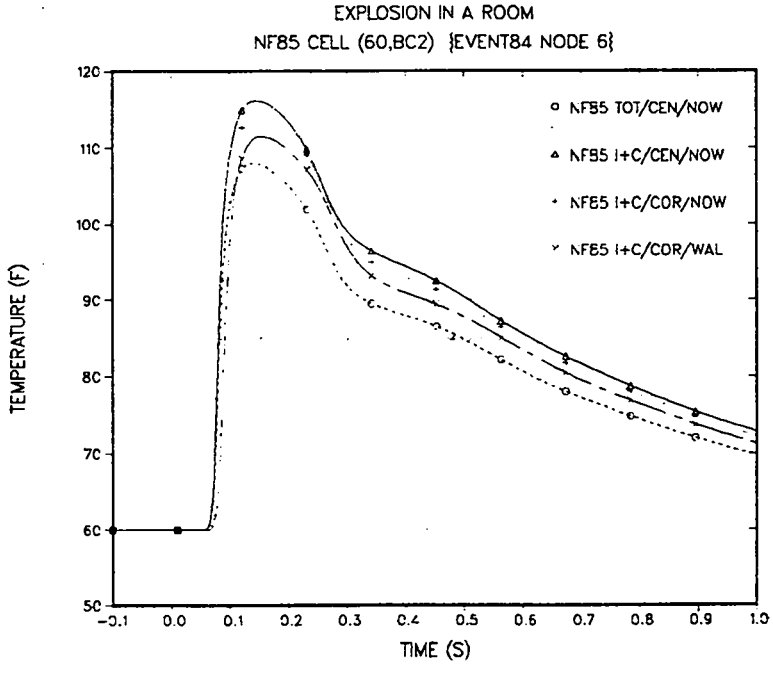

Fig. 20.
Air temperature from variations of the "Explosion in a Room" sample problem (Node 6).

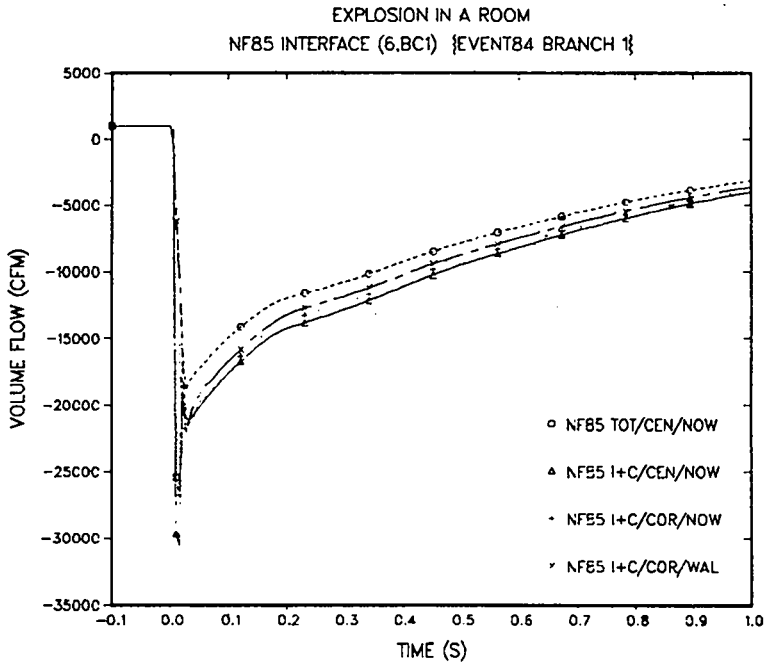

Fig. 21.
Air volume flow from variations of the "Explosion in a Room" sample problem (Branch 1).

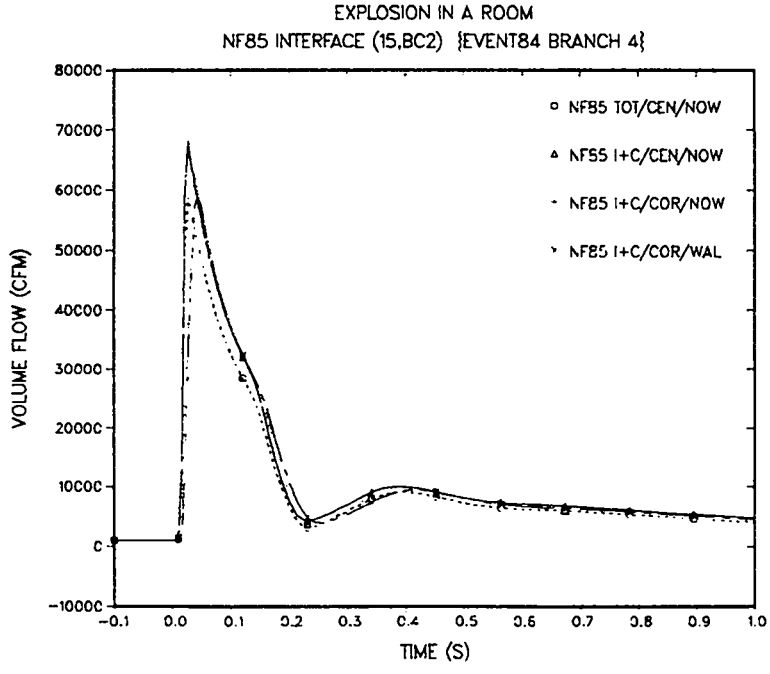

Fig. 22.
Air volume flow from variations of the "Explosion in a Room" sample problem (Branch 4).

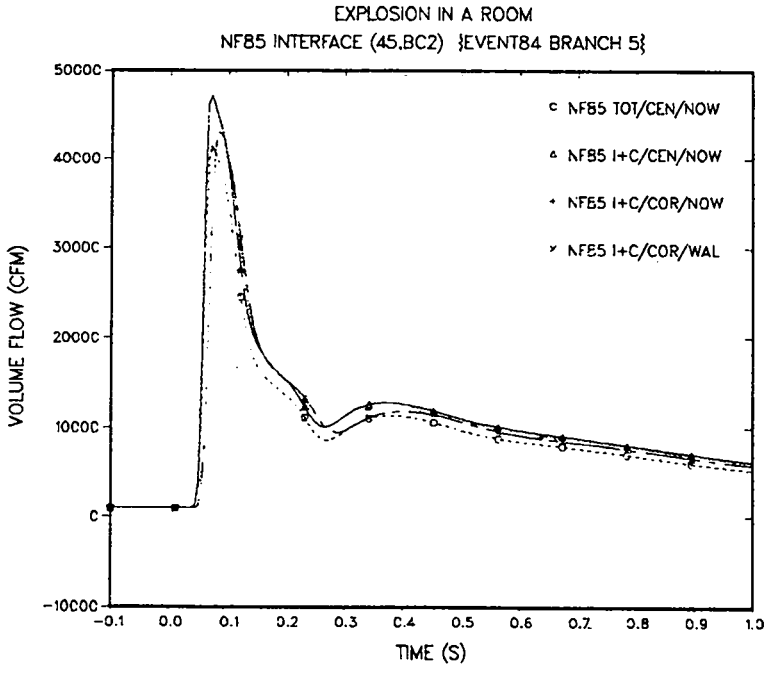

Fig. 23.
Air volume flow from variations of the "Explosion in a Room" sample problem (Branch 5).

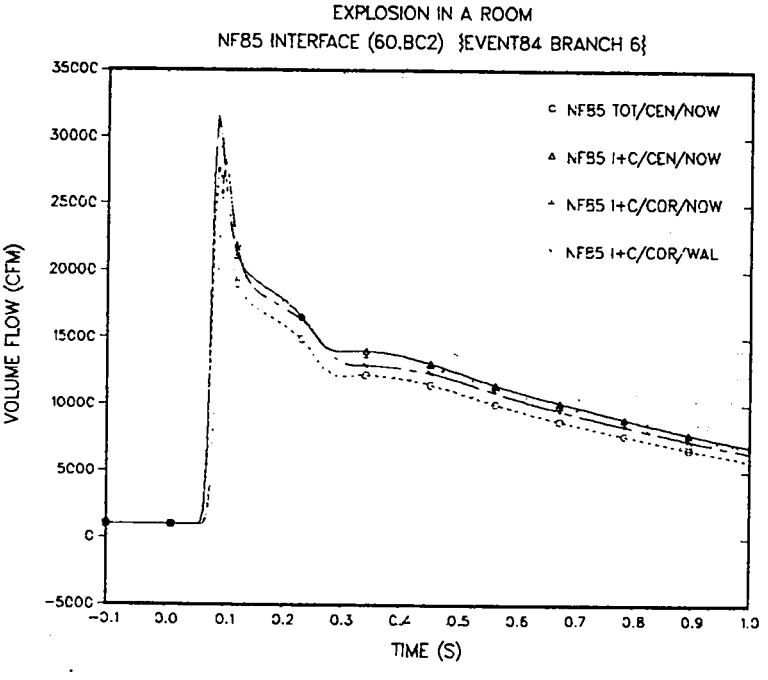

Fig. 24.
Air volume flow from variations of the "Explosion in a Room" sample problem (Branch 6).

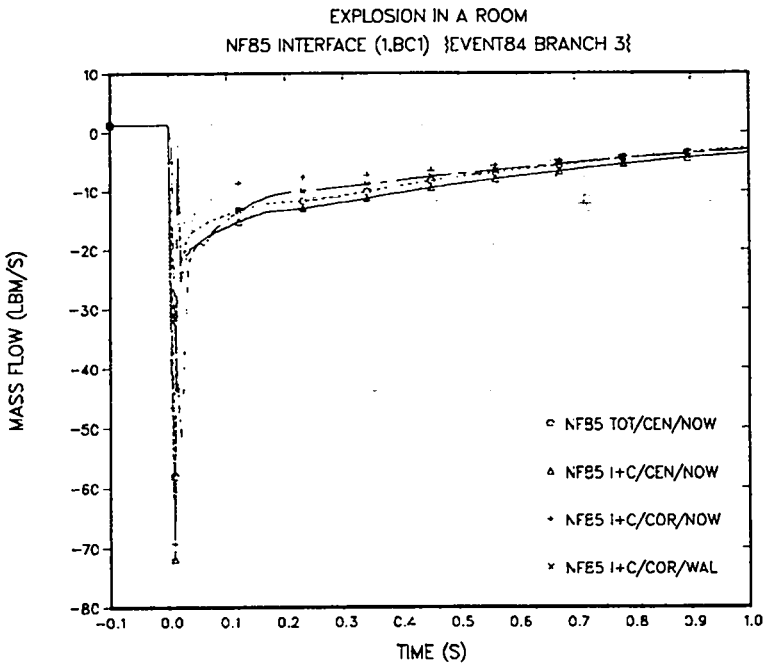

Fig. 25.
Air mass flow from variations of the "Explosion in a Room" sample problem (Branch 3).

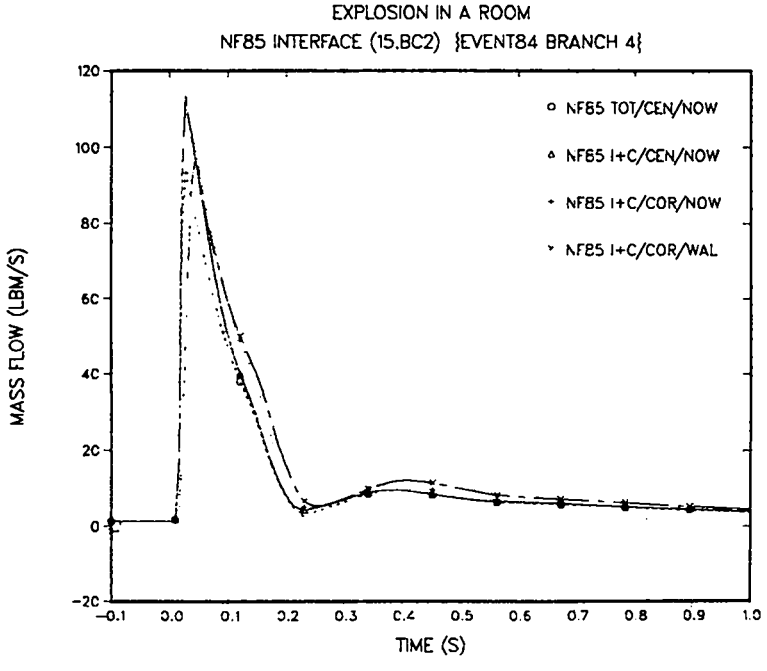

Fig. 26.
Air mass flow from variations of the "Explosion in a Room" sample problem (Branch 4).

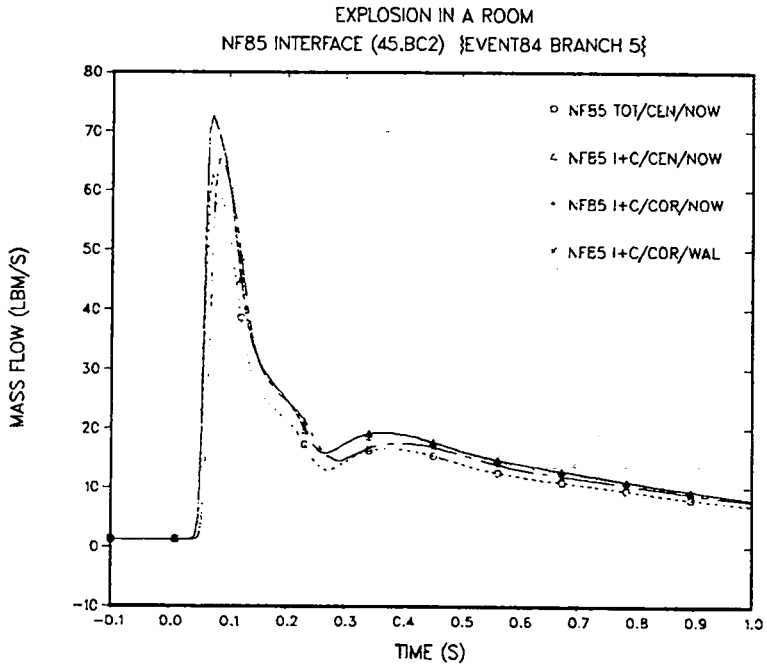

Fig. 27.
Air mass flow from variations of the "Explosion in a Room" sample problem (Branch 5).

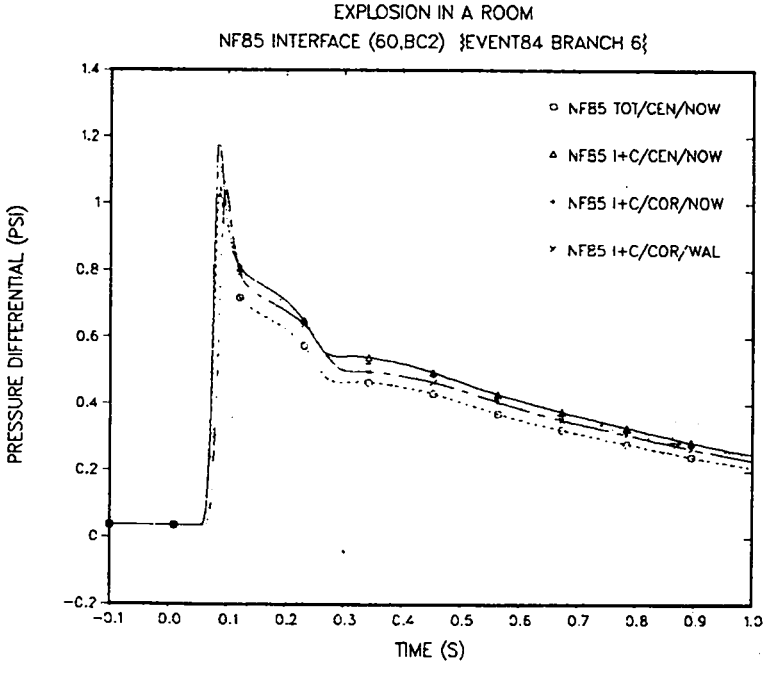

Fig. 28.
Air mass flow from variations of the "Explosion in a Room" problem (Branch 6).

EVENT84 nodes 2, 4, 5, and 6. From these results, we observe only a small effect on air pressure, volume flow, mass flow, and differential pressure across the filter from these variations. Varying the combustion energy from 6566 Btu to 6236 Btu (a 5% decrease) had the biggest effect--reducing these parameter values by 10% to 30%. On the other hand, a surprisingly large effect on air temperature is observed from these variations. Moving the explosion to the corner of the room significantly increases the air temperature in Figs. 17 and 18 as a result of multiple pressure (shock and rarefaction) wave reflections and interactions in the room. This tends to bottle up the effect of the explosion and delay its effect on the duct vents as shown in Figs. 19 and 20. Modeling an internal wall in the room shortens the time frame of pressure wave interactions because of the shorter distances of wave travel within the room. At the same time, it further bottles up the effect of the explosion, delaying its effect on the remainder of the room in Fig. 18 and the vents in Figs. 17 and 19. The air temperature shown in Fig. 20 is not affected by these events. The explosion effects on the air temperature behind the material front, which has not yet reached the end of the long duct after 1.0 s.

C. Interfacing and Comparing NF85 and EVENT84 Results

EVENT84 is an efficient computer code for analyzing gas-dynamic transients in airflow networks. It has an explosion model but lacks the multidimensional analysis capability needed to model accurately the effects of an explosion in the near field. NF85 was developed to provide the multidimensional modeling capability that EVENT84 lacks for the room in which the explosion occurs. At the near-field/far-field interface, NF85 is programmed to define a time-dependent boundary condition from its solution; EVENT84 then uses it to analyze the remaining far-field region. NF85 provides a stand-alone analysis capability (as shown in the sample-problem applications thus far), and it also interfaces with EVENT84 to model accurately the effect of an internal explosion on a complicated airflow network system.

In this section, the interfacing between NF85 and EVENT84 for the sample problem will be demonstrated. The importance of NF85 modeling a portion of the far field with its one-dimensional boundary-condition regions to account for the far-field feedback effect on the near-field solution also will be discussed. The results from four calculations will be compared: the "base case" NF85 1+C/CEN/NOW solution; the EVENT84 sample-problem solution using its explosion-

chamber combustion model; and two EVENT84 solutions for the two vent ducts using the NF85-solution boundary conditions at the room/vent interfaces. The first set of NF85 interface boundary conditions is defined from the "base case" NF85 I+C/CEN/NOW solution. This represents the use of an NF85 solution where no approximation of the feedback effect from the far field have been made. The second set of NF85 boundary conditions is defined from an NF85 calculation of only the three-dimensional room. Here the feedback effect from the far field is approximated by assigning the steady-state flow resistance of each ventilation-duct system (through an appropriate CFZV value as described in Sec. V.A) to its room/vent interfaces on the three-dimensional region's external boundary. The EVENT84 boundary condition defined by NF85 was a time-dependent table of air pressure and temperature values averaged over the three-dimensional region's mesh cells adjacent to each vent interface. The table spans the time interval of 0.0 to 1.0 s in time increments of 0.01 s.

Figures 29 to 44 show some of the air pressure, temperature, volume flow, mass flow, and pressure differential results from those four calculations. The same locations that were considered for the problem-variation results in the previous section are being looked at here. Figures 29 to 32 show the air-pressure change evaluated by EVENT84 to be 30% to 90% larger than that evaluated by NF85. However, the EVENT84+BC (NF85{3D+2BC}) calculation for the two ventilation ducts (using the same NF85 solution to define the room/vent-interface boundary conditions) determines the air pressure change to be the same as that evaluated by NF85 for problem times beyond 0.5 s. For earlier times, the EVENT84-evaluated air pressures rise and fall slower than the NF85-evaluated air pressures because EVENT84 evaluates the air pressure in larger-volume nodes. It appears that the large air-pressure difference between the EVENT84 and NF85 solutions is a result of how they model the explosion in the room. How much of that difference results from the difference in explosion energy evaluated by their combustion models and how much is a result of modeling multidimensional effects is not known. Reevaluating EVENT84 with the 6566-Btu combustion energy evaluated by NF85 being input to the EVENT84 calculation would show how much of the air pressure difference is caused by multidimensional effects.

Using boundary conditions defined from the NF85{3D+2BC} and NF85{3D ONLY} solutions, the EVENT84 calculations show significantly different air pressures in Figs. 29 and 32. Modeling the ventilation ducts by their steady-state flow resistance applied at the room/vent interface in the NF85 {3D ONLY} calculation

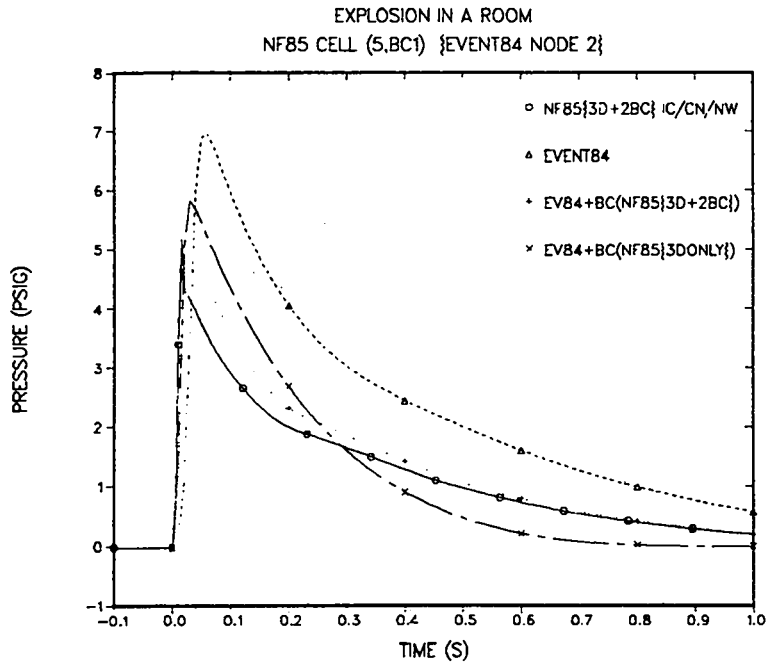

Fig. 29.
Air pressure in the "Explosion in a Room" sample problem evaluated by NF85, EVENT84, and EVENT84+BC(NF85) (Node 4).

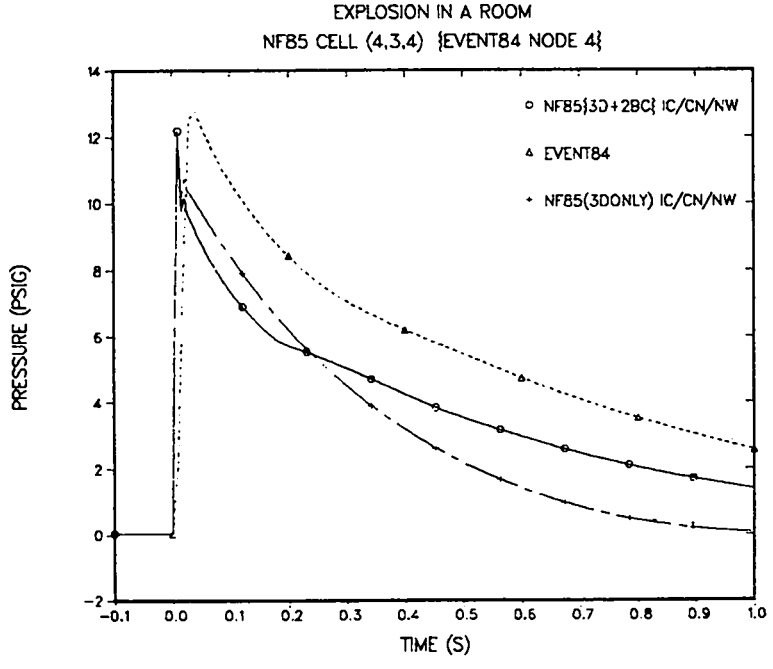

Fig. 30.
Air pressure in the "Explosion in a Room" sample problem evaluated by NF85, EVENT84, and EVENT84+BC(NF85) (Node 4).

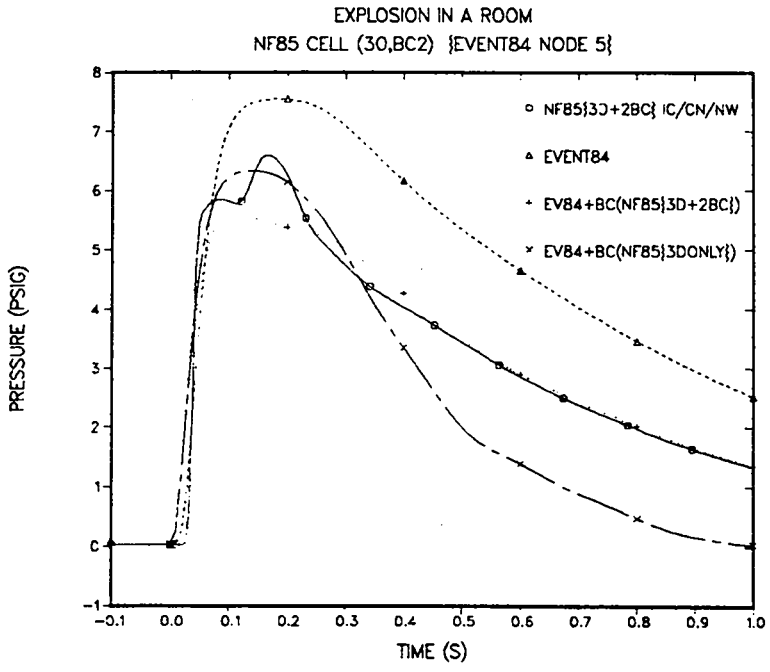

Fig. 31.
Air pressure in the "Explosion in a Room" sample problem evaluated by NF85, EVENT84, and EVENT84+BC(NF85) (Node 6).

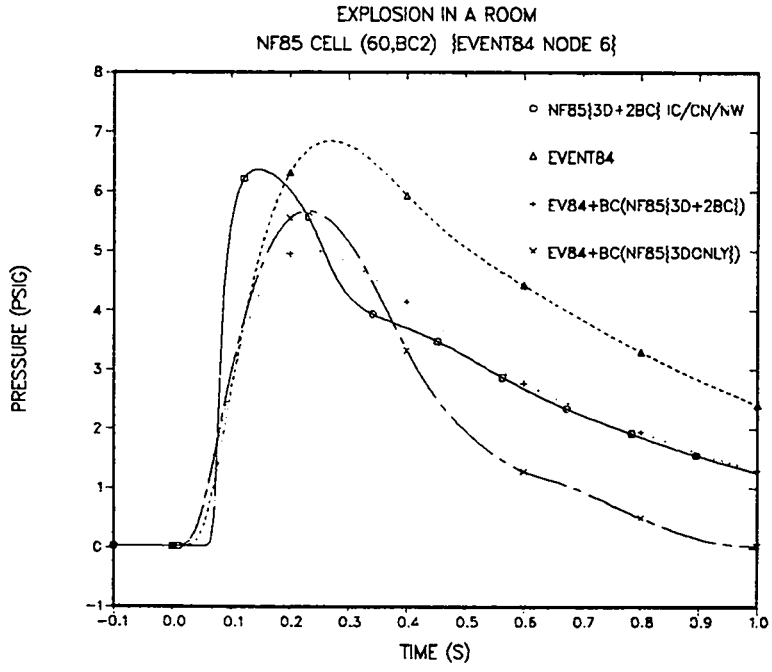

Fig. 32.
Air pressure in the "Explosion in a Room" sample problem evaluated by NF85, EVENT84, and EVENT84+BC(NF85) (Node 2).

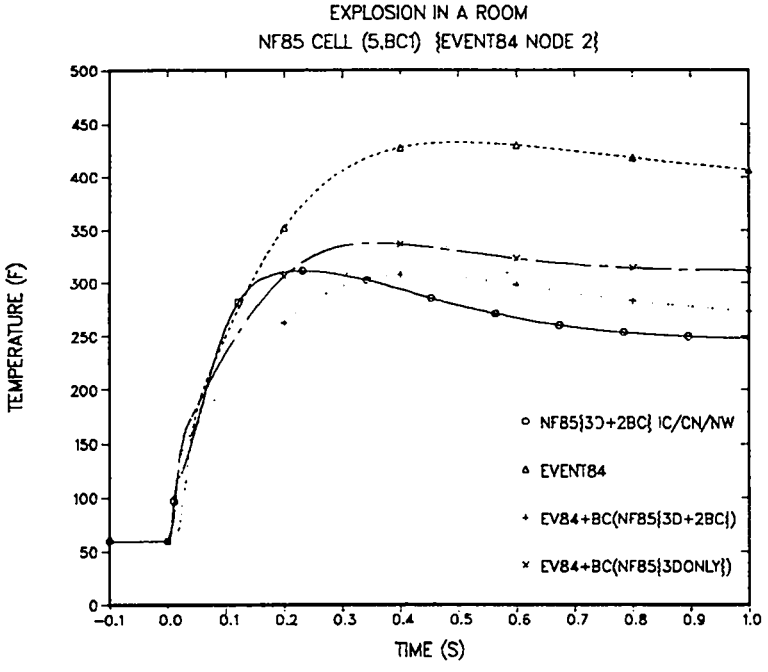

Fig. 33.
Air temperature in the "Explosion in a Room" sample problem evaluated by NF85, EVENT84, and EVENT84+BC(NF85) (Node 2).

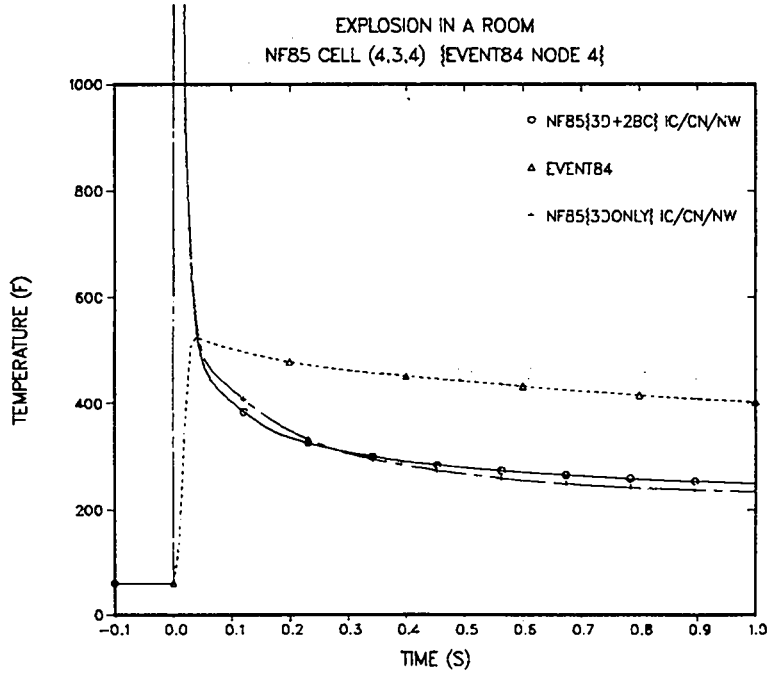

Fig. 34.
Air temperature in the "Explosion in a Room" sample problem evaluated by NF85, EVENT84, and EVENT84+BC(NF85) (Node 4).

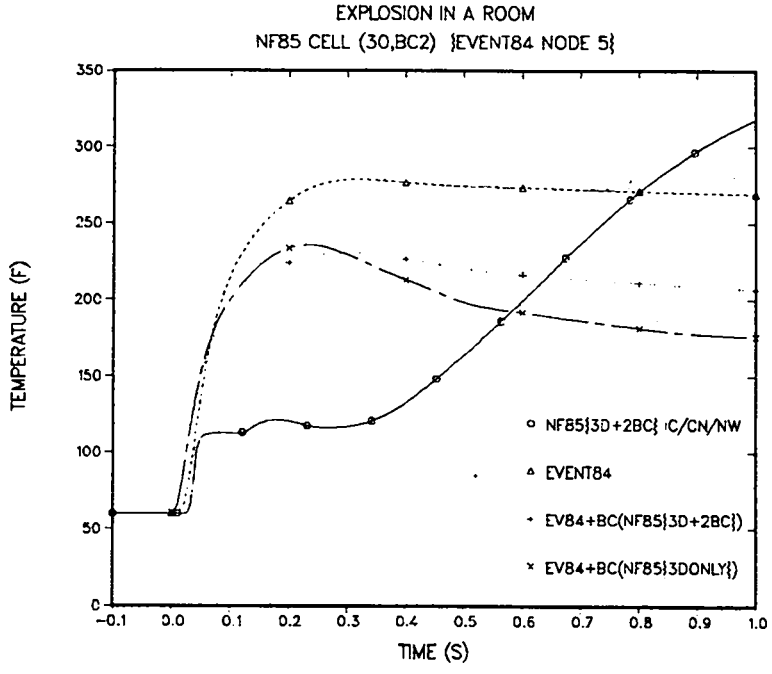

Fig. 35.
Air temperature in the "Explosion in a Room" sample problem evaluated by NF85, EVENT84, and EVENT84+BC(NF85) (Node 5).

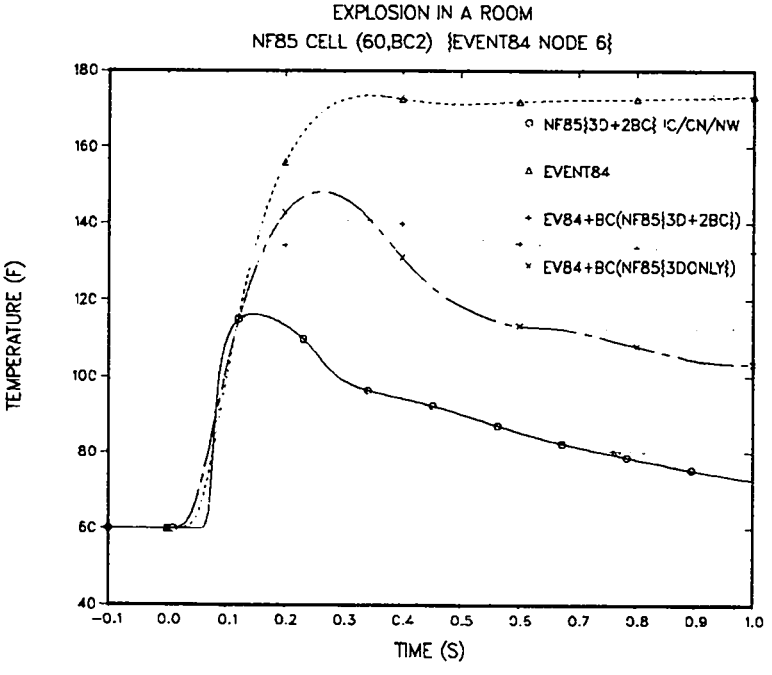

Fig. 36.
Air temperature in the "Explosion in a Room" sample problem evaluated by NF85, EVENT84, and EVENT84+BC(NF85) (Node 6).

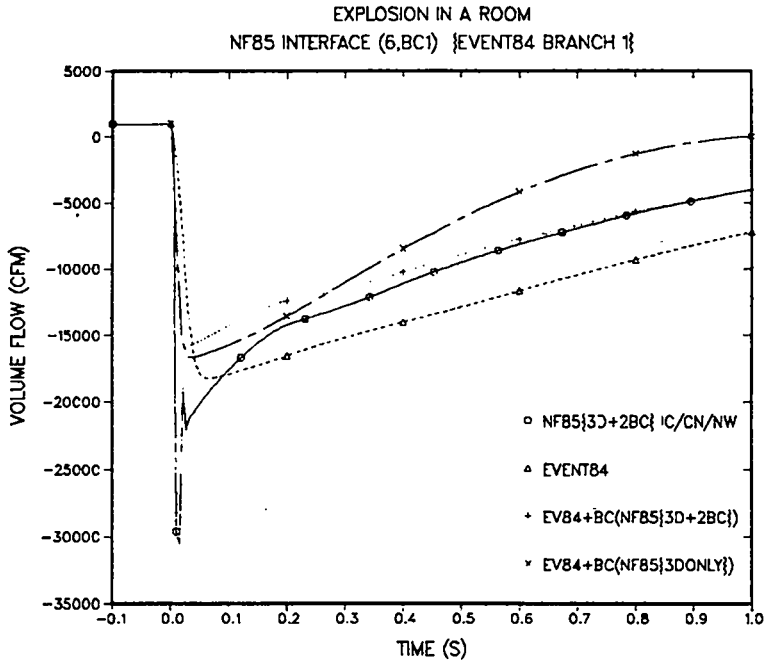

Fig. 37.
Air volume flow in the "Explosion in a Room" sample problem evaluated by NF85, EVENT84, and EVENT84+BC(NF85) (Branch 1).

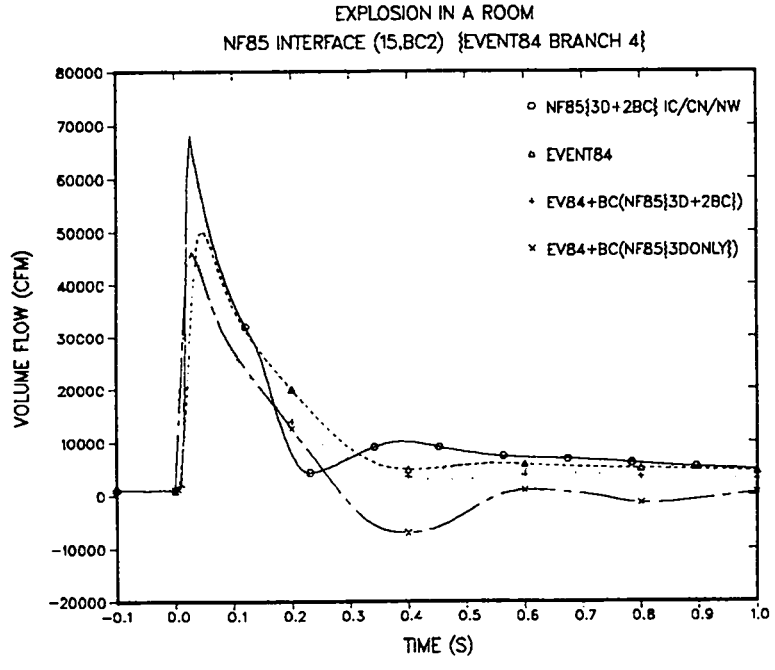

Fig. 38.
Air volume flow in the "Explosion in a Room" sample problem evaluated by NF85, EVENT84, and EVENT84+BC(NF85) (Branch 4).

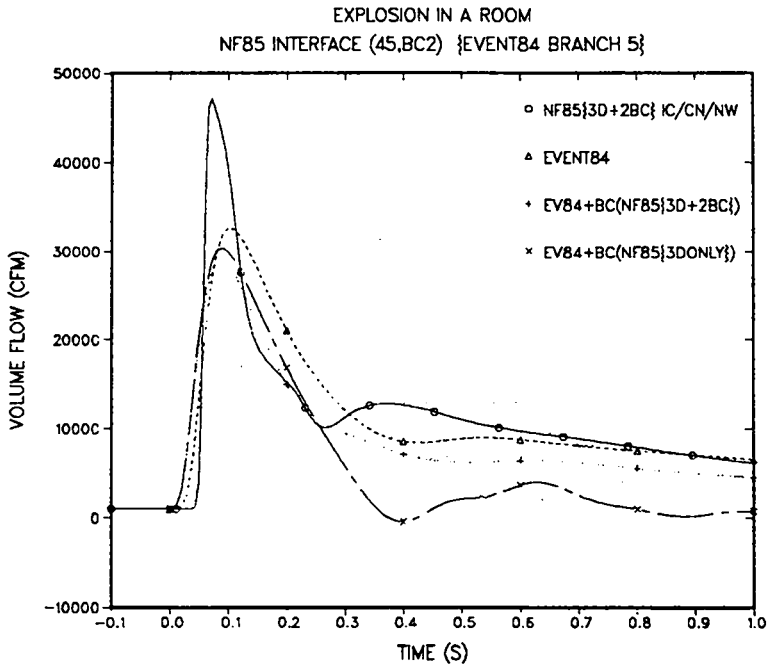

Fig. 39.
Air volume flow in the "Explosion in a Room" sample problem evaluated by NF85, EVENT84, and EVENT84+BC(NF85) (Branch 5).

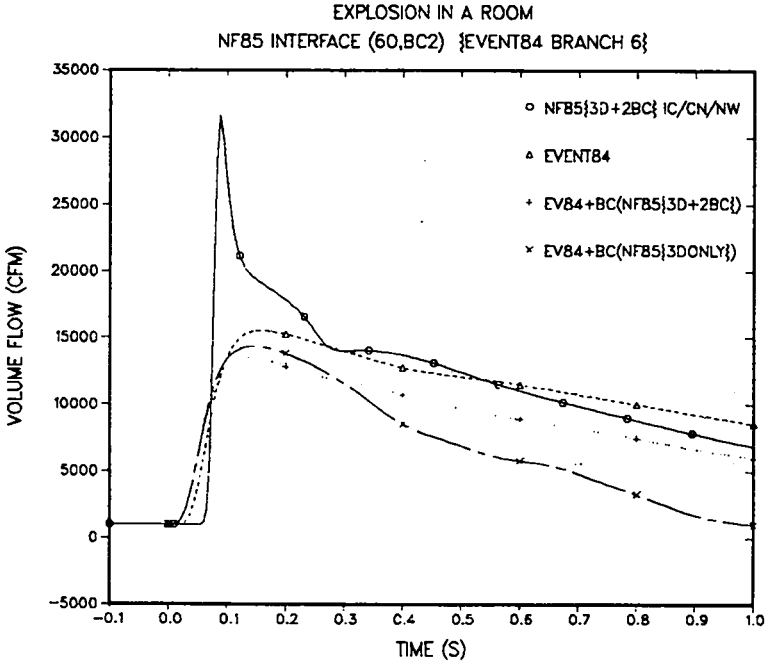

Fig. 40.
Air volume flow in the "Explosion in a Room" sample problem evaluated by NF85, EVENT84, and EVENT84+BC(NF85) (Branch 6).

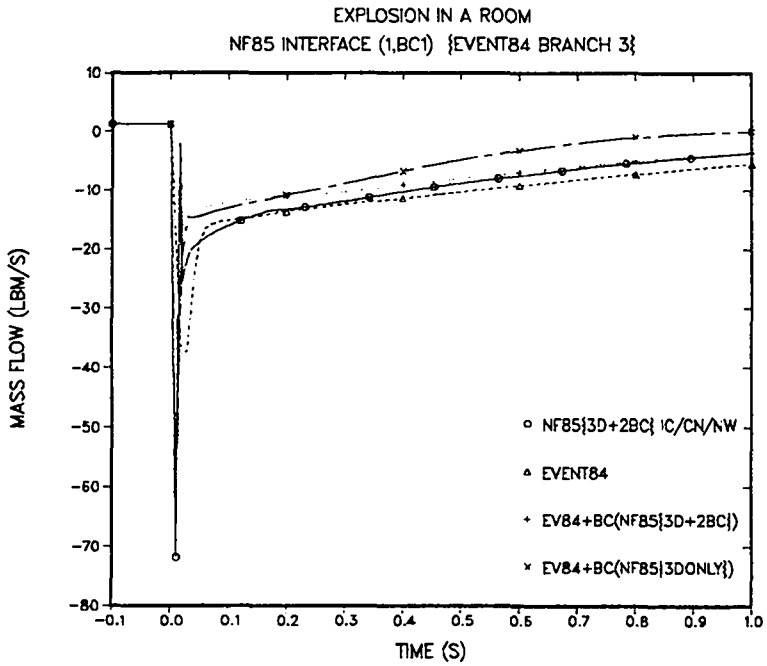

Fig. 41.
Air mass flow in the "Explosion in a Room" sample problem evaluated by NF85, EVENT84, and EVENT84+BC(NF85) (Branch 5).

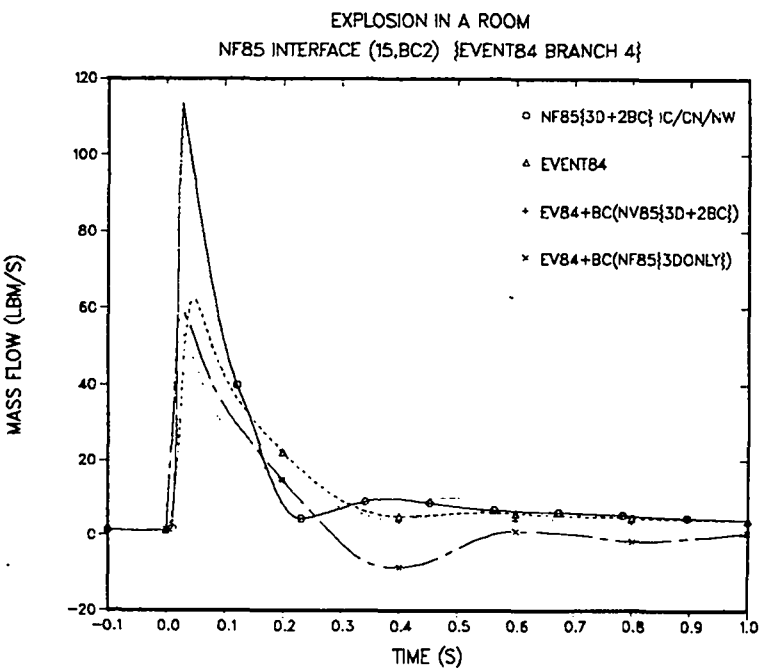

Fig. 42.
Air mas flow in the "Explosion in a Room" sample problem evaluated by NF85, EVENT84, and EVENT84+BC(NF85) (Branch 5).

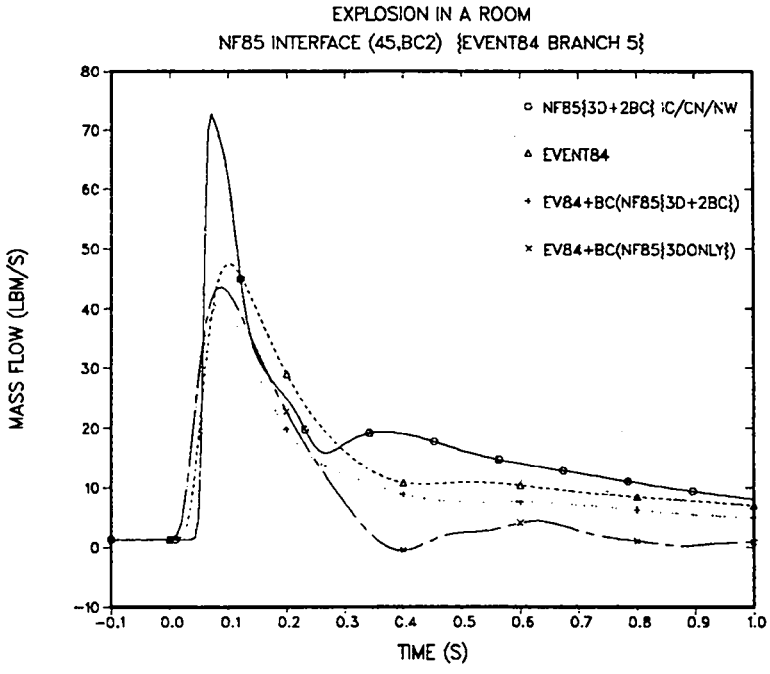

Fig. 43.
Air mass flow in the "Explosion in a Room" sample problem evaluated by NF85, EVENT84, and EVENT84+BC(NF85) (Branch 5).

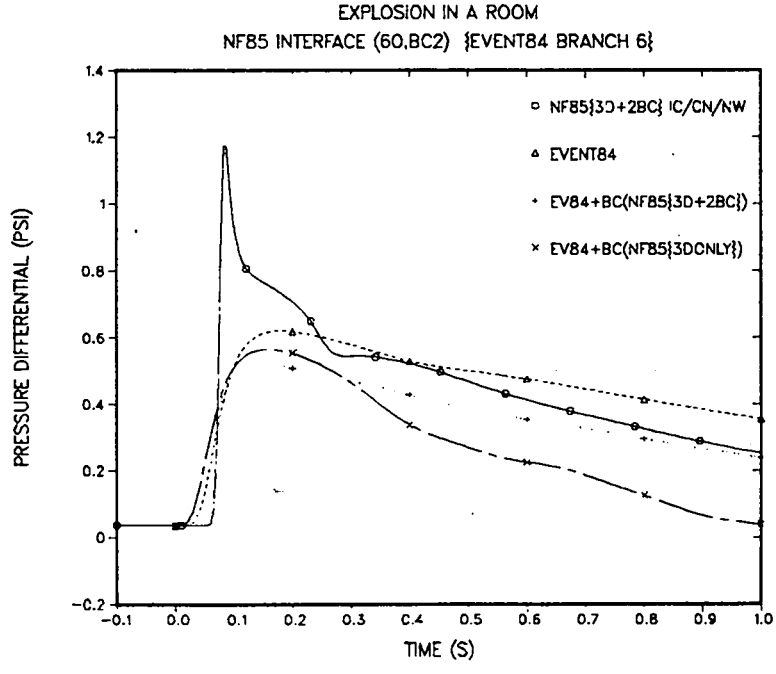

Fig. 44.
Air pressure differential across the filter in the "Explosion in a Room" sample problem evaluated by NF85, EVENT84, and EVENT84-BC(NF85).

is the cause for this difference. Moving the large resistance of the filter to the room/vent interface removes 400 ft^3 of long-duct volume from the effective low flow-resistance volume of the room. With less volume, the air pressure before 0.3 s in the NF85{3D ONLY} calculation is larger in the room (and in the EVENT84 boundary condition). With higher air pressures from the explosion, the blower in each ventilation duct changes from driving the air to being driven by the air, thus introducing airflow resistance. The NF85{3D ONLY} calculation does not model this added resistance, which results in larger air velocities at the room/vent interface and causes the air pressure in the room (and in the EVENT84 boundary condition) to fall faster. Here is a clear example of how important it is to correctly approximate the feedback effect from the far field on the near-field solution if NF85 is to determine an accurate boundary condition for EVENT84.

The air-temperature plots in Figs. 33 to 36 show a significant difference between all calculations. In Figure 35, the higher air temperature behind the material front in the NF85 calculation (because of pressure-wave reflection/interaction heating the air in the room) is observed to occur all the way to the shock front in the EVENT84 calculations. EVENT84 evaluates air temperatures that rise and stay higher than the air temperatures evaluated by NF85. Upon comparing the momentum and energy equations evaluated by EVENT84 and NF85, one finds that EVENT84 does not model momentum convection, and the time rate of change of total energy is assigned to internal energy only. Not modeling momentum convection is based on the EVENT84 assumption of incompressibility for the momentum equation only. Both these effects tend to bottle up the explosion for a longer period of time, causing higher air pressures and temperatures. Assigning the total-energy changes to the internal energy of air results in higher air temperatures. These approximations probably were made to the EVENT84 working equations for simplicity and because a very coarse spatial mesh poorly approximates momentum convection. These approximations also make the air pressures and temperatures evaluated by EVENT84 conservatively high.

ACKNOWLEDGMENT

The NF85 computer program was developed from the SETS3D computer program written by Susan Woodruff. SETS3D is a test program in three-dimensional geometry that implemented the semi-implicit fluid-dynamics solution algorithm and

stability-enhancing two-step method developed by John Mahaffy. The author wishes to thank Susan and John for their assistance and advice during the development of NF85; Jeffrey Moore, who as project manager provided many ideas and suggestions to enhance the utility of NF85; and William Gregory, who documented the shock-transmission experiments analyzed with NF85 in Appendix D.

APPENDIX A

SEMI-IMPLICIT, FLUID-DYNAMICS EQUATIONS

The fluid-dynamics, partial-differential equations governing the behavior of air are presented in Sec. II.B by Eqs. (2) to (4). Time-differencing these equations with a semi-implicit formulation gives the following equations:

$$(\rho^{n+1} - \rho^n)/\Delta t + \underline{\nabla} \bullet \rho^n \underline{V}^{n+1} = m_s^{n+\frac{1}{2}} \quad , \tag{A-1}$$

$$(\underline{V}^{n+1} - \underline{V}^n)/\Delta t + \underline{V}^n \bullet \underline{\nabla}\, \underline{V}^{n+1} + \beta(\underline{V}^{n+1} - \underline{V}^n) \bullet \underline{\nabla}\, \underline{V}^n = - \underline{\nabla} P^{n+1}/\rho^n - K^n |\underline{V}^n| (2\underline{V}^{n+1} - \underline{V}^n) + \underline{g} \quad , \text{ and} \tag{A-2}$$

$$(\rho^{n+1} e^{n+1} - \rho^n e^n)/\Delta t + \underline{\nabla} \bullet \rho^n e^n \underline{V}^{n+1} = -P^{n+1}\, \underline{\nabla} \bullet \underline{V}^{n+1} + m_s^{n+\frac{1}{2}}\, e_s^{n+\frac{1}{2}} \tag{A-3}$$

for air mass, motion, and energy, where

Δt is the time-step size interval from time t^n to t^{n+1} ($\Delta t = t^{n+1} - t^n$),
β is 0 when $\Delta\, \underline{V}^n \bullet r_\ell \leq 0$ and 1 when $\nabla\, \underline{V}^n \bullet r_\ell > 0$, and
r_ℓ is a unit vector for coordinate direction ℓ.

All the other parameters are defined in Sec. II.B. Parameters with superscript n are defined at time t^n and have known values; parameters with superscript n+1 are defined at time t^{n+1} and have unknown values that are to be solved for. The explosion-source parameters m_s and e_s have superscript n+½, which defines their known average value over the time step.

If all the terms in the above equations except the time-derivative terms have only superscript n, the time-differencing formulation would be explicit. This requires that the time-step size be less than the sonic Courant limit (the minimum time for a pressure wave to cross a mesh cell) to obtain a numerically stable solution. If, on the other hand, all the terms in the above equations except the time-derivative terms have only superscript n+1, the time differencing formulation would be implicit. Any time-step size would yield a numerically stable solution, but the extensive nonlinear form of the unknown parameters makes the numerical solution computationally demanding. The semi-implicit formulation, which defines only the pressure and some of the velocities at time t^{n+1}, provides a compromise. There is enough feedback of the time t^{n+1} solution information to stabilize the solution for time steps greater than the sonic Courant limit but less than the material Courant limit (the minimum time for air to cross a mesh cell) while making a reasonably efficient numerical solution possible. The air pressure and velocity, which are defined at time t^{n+1}, are the most sensitive parameters to the solution's spatial coupling effects. Allowing them to vary in a consistent manner rather than constraining them to their known time t^n values when satisfying the gas-dynamic equations gives the needed degrees of freedom in the solution to dampen numerical-solution error. In Eq. (A-2), the semi-implicit approximation of the $\underline{V}\cdot\underline{\nabla}\,\underline{V}$ terms by $\underline{V}^n\cdot\underline{\nabla}\,\underline{V}^{n+1} + \beta(\underline{V}^{n+1}-\underline{V}^n)\cdot\nabla\underline{V}^n$ and $K|\underline{V}|\underline{V}$ term by $K^n|\underline{V}^n|(2\underline{V}^{n+1} - \underline{V}^n)$ may seem unusual. This form is a linearized approximation of their implicit forms $\underline{V}^{n+1}\cdot\underline{\nabla}\,\underline{V}^{n+1}$ and $K^n|\underline{V}^{n+1}|\underline{V}^{n+1}$. Defining $\beta = 0$ and 1 provides two such approximations for $\underline{V}\cdot\underline{\nabla}\,\underline{V}$ that a numerical study[3,4] has shown are stable and accurate under fluid compression and expansion, respectively.

Spatial differencing [Eqs. (A-1) through (A-3)] is a more complicated procedure, especially when done for a three-dimensional, cartesian or cylindrical geometry region of solution. The dot product of the air-motion equation [Eq. A-2] is taken with respect to the unit vector for each of the three coordinate directions. This results in three motion equations defining the air-velocity component for each coordinate direction. In three-dimensional geometry, five partial-differential equations are defined. Adding the equation of

state defined in Sec. II.C gives six equations that are to be solved for the six unknowns: P^{n+1}, ρ^{n+1}, e^{n+1}, and the three air-velocity components $\underline{V}^{n+1}\cdot r_{\ell}$ for $\ell = \ell_i, \ell_j, \ell_k$.

Just as time was divided into time-step intervals to time-difference these equations for numerical solution, the spatial region of solution is partitioned with an imaginary grid overlay into mesh-cell volumes. The air parameters are defined in a staggered fashion within this spatial mesh. The thermodynamic properties P, ρ, and e are defined at the mesh-cell centers by their average value over the mesh-cell volume; the velocity components $\underline{V}\cdot r_{\ell}$ are defined on the mesh-cell side (interface) that is normal to their component direction by their average value over the mesh-cell side area. For the $\ell_i{}^{th}$ direction, the velocity component defined on the mesh-cell side interface between mesh cell i and i+1 is $V_{i+\frac{1}{2}} = \underline{V}\cdot r_{\ell i}$. For the purpose of reference and storage, $V_{i+\frac{1}{2}}$ will be associated with mesh cell i; the $V_{i-\frac{1}{2}}$ velocity component on the other side of mesh cell i will be associated with mesh cell i-1. In three dimensions, ℓ has three directions: $r_{\ell i}$, $r_{\ell j}$, and $r_{\ell k}$. Associated with a mesh cell with its center at coordinate location (i,j,k) are the three velocity components $V_{i+\frac{1}{2}jk}$, $V_{ij+\frac{1}{2}k}$, and $V_{ijk+\frac{1}{2}}$. The velocity components are defined on the mesh-cell side interfaces because they convect air mass (ρ), momentum ($\rho\underline{V}$), and energy (ρe) across those interfaces. The thermodynamic parameters P, ρ, and e define the physical state of the air in each mesh cell. P is an important driving force for convection; ρ and e are the properties of air that $\underline{V}$ convects.

Spatial differencing Eqs. (A-1) and (A-3) and the directional dot products of Eq. (A-2) involves integrating the terms of these equations over the volume of each mesh cell. The motion equations have as their mesh-cell volume the adjacent halves of the two-mesh cells on each side of the interface where the motion equation's velocity component is defined.

With the above parameter definitions, this procedure is straightforward except for the terms with gradient $\underline{\nabla}$ and divergence $\underline{\nabla}\cdot$ operators. The pressure gradient term in Eq. (A-2), dot-producted with $r_{\ell i}$, has the finite-difference approximation form

$$(\underline{\nabla}P^{n+1}/\rho^{n})\cdot\underline{\Delta}_{\ell_i} = [(P^{n+1}_{i+1jk} - P^{n+1}_{ijk})/\Delta X_{i+\frac{1}{2}}]/\rho^{n}_{i+\frac{1}{2}jk} \quad , \qquad \text{(A-4)}$$

where $\Delta X_{i+\frac{1}{2}} = \frac{1}{2}(\Delta X_i + \Delta X_{i+1})$ and ΔX_i is the length of the (i,j,k) mesh cell in the $r_{\ell i}$ direction and $\rho^n{}_{i+\frac{1}{2}jk} = \frac{1}{2}(\Delta X_i \rho_{ijk} + \Delta X_{i+1}\, \rho^n{}_{i+1jk})/\Delta X_{i+\frac{1}{2}}$. For the Eq. (A-2) momentum-convection term $(\underline{V}\cdot\underline{\nabla}\,\underline{V})\cdot r_{\ell}$, we need to add to our velocity-component notation a subscript denoting the component direction because the interface location for the velocity is no longer unique to a given velocity component. Where $V_{i+\frac{1}{2}jk}$ defined V_x at $(i+\frac{1}{2},j,k)$ above, now $V_{xi+\frac{1}{2}jk}$, $V_{yi+\frac{1}{2}jk}$, and $V_{zi+\frac{1}{2}jk}$ will be defined on the $(i+\frac{1}{2}, j, k)$ interface when defining the finite-difference approximation form for $[\underline{V}^n\cdot\underline{\nabla}\,\underline{V}^{n+1} + \beta(\underline{V}^{n+1}-\underline{V}^n)\cdot\underline{\nabla}\,\underline{V}^n]\cdot r_{\ell i}$:

$$
\frac{V^n_{x_{i+\frac{1}{2}jk}}}{\Delta x_{i+\frac{1}{2}}}\; W^n_{V_{i+\frac{1}{2}jk}}\; \frac{FA_{i+\frac{1}{2}jk}}{FA_{i+1jk}}\; \frac{FA_{i+\frac{1}{2}jk}}{FA_{i+1jk}}\, \tilde{V}^{n+1}_{x_{i+\frac{1}{2}jk}} - \frac{FA_{i-\frac{1}{2}jk}}{FA_{ijk}}\, \tilde{V}^{n+1}_{x_{i-\frac{1}{2}jk}}
$$

$$
+\; 1 - W^n_{V_{i+\frac{1}{2}jk}}\; \frac{FA_{i+\frac{1}{2}jk}}{FA_{ijk}}\; \frac{FA_{i+3/2jk}}{FA_{i+1jk}}\, \tilde{V}_{x_{i+3/2jk}} - \frac{FA_{i+\frac{1}{2}jk}}{FA_{ijk}}\, \tilde{V}^{n+1}_{x_{i+\frac{1}{2}jk}} \qquad \text{(A-5)}
$$

$$
+\; \frac{\max(V^n_{y\,i+\frac{1}{2}j-\frac{1}{2}k,}\, 0)}{\Delta y_j}\; \tilde{V}^{n+1}_{x_{i+\frac{1}{2}jk}} - \tilde{V}^{n+1}_{x_{i+\frac{1}{2}j-1k}} + \frac{\min(V^n_{y\,i+\frac{1}{2}j+\frac{1}{2}k,}\, 0)}{\Delta y_j}\; \tilde{V}^{n+1}_{x_{i+\frac{1}{2}j+1k}} - \tilde{V}^{n+1}_{x\,i+\frac{1}{2}jk}
$$

$$
+\; \frac{\max(V^n_{z\,i+\frac{1}{2}jk-\frac{1}{2},}\, 0)}{\Delta z_k}\; \tilde{V}^{n+1}_{x_{i+\frac{1}{2}jk}} - \tilde{V}^{n+1}_{x_{i+\frac{1}{2}jk-1}} + \frac{\min(V^n_{z\,i+\frac{1}{2}jk+\frac{1}{2},}\, 0)}{\Delta z_k}\; \tilde{V}^{n+1}_{x_{i+\frac{1}{2}jk+\frac{1}{2}}} - \tilde{V}^{n+1}_{x_{i+\frac{1}{2}jk}}
$$

$$
+\; \beta\, \frac{V^{n+1}_{x\,i+\frac{1}{2}jk} - V^n_{x\,i+\frac{1}{2}jk}}{\Delta X_{i+\frac{1}{2}}}\; W^n_{V_{i+\frac{1}{2}jk}}\; \frac{FA_{i+\frac{1}{2}jk}}{FA_{i+1jk}}\; \frac{FA_{i+\frac{1}{2}jk}}{FA_{i+1jk}}\, V^n_{x_{i+\frac{1}{2}jk}} - \frac{FA_{i-\frac{1}{2}jk}}{FA_{ijk}}\, V^n_{x_{i-\frac{1}{2}jk}}
$$

$$
+\; (1 - W^n_{V_{i+\frac{1}{2}jk}}\; \frac{FA_{i+\frac{1}{2}jk}}{FA_{ijk}}\; \frac{FA_{i+3/2jk}}{FA_{i+1jk}}\, V^n_{x_{i+3/2jk}} - \frac{FA_{i+\frac{1}{2}jk}}{FA_{ijk}}\, V^n_{x_{i+\frac{1}{2}jk}}\;,
$$

where

$$
W^n_{V_{i+\frac{1}{2}jk}} = 0 \text{ if } V^n_{x_{i+\frac{1}{2}jk}} \geq 0 \text{ or } 1 \text{ if } V^n_{x_{i+\frac{1}{2}jk}} < 0\;,
$$

$FA_{i+\frac{1}{2}jk}$ = the flow area through the $(i+\frac{1}{2},j,k)$ interface,

$$FA_{ijk} = Vol_{ijk}/\Delta X_i,\ FA_{i\pm1jk} = Vol_{i\pm1jk}/\Delta X_{i\pm1},$$

$\tilde{V}_X^{n+1}$ = velocities are the previous power-iteration values of V_X^{n+1} velocities, and

β = 0 if the bracketed quantity in the β term above is less than zero or if $V^n_{x_{i+\frac{1}{2}jk}}$ and $V^{n+1}_{x_{i+\frac{1}{2}jk}}$ differ in numerical sign, or

β = 1 otherwise.

Note that in the above approximation form for $(\underline{V}^n \cdot \underline{\nabla}\underline{V}^{n+1}) \cdot r_{\ell i}$, only transverse convection into the $(i+\frac{1}{2},j,k)$ cell is evaluated. Transverse convection is neglected in the β-factored term. The above definition of β has been expanded to define $\beta = 0$ when $V_{x\,i+\frac{1}{2}jk}$ changes its sign (direction) during the time step. A similar approximation form applies when $\underline{V} \cdot \underline{\nabla}\,\underline{V}$ is dot producted with $r_{\ell j}$ or $r_{\ell k}$ to define the finite-differenced motion equation for the other two directions. This gives the cartesian-geometry form for the $(\underline{V} \cdot \underline{\nabla}\,\underline{V}) \cdot r_\ell$ term; for the cylindrical-geometry form, Δx is replaced Δr, Δy is replaced by $r\Delta\theta$, and the FA/FA ratios are replaced by unity in the r- and θ-direction motion equations. Numerical testing of various approximations for stability, accuracy, and computational efficiency provided the basis for selecting the above approximation form (Refs. 3 and 4).

The finite-difference form for the divergence operator term $\underline{\nabla} \cdot (Q^n V^{n+1})$ convecting the quantity $Q^n = \rho^n$, $\rho^n e^n$, or 1 in Eqs. (A-1) and (A-3) is based on a donor-cell approximation:

$$\underline{\nabla} \cdot (Q^n \underline{V}^{n+1}) = (\langle Q^n V^{n+1}\rangle_{i+\frac{1}{2}jk} - \langle Q^n V^{n+1}\rangle_{i-\frac{1}{2}jk})/\Delta x_i$$

$$+ (\langle Q^n V^{n+1}\rangle_{ij+\frac{1}{2}k} - \langle Q^n V^{n+1}\rangle_{ij-\frac{1}{2}k})/\Delta y_j$$

$$+ (\langle Q^n V^{n+1}\rangle_{ijk+\frac{1}{2}} - \langle Q^n V^{n+1}\rangle_{ijk-\frac{1}{2}})/\Delta z_k \quad .$$

The quantity Q^n is convected from the upstream mesh cell. For the $i+\frac{1}{2}jk$ interface,

$$\langle Q^n V^{n+1} \rangle_{i+\frac{1}{2}jk} = Q^n_{ijk} V^{n+1}_{i+\frac{1}{2}jk} \quad \text{if} \quad V^{n+1}_{i+\frac{1}{2}jk} \geq 0$$

$$= Q^n_{i+1jk} V^{n+1}_{i+\frac{1}{2}jk} \quad \text{if} \quad V^{n+1}_{i+\frac{1}{2}jk} < 0. \tag{A-7}$$

In the process of solving for $V^{n+1}_{i+\frac{1}{2}jk}$, first the numerical sign of $V^n_{i+\frac{1}{2}jk}$ is used to determine from which neighboring mesh cell the known value of Q^n is obtained. When the evaluated sign of $V^{n+1}_{i+\frac{1}{2}jk}$ is different, the calculation is repeated to convect the other neighboring mesh cell's Q^n.

These finite-difference approximations are applied to Eqs. (A-1) to (A-3) to obtain the equations that NF85 will solve with a Newton iteration method. Each of the motion equations is rearranged to obtain the unknown velocity component V^{n+1}_{ℓ} (where $\ell = x_{i+\frac{1}{2}jk}$, $y_{ij+\frac{1}{2}k}$, or $z_{ijk+\frac{1}{2}}$) as a linear function of the unknown pressures in the two mesh cells adjacent to its interface. These unknown velocity and pressures are replaced by the sum of their current-estimate iteration value and their change in value that is to be determined,

$$V^{n+1}_{\ell} = \tilde{V}^{n+1}_{\ell} + \Delta V^{n+1}_{\ell} \quad \text{and} \tag{A-8}$$

$$P^{n+1}_{\ell\pm\frac{1}{2}} = \tilde{P}^{n+1}_{\ell\pm\frac{1}{2}} + \Delta P^{n+1}_{\ell\pm\frac{1}{2}} \quad ,$$

to give

$$\Delta V^{n+1}_{\ell} = \bar{V}_{\ell} + \bar{\Delta V}_{\ell} \left(S_{\ell} \Delta P^{n+1}_{\ell-\frac{1}{2}} + Sm_{\ell} \Delta P^{n+1}_{\ell+\frac{1}{2}} \right) \quad , \tag{A-9}$$

where for $\ell = x_{i+\frac{1}{2}jk}$, $\ell-\frac{1}{2} = ijk$ and $\ell+\frac{1}{2} = i+1jk$;

$= y_{ij+\frac{1}{2}k}$, $\ell-\frac{1}{2} = ijk$ and $\ell+\frac{1}{2} = ij+1k$; and

$= z_{ijk+\frac{1}{2}}$, $\ell-\frac{1}{2} = ijk$ and $\ell+\frac{1}{2} = ijk+1$.

Rearranging the finite-difference form of the motion equations and substituting Eq. (A-8) gives expressions that are represented by $\bar{V}_{\ell}$, $\bar{\Delta V}_{\ell}$, S_{ℓ}, and Sm_{ℓ} in

Eq. (A-9). These expressions are defined by parameters with known values from the beginning-of-time-step condition or from the previous Newton iteration's end-of-time-step condition. Those latter parameter, s $V_{\ell}^{\sim n+1}$ and $P_{\ell\pm\frac{1}{2}}^{\sim n+1}$, are defined by V_{ℓ}^{n} and $P_{\ell\pm\frac{1}{2}}^{n}$ before the first Newton iteration and for subsequent iterations by $\tilde{V}_{\ell}^{n+1} + \Delta V_{\ell}^{n+1}$ and $\tilde{P}_{\ell\pm\frac{1}{2}}^{n+1} + \Delta P_{\ell\pm\frac{1}{2}}^{n+1}$ from the previous iteration. Subroutine TF3DE evaluates these expressions represented by $\bar{V}_{\ell}$, $\bar{\Delta V}_{\ell}$, S_{ℓ}, and Sm_{ℓ} in Eq. A(9) for all mesh-cell interfaces in all three directions before each Newton iteration.

Eqs. (A-1) and (A-3), with the divergence-operator finite-difference approximation applied, are reduced to being a linear function of the unknown change in the air pressure and temperature. This is done first to the air density ρ_{ijk}^{n+1} by a linear approximation based on the air EOS, $\rho = P/[(\gamma-1)C_v T]$, where $e = C_v T$.

$$\rho_{ijk}^{n+1} = \tilde{\rho}_{ijk}^{n+1} + (d\rho/dP)_{ijk}^{n} \Delta P_{ijk}^{n+1} + (d\rho/dT)_{ijk}^{n} \Delta T_{ijk}^{n+1} \quad , \qquad \text{(A-10)}$$

where $\tilde{\rho}_{ijk}^{n+1}$ is ρ_{ijk}^{n} for the first iteration and ρ_{ijk}^{n+1} from the previous iteration for subsequent iterations,

$$(d\rho/dP)_{ijk}^{n} = 1/[(\gamma-1)e_{ijk}^{n}] \quad ,$$

$$(d\rho/dT)_{ijk}^{n} = -\rho_{ijk}^{n} C_v/e_{ijk}^{n} \quad , \text{ and}$$

$$e_{ijk}^{n} = C_v T_{ijk}^{n} \quad ,$$

The air temperature definition of the air interval energy per unit mass, $e_{ijk}^{n+1} = C_v T_{ijk}^{n+1} = C_v \tilde{T}_{ijk}^{n+1} + C_v \Delta T_{ijk}^{n+1}$, is used to define e_{ijk}^{n+1} as a linear function of the unknown change in the air pressure and temperature:

$$e_{ijk}^{n+1} = \tilde{e}_{ijk}^{n+1} + (de/dP) \Delta P_{ijk}^{n+1} + (de/dT) \Delta T_{ijk}^{n+1} \quad , \qquad \text{(A-11)}$$

where $\tilde{e}^{n+1}_{ijk}$ is e^{n}_{ijk} for the first iteration and e^{n+1}_{ijk} from the previous iteration for subsequent iterations,

$$(de/dP) = 0 \quad , \text{ and}$$

$$(de/dT) = C_v \quad .$$

Equations (A-8) to (A-11) now are substituted for V^{n+1}_{ℓ} ($\ell = x_{i\pm\frac{1}{2}jk}$, $y_{ij\pm\frac{1}{2}k}$, and $z_{ijk\pm\frac{1}{2}}$), ρ^{n+1}_{ijk}, and e^{n+1}_{ijk} in the spatial finite-difference approximated equations [Eqs. (A-1) and (A-3)]. Rearranging the terms of these two equations for mesh cell (i,j,k) with the ΔP^{n+1}_{ijk} and ΔT^{n+1}_{ijk} unknowns on the left-hand side of the equations and all other terms on the right-hand side of the equations gives

$$a_{11}\,\Delta P^{n+1}_{ijk} + a_{12}\,\Delta T^{n+1}_{ijk} = \rho_{rhs} + \sum_{m=1}^{6} c_{1m}\,\Delta P^{n+1}_{\ell m} \quad \text{and}$$

$$a_{21}\,\Delta P^{n+1}_{ijk} + a_{22}\,\Delta T^{n+1}_{ijk} = e_{rhs} + \sum_{m=1}^{6} c_{2m}\,\Delta P^{n+1}_{\ell m} \quad , \tag{A-12}$$

where $\ell 1 = i-\frac{1}{2}jk$, $\ell 2 = i+\frac{1}{2}jk$, $\ell 3 = ij-\frac{1}{2}k$ and
$\ell 4 = ij+\frac{1}{2}k$, $\ell 5 = ijk-\frac{1}{2}$, and $\ell 6 = ijk+\frac{1}{2}$.

Subroutine TF3DI and evaluates the a_{11}, a_{12}, c_{1m}, ρ_{rhs}, a_{21}, a_{22}, c_{2m}, and e_{rhs} expressions using known parameter values. Then subroutine TF3DI solves Eq. (A-12)'s two equations for ΔP^{n+1}_{ijk} and ΔT^{n+1}_{ijk} by inverting the 2-by-2 coefficient matrix "a" of Eq. (A-12), giving

$$\Delta P^{n+1}_{ijk} = \Delta \tilde{P}^{n+1}_{ijk} + \sum_{m=1}^{6} c1P_m\,\Delta P^{n+1}_{\ell m} \quad \text{and}$$

$$\Delta T^{n+1}_{ijk} = \Delta \tilde{T}^{n+1}_{ijk} + \sum_{m=1}^{6} c2P_m\,\Delta P^{n+1}_{\ell m} \quad , \tag{A-13}$$

where $\Delta \tilde{P}^{n+1}_{ijk}$, $\Delta \tilde{T}^{n+1}_{ijk}$, $c1P_m$, and $c2P_m$ are the known-parameter expressions ρ_{rhs}, e_{rhs}, c_{1m}, and c_{2m}, respectively, multiplied by the inverted "a" matrix.

The first equation of Eq. (A-13) defines the unknown change in pressure in mesh cell (i,j,k) to be a linear function of the unknown change in pressure in each of its six neighboring mesh cells. Move all terms with the ΔP unknowns to the left-hand side of this equation. When considering all mesh cells, this equation becomes a matrix equation with a banded coefficient matrix having seven diagonals with nonzero elements. Subroutine STDIR inverts this coefficient matrix and solves for the pressure change in all mesh cells. With these pressure changes known, subroutine FF3D substitutes them into the second equation of Eq. (A-13) to solve for the temperature change in all mesh cells and into Eq. (A-9) to solve for the velocity change on all mesh-cell interfaces. The evaluated changes in velocity, pressure, and temperature are substituted into Eq. (A-8) and $T^{n+1}_{ijk} = \tilde{T}^{n+1}_{ijk} + \Delta T^{n+1}_{ijk}$ to determine the values of these parameters at time t^{n+1} based on the above linearized equations. The air internal energy and density parameters are evaluated by subroutine THERMO from $e^{nh}_{jk} = C_v T^{n+1}_{ijk}$ and the air EOS rather than from their linearized Eqs. (A-10) and (A-11).

This solution is only a Newton's method iterative estimate of the desired solution because linear approximations have been applied to some of the equations solved. To converge the evaluated solution to the desired solution, a Newton's method pressure iteration is performed beginning with the reevaluation of Eq. (A-9). Each iteration updates the ~ superscripted parameters by adding to them their Δ values determined in the previous iteration pass. The iterative procedure is assumed to have converged to the desired solution when the following convergence tests are satisfied in subroutine HOUT.

1. Maximum fractional change in air pressure = VARER = $\max_{ijk}\left(\left|\Delta P^{n+1}_{ijk}\right| / \tilde{P}^{n+1}_{ijk}\right)$ $\leq$ EPSO (an input-specified pressure convergence-criterion parameter)

2. Maximum change in air temperature - DTVLM = $-2\ K \leq \Delta T^{n+1}_{ijk}) \leq 2\ K$ = DTVUM for all ijk mesh cells of DTVLM and DTVUM are defined by subroutine BLKDAT)

3. No velocity component has changed numerical sign as a result of the last ΔV^{n+1}_{ℓ} evaluation

If all three of these criteria are not satisfied concurrently after NOITMX pressure iterations (NOITMX = 10 defined by subroutine BLKDAT), NF85 reduces the

time-step size in subroutine TIMSTP and repeats (with a backup calculation) the entire time-step solution procedure. Reducing the time-step size below the input-specified minimum time-step size DTMIN aborts the calculation.

APPENDIX B

STABILITY-ENHANCING, TWO-STEP METHOD EQUATIONS

The procedure of solving the semi-implicit, fluid-dynamic equations presented in Appendix A is numerically stable if the time-step size is less than the material Courant limit (the minimum time for air to be convected across a mesh cell). This requirement can limit the time-step size used to evaluate the equilibrium overpressure condition a few seconds after an explosion or the steady-state condition before an explosion occurs. To reduce the computational effort in such situations, larger time steps are desirable so that fewer time-step evaluations are needed to analyze a problem time interval of interest.

The stability-enhancing, two-step (SETS) method[3,4] was developed by John Mahaffy to provide further spatial coupling of the air state across the region of solution. Some additional implicitness is added to the equations to provide numerical stability when the time-step size exceeds the material Courant limit. Rather than add that implicitness to the equations defined in Appendix A (which would further complicate their numerical-solution procedure), the implicitness is added through the further evaluation of a separate set of stabilizer equations. The solution procedure becomes a two-step method: solve the basic (semi-implicit) equations as described in Appendix A and solve a set of stabilizer equations.

Although the SETS-method evaluation step could be used all the time, it is needed for numerical stability of the solution only when the time-step size exceeds the material Courant limit. To reduce computational effort, NF85 uses the SETS method when the time step exceeds 80% of the material Courant limit time-step size. Subroutine NEWDLT sets variable NSTAB to 1 as a flag to indicate that the SETS stabilizer equations are to be evaluated. Their evaluation

continues each time step until the time step decreases below 75% of the material Courant limit time-step size. Variable NSTAB is set to 0 as a flag to discontinue evaluation of the SETS stabilizer equations. In the SETS method, the stabilizer equations are evaluated once each time step, which increases the computational effort per time step by approximately 20%. This results in the computational effort of NF85 being reduced with the SETS method when the time-step size exceeds 120% of the material Courant limit. During the transition from time steps of 80% to 120% of the material Courant limit, an average 15% additional computational effort is required.

In the two-step procedure, the stabilizer equations can be evaluated either before or after the basic equations. One ordering that is always stable and is used by NF85 begins with evaluating the stabilizer equations of motion, is followed by the pressure iteration (Newtons method) solution of the basic equations, and ends with evaluating the stabilizer mass and energy equations.

The time-differenced stabilizer equation of motion has the form

$$(\tilde{\underline{V}}^{n+1} - \underline{V}^n)/\Delta t + \underline{V}^n \cdot \nabla \tilde{V}^{n+1} + \beta(\tilde{\underline{V}}^{n+1} - \underline{V}^n) \cdot \underline{\nabla}\, \underline{V}^n =$$

$$-\underline{\nabla}\, P^n/\rho^n - K^n |\underline{V}^n|(2\tilde{\underline{V}}^{n+1} - \underline{V}^n) + \underline{g} \quad . \tag{B-1}$$

Equation (B-1) differs from the semi-implicit equation of motion [Eq. (A-2)] by having beginning- rather than end-of-time-step air pressures. Spatial differencing Eq. (B-1) is done in the same way as for Eq. (A-2) in Appendix A except that $\tilde{\underline{V}}^{n+1}$ in the $\underline{V}^n \cdot \underline{\nabla}\, \tilde{\underline{V}}^{n+1}$ term is to be evaluated simultaneously with all other $\tilde{\underline{V}}^{n+1}$ in the equation rather than with their previous iteration value. The stabilizer equation of motion for each of the three coordinate directions over the region of solution becomes a matrix equation with a coefficient matrix having seven diagonals of nonzero elements. These matrix equations are defined and solved by subroutines FEMOMX, FEMOMY, and FEMOMZ in the same manner as the pressure-change matrix equation [Eq. (A-13)]. The solution for the unknown $\tilde{V}^{n+1}$ where ℓ = x or r, y or t, and z is used rather than V_ℓ^n to define $\tilde{V}_\ell^{n+1}$ for the first iteration solution of the basic equations of motion.

After the basic equations are solved by convergence of the pressure iteration, all end-of-time-step air parameters have had their values determined.

Solving the stabilizer mass and energy equations reevaluates the air density ρ^{n+1} and internal energy e^{n+1}. These time-differenced equations differ from their basic equations by convecting these quantities with a fully implicit approximation:

$$(\rho^{n+1} - \rho^n)/\Delta t + \underline{\nabla} \cdot \rho^{n+1} \underline{V}^{n+1} = m_s^{n+\frac{1}{2}} \quad \text{and} \tag{B-2}$$

$$(\rho^{n+1}e^{n+1} - \rho^n e^n)/\Delta t + \underline{\nabla} \cdot \rho^{n+1}e^{n+1}\underline{V}^{n+1} = \tag{B-3}$$

$$-P^{n+1} \underline{\nabla} \cdot \underline{V}^{n+1} + m_s^{n+\frac{1}{2}} e_s^{n+\frac{1}{2}} \quad .$$

Spatial differencing Eqs. (B-2) and (B-3) is done with a donor-cell approximation in the same way that Eqs. (A-1) and (A-3) were spatially differenced. With known values for $\underline{V}^{n+1}$ and P^{n+1} from the solution of the basic equations, Eqs. (B-2) and (B-3) over the region of solution become matrix equations having the same coefficient matrix with seven diagonals of nonzero elements.

Although this coefficient matrix has the same nonzero-element form as the pressure-change and velocity coefficient matrices discussed earlier, this coefficient matrix may not be diagonally dominant. A diagonally dominant matrix satisfies the matrix property that the sum of the absolute value of all off-diagonal elements in any row or column of the matrix is less than the absolute value of their main-diagonal element. The pressure-change and velocity coefficient matrices are diagonally dominant and can be inverted by direct or iterative algorithms. NF85 inverts these coefficient matrices directly into the product of banded lower and upper triangular matrices without pivoting using the CALMATH library routines BGLSDC and BGLSSL. For the density and internal energy coefficient matrix, NF85 performs a direct inversion with partial pivoting in subroutine STBME by calling the CALMATH library routines SGBFA and SGBSL.

The solution of the stabilizer mass and energy equations gives new values for the air density and internal energy that are close approximations to their values from a fully implicit solution. That closeness provides the numerical stability of a fully implicit approximation under almost all conditions encountered. The SETS method is said to be conditionally stable. It can become un

stable when parameters defined at the beginning of the time step undergo a rapid variation in time. K^n is such a parameter. This situation is avoided by the internal time-step size adjustment procedure in NF85 reducing the time-step size when events are encountered that cause a rapid transient. The user needs to be aware that temporary oscillations that develop after a rapid change in a slow transient may be the result of numerical instability.

NF85 completes the time-step solution by evaluating consistent air temperature and pressure values from the air density and internal energy solutions of the stabilizer mass and energy equations. The relationship $T^{n+1}_{ijk} = e^{n+1}_{ijk}/C_v$ defines the air temperature; the air EOS $P^{n+1}_{ijk} = (\gamma-1)\,\rho^{n+1}_{ijk}\,e^{n+1}_{ijk}$ defines the air pressure.

APPENDIX C

ONE-DIMENSIONAL, BOUNDARY-CONDITION REGION FLUID-DYNAMIC EQUATIONS

The fluid-dynamic equations for the one-dimensional, boundary-condition regions have the form of the three-dimensional region, cartesian-coordinate equations (defined in Appendices A and B) after being simplified to model only one-dimensional dependence. They will not be rewritten here because this is quite straightforward. What will be discussed here is how these one-dimensional equations are coupled (interfaced) to the three-dimensional equations and how they are solved.

NF85 restricts the user to coupling a one-dimensional, boundary-condition region to a rectangular subarea of mesh-cell interfaces on the external boundary of the three-dimensional region. Such a region can not be attached to an internal interface of mesh cells within the three-dimensional region. Modeling a vent duct whose open end is internal to the room rather than at the room's external wall can be done by defining zero flow areas to the internal mesh-cell interfaces in order to model the vent duct's wall sides within the room.

The one-dimensional region's mesh cells are numbered starting at the three-dimensional region interface. Mesh cell 1 is coupled by convection to mesh cell 2 and to all the three-dimensional region mesh cells whose external-boundary interface lies within the rectangular subarea of attachment. That subarea can range from a fraction of the external-interface flow area of one mesh cell to as much as the summed external interface of all mesh cells adjacent to the three-dimensional region's external-boundary side. There is one restriction required by the bandedness of the matrices being solved by CALMATH routines. The rectangular subarea can have only one or two mesh cells in the z-coordinate direction. In cartesian coordinates, this restriction generally can be circumvented by proper selection of the z-coordinate direction. In cylindrical geometry, the z-direction dimension of the attached duct may need to be modeled smaller than it actually is with two z-direction mesh-cell interfaces, or the Δz dimensions of those two axial levels may need to be sized to the duct dimension. If the z-direction duct dimension is reduced, the dimension in the other direction should be increased to conserve flow area at the room/duct interface.

The basic (semi-implicit) equations for a three-dimensional region with one-dimensional, boundary-condition regions attached need to be coupled over the entire region of solution when solving the pressure-change matrix equation. The basic equations for each one-dimensional region are defined in Appendix A for the three-dimensional region [Eqs. (A-8) to (A-13)]. Each one-dimensional region has a pressure-change matrix equation defined by

$$\Delta P_i^{n+1} = \Delta \tilde{P}_i^{n+1} + \sum_{m=1}^{2} c1P_{im} \Delta P_{\ell m}^{n+1} \quad , \tag{C-1}$$

where

$$i = 1, 2, \ldots, NBC, \ \ell 1 = i - 1, \ \ell 2 = i + 1 \text{ and}$$

$$\Delta P_0^{n+1} = \sum_{\ell} FA_{\ell+\frac{1}{2}} \Delta P_{\ell}^{n+1} / \sum_{\ell} FA_{\ell+\frac{1}{2}} \quad ,$$

where ℓ sums over all ijk mesh cells with a side interface of flow area $FA_{\ell+\frac{1}{2}}$ within the rectangular subarea of attachment to the one-dimensional region.

Equation (C-1) defines a matrix equation with a tridiagonal coefficient matrix. The first row of the matrix equation has its ΔP_{ℓ}^{n+1} unknown terms kept on the right-hand side of the equation. Subroutine STDIR inverts this coefficient matrix and solves for each of the ΔP_{i}^{n+1} unknowns in the one-dimensional region as a function of the ΔP_{ℓ}^{n+1} unknowns from the three-dimensional region.

$$\Delta P_{i}^{n+1} = \Delta P_{i}^{rhs} + C_{i}^{rhs} \left(c1P_{11} / \sum_{\ell} FA_{\ell+1/2}\right) \sum_{\ell} FA_{\ell+1/2} \Delta P_{\ell}^{n+1} \qquad (C\text{-}2)$$

$$i = 1, 2, \ldots, NBC.$$

From each of the one-dimensional regions, the Eq. (C-2) for i = 1 is substituted into the pressure-change matrix [Eq. (A-13)] to eliminate all $\Delta P_{\ell+1}^{n+1} \equiv \Delta P_{i=1}^{n+1}$ outside the external boundary at open-flow interfaces where one-dimensional regions are attached. The resulting matrix equation has only ΔP_{ijk}^{n+1} unknowns at (i,j,k) mesh cells within the three-dimensional region's external boundary. The matrix equation is solved in the manner of Appendix A because coupling to all one-dimensional regions has been eliminated by the above substitution. From this solution, all ΔP_{ℓ}^{n+1} in Eq. (C-2) are known; evaluating Eq. (C-2) determines ΔP_{i}^{n+1} for all mesh cells in the one-dimensional regions. From the equations defined to determine Eq. (A-13) for the three-dimensional region and Eq. (C-1) for the one-dimensional regions, all other air parameters (T^{n+1}, V^{n+1}, ρ^{n+1}, and e^{n+1}) can be evaluated throughout the region of solution. This procedure is re-evaluated within a Newton's-method pressure iteration until the three convergence criteria defined at the end of Appendix A are satisfied throughout the three-dimensional region and the one-dimensional regions of solution.

When the SETS method is applied, the three-dimensional stabilizer equations defined in Appendix B are simplified to model only one-dimensional dependence in the one-dimensional, boundary-condition regions. Solving the stabilizer equation of motion is done progressively by following the direction of information flow as it is convected by the donor-cell approximation. First, the stabilizer equation of motion is solved in each one-dimensional region that has an interface air velocity directed into the three-dimensional region. The solution of the stabilizer equation of motion in these regions is uncoupled from the three-dimensional

region. The stabilizer equations of motion in the three-dimensional region then are evaluated using the known in-flow velocities from the one-dimensional regions. Finally, the remaining one-dimensional regions have their stabilizer equation of motion evaluated using the known velocities at their interface that flow out of the three-dimensional region. Solving these matrix equations in the one-dimensional regions involves inverting tridiagonal coefficient matrices; solving the three stabilizer-equation-of-motion matrix equations in the three-dimensional region involves inverting seven-diagonal coefficient matrices.

A similar procedure is used to evaluate the stabilizer mass and energy equations. Here the quantity being convected across a region interface is the unknown that couples the solution of one region to the other region. The downstream region's solution is coupled to the upstream region's solution; however, the reverse is not true. All one-dimensional regions with interface velocities directed into the three-dimensional region have their stabilizer mass and energy equations evaluated first, then the equations of the three-dimensional region are evaluated, and finally the remaining one-dimensional regions are evaluated to complete the time-step solution.

APPENDIX D

NF85 INITIAL EXPERIMENTAL VERIFICATION

The NF85 computer code has been verified by shock-transmission experiments. These experiments were designed to evaluate the code's ability to calculate shock reflection and interaction as well as transmission. The experimental set-up, NF85 computer model, and experimental/calculative results will be discussed.

I. TEST EQUIPMENT

A. Two-Dimensional Shock Transmission Set-Up

Figure D-1 is a schematic showing a plan view of the experimental apparatus, which is located on the campus of New Mexico State University in Las Cruces, New Mexico. This test facility is operated under contract to the Los Alamos National Laboratory. The shock tube is connected to the experimental apparatus with a 0.305-m (1-ft)-i.d. pipe that is 2.72 m (8.92 ft) long. The focus of these experiments was to obtain two-dimensional data in the transition region where the shock tube (0.91 m i.d.) connects to the smaller (0.305 m i.d.) pipe.

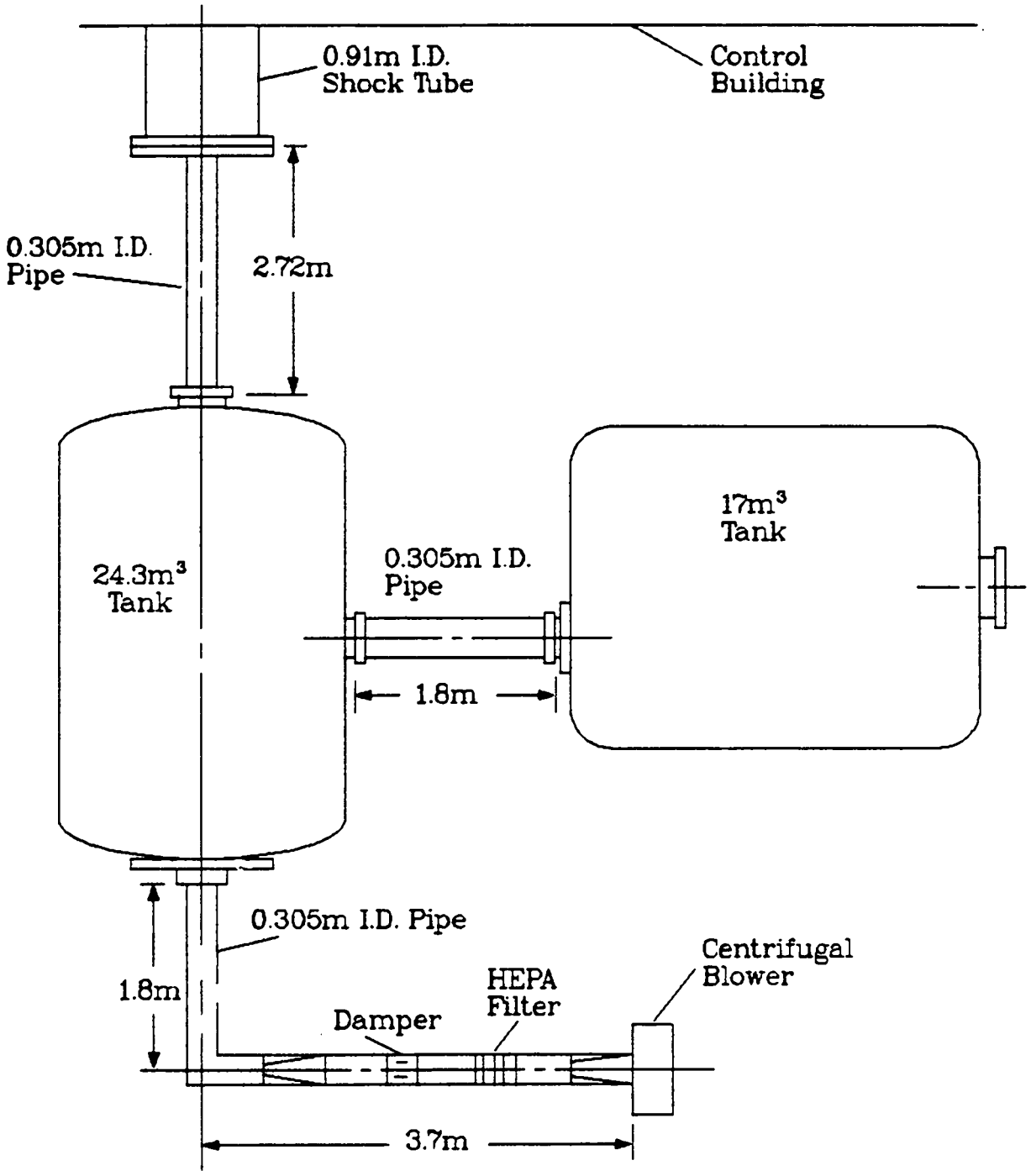

Fig. D-1.
Plan view of the model ventilation system.

The shock tube consists of a 0.91-m (3-ft)-diam tube 48 m (160 ft) long. The driven (low-pressure) section of the shock tube is 36 m (118 ft) long. The driver (high-pressure) section has a variable length, but for this study, it was fixed at 3.0 m (10 ft). A complete description of the shock tube is given by Smith and Gregory.[10] At the end of the driven section of the shock tube, an abrupt contraction was constructed to a 0.305-m (1-ft)-diam pipe 2.72 m (8.92 ft) long that leads into the small ventilation systems.

Pressure measurements were taken at eight locations, which are shown in Fig. D-2 and labeled 1 through 8. Channel 1 is on the side wall of the shock tube 0.91 m (3 ft) ahead of the abrupt contraction. Channels 2, 3, and 4 are located on the dead-end portion of the abrupt contraction (area-reducing plate) at the radial positions of 0.35 m (1.16 ft), 0.28 m (0.92 ft), and 0.20 m (0.67 ft), respectively. These three measurements are referred to as "head-on pressure measurements." Channels 5, 6, 7, and 8 were located at positions on the 0.30-m (1-ft)-diam pipe (Fig. D-2). These four measurements were side-on pressure measurements. All eight channels used Kulite model XT-190 miniature pressure transducers with a range of 0 to 689 kPa (0 to 100 psi). The experimental data were digitized and recorded by a CAMAC data acquisition system using a DEC PDP11/10 digital computer.

All eight pressure transducers were calibrated against a pressure standard before each experiment. The driver of the shock tube then was pressurized to the desired driven pressure, and the diaphragm was ruptured. The resulting shock wave traveled down the shock tube and, upon passing a triggering pressure transducer, automatically started the data acquisition system.

II. COMPUTER CODE MODELING

A. NF85 Shock Transmission Model

The shock-transmission tests have been analyzed by the NF85 computer program to provide a benchmark for determining the ability of NF85 to evaluate shock-wave transmission, reflection, and interaction. A multidimensional region in (r,z) cylindrical geometry with a (9,24) spatial mesh was used to model the vicinity of the cross-section-area-reduction plate at the open end of the shock tube. By neglecting the small effect of gravitational acceleration normal to the axial (z) direction, azmuthal (θ) dependence was eliminated to reduce calculational effort. Radial (r) dependence was evaluated to model its effect at the

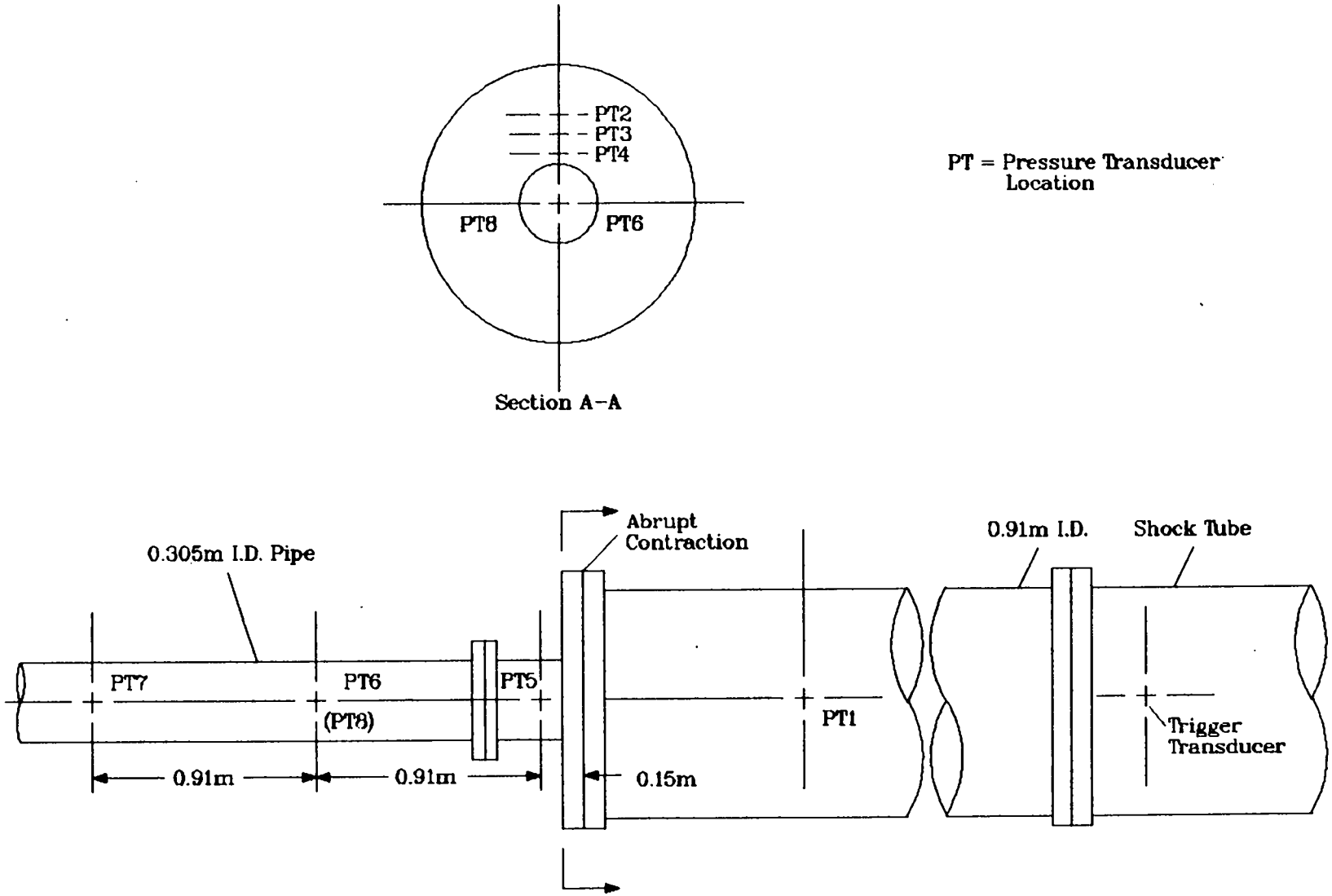

Fig. D-2.
Location of pressure transducers for shock-transmission tests.

area-reduction plate where partial reflection and transmission of the shock-wave pulse occurs. Almost all of the 0.91-m (3-ft)-diam shock tube was modeled by a one-dimensional region with 750 mesh cells attached at the z = 0 boundary face of the (r,z) region. At the z = 24 boundary face of the (r,z) region, another one-dimensional region with 179 mesh cells was attached to model a 0.30-m (1-ft)-diam pipe, a 24.3-m^3 (859-ft^3) tank, and another 0.30-m (1-ft)-diam pipe, all of which are down-stream of the area-reduction plate. Figure D-3 is a diagram of the mesh-cell spatial model of the shock-transmission experiment. Darkened mesh cells indicate the location of the eight pressure transducers in the experiment.

III. EXPERIMENTAL AND CODE MODELING RESULTS

A. Shock Transmission Test/NF85

The shock-transmission tests measure air pressure at eight locations in the vicinity of the area-reduction plate as a shock-wave pulse passes through the region. The shock-wave pulse is generated by breaking two diaphragms between the high and low (atmospheric) air-pressure ends of the shock tube. The shock-wave front travels down the low-pressure length of the shock tube at essentially the sonic velocity of the air medium ahead of it. It is followed by an air-mass front moving at the much lower air velocity. In the opposite direction, a rarefaction- (expansion-) wave front travels up the high-pressure length of the shock tube until it reaches the closed end, where it is reflected. It then travels down the high-pressure plus low-pressure lengths of the shock tube at the sonic plus air-mass velocity. The expansion wave has both a front and a tail; the tail travels at a slightly slower velocity. Very quickly the expansion wave catches up to the air-mass front and passes through it. Eventually the expansion wave catches up to the shock wave, but this does not happen in the experiment until after both waves have passed the pressure transducer locations. The pressure transducers measure a shock-wave pulse where the air pressure rises initially when the shock-wave front crosses the transducer location. A short time later, the expansion-wave front crosses the transducer location, causing the air pressure to fall until the expansion-wave tail crosses the transducer location.

This shock-transmission test provides a very sensitive benchmark for calculating shock- and expansion-wave transmission, reflection, and interaction.

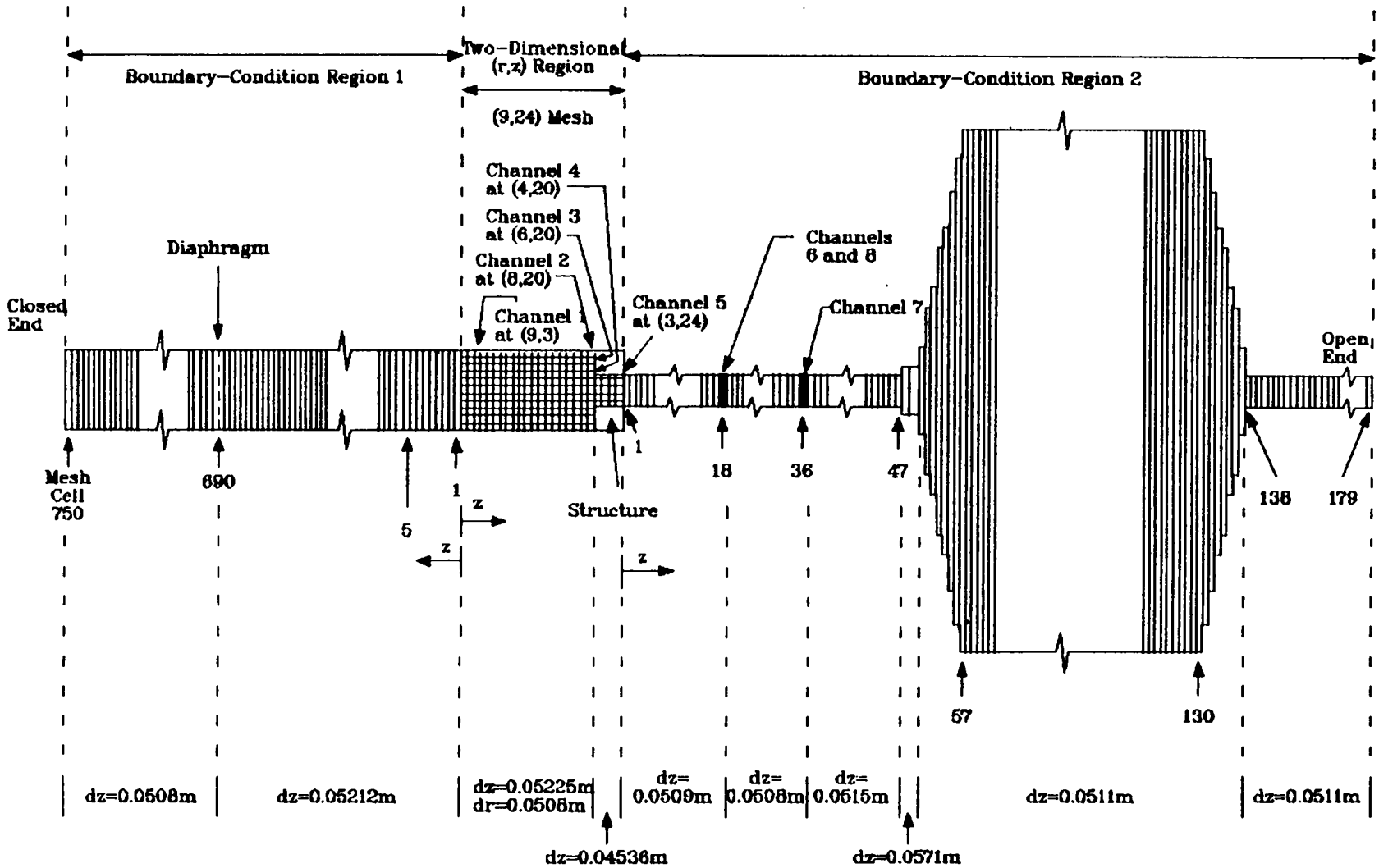

Fig. D-3.
Mesh-cell spatial model used by the NF-85 Computer Program to analyze the shock transmission tests.

The channel 1 pressure transducer first encounters the shock-wave front and then encounters its front partially reflected from the area-reduction plate. Soon thereafter it encountered the expansion-wave that was reflected from the shock tube's high-pressure end and had interacted with the air-mass front and the partially reflected shock front. The pressure transducers of channels 2, 3, and 4 measure the air pressure at the area-reduction reflecting surface. The pressure transducers of channels 5, 6, 7, and 8 encounter the shock and expansion waves that have been partially transmitted through the abrupt area-reduction plate opening.

NF85 was used to evaluate the shock-transmission tests in three different ways.

1. The calculation starts at the breaking of the diaphragms using the numerical model in Fig. D-3 with the shock and air-mass fronts initially 36.1 m (118 ft) from the channel 1 location.

2. The calculation starts from an analytic solution for the shock pulse after it has traveled down the shock tube and is approximately 0.13 m (0.43 ft) from the channel 1 location using the numerical model in Fig. D-3.

3. The calculation is done in two stages: First, only the shock tube is modeled with the 750-mesh-cell region 1 attached to a one-cell multidimensional region, and the test is analyzed from the breaking of the diaphragms until the shock front is approximately 0.13 m (0.43 ft) from the channel 1 location; the second stage uses the restart data dump from region 1 instead of the analytic solution as the initial condition for a calculation similar to 2.

Computational statistics from the nine shock-transmission tests analyzed are shown in Table D-I. The second procedure described above was used to analyze all the tests for 0.065 s with the total number of time steps and Cray-1 computer time required by NF85 for each test reported in the left half of the table. The right half of the table reports the same statistics when using the first procedure for tests with shock-front overpressures of 20.7, 21.8, 22.4,

TABLE D-I

NF85-CALCULATION STATISTICS FROM ANALYZING THE NUMS SHOCK-TRANSMISSION TESTS

Pressure Difference Across Diaphragms (psi)	Shock-Front Overpressure (psi)	Calculated from Analytic Solution			Calculated From Diaphragm Break			Transmission Time to the Area-Reduction End of the Shock Tube		
		Problem Time (s)	Time Steps	CRAY Time (s)	Problem Time (s)	Time Steps	CRAY Time (s)	Analytic (s)	Calc. (s)	Error (%)
6.830	3.000	0 to 0.065	186*	69.4*	0 to 0.160	199	87.9	0.09642	0.09530	-1.12
7.250	3.163	0 to 0.065	105	42.4	0 to 0.160	199	88.8	0.09700	0.09583	-1.13
7.500	3.257	0 to 0.065	105	42.8	0 to 0.160	199	89.2	0.09639	0.09531	-1.11
58.000	15.646	0 to 0.065	688	307.9	0 to 0.074	0 to 1665	127.6			
					to 0.140	to 2301	305.4			
							433.0	0.07418	0.07894	+6.40
58.000	15.653	0 to 0.065	685	306.4	0 to 0.076	0 to 1697	129.6			
					to 0.140	to 2294	293.2			
							442.8	0.07445	0.07926	+6.46
59.985	16.000	0 to 0.065	690	314.7	0 to 0.140	0 to 2403	917.0	0.07423	0.07899	+6.42
60.000	16.012	0 to 0.065	706	316.0	0 to 0.076	0 to 1775	135.1			
					to 0.140	to 2396	301.4			
							436.5	0.07444	0.07935	+6.60
90.000	20.547	0 to 0.065	1248	553.2	0 to 0.072	0 to 2759	208.8			
					to 0.140	to 3622	401.5			
							610.3	0.06954	0.07575	+8.92
98.000	21.603	0 to 0.065	1395	620.0	0 to 0.070	0 to 2933	223.3			
					to 0.135	to 3881	430.1			
							653.4	0.06808	0.07436	+9.21

*This calculation's time-step size was constrained for most of the analysis by a maximum time-step size of 0.0005 s; the other calculations used a maximum time-step size of 0.0001 s.

and 110.2 kPa (3.000, 3.163, 3.257, and 16.000 psi) and the third procedure for the other tests. The first and third procedures give the same solution, but we see in Table D-I that the Cray-1 computer times for the 107.8, 107.85, and 110.3 kPa (15.646, 15.653, and 16.012 psi) shock-front overpressure tests evaluated with the third procedure required half the calculative effort of the 110.2-kPa (16.000-psi) test with the first procedure. The second procedure required a half to a third of the calculative effort of the first procedure. At the far right of Table D-I is a comparison of the analytic and calculated transmission times for the shock-wave front to reach the area-reduction plate. The transmission times for small shock-front overpressures are calculated accurately with a trend toward overestimating the times as the shock-front overpressures increase. Determining the time at which the shock front reaches the area-reduction plate was based on realizing half the shock-front overpressure rise at the plate.

Time plots of calculated air pressure and pressure transducer measurements are shown in Figs. D-4 through D-6 for the 21.8-, 110.3-, and 141.5-kPa (3.163-, 16.012-, and 20.547-psi) shock-front overpressure tests, respectively. Results from seven of the eight pressure-transducer locations are shown with results from channel 3 omitted because of their similarity to channel 2 and 4 results. The results from the tests are of two different forms: The 20.7-, 21.8-, and 22.4-kPa (3.000-, 3.163-, and 3.257-psi) shock-front overpressure tests have similar results and the other tests with shock-front overpressures greater than 103.35 kPa (15 psi) have similar results. An example of this similarity can be seen by comparing Figs. D-5 and D-6.

The pressure transducer measurements are plotted (points) along with NF85 calculative results using the first or third procedure shown by the dotted curve (labeled 36.1 m, the initial distance of the shock-wave front from channel 1) and using the second procedure shown by the solid curve (labeled 0.13 m). The first or third procedure is more convenient for the NF85 user because the entire solution, starting with the breaking of the diaphragms, is evaluated by NF85. However, having NF85 evaluate the shock-wave pulse transmission down the 36-m (118-ft) length of the shock tube low-pressure section introduces spatial smearing to the solution. The second procedure avoids this numerical-solution error by starting with the analytic solution for the shock-front pulse just before it reaches channel 1.

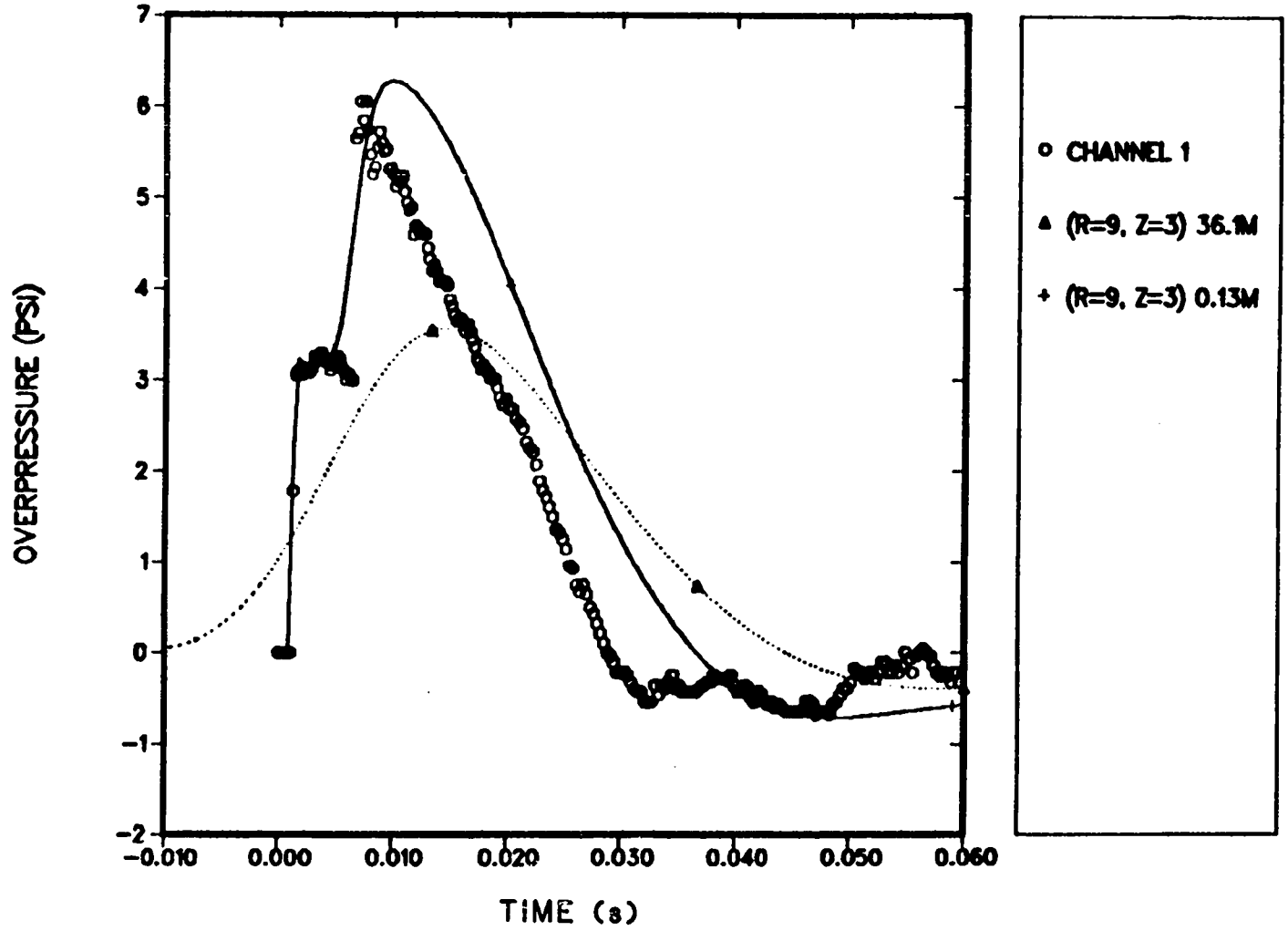

Fig. D-4.
Shock transmission test with 21.8-kPa (3.163-psi) shock overpressure.

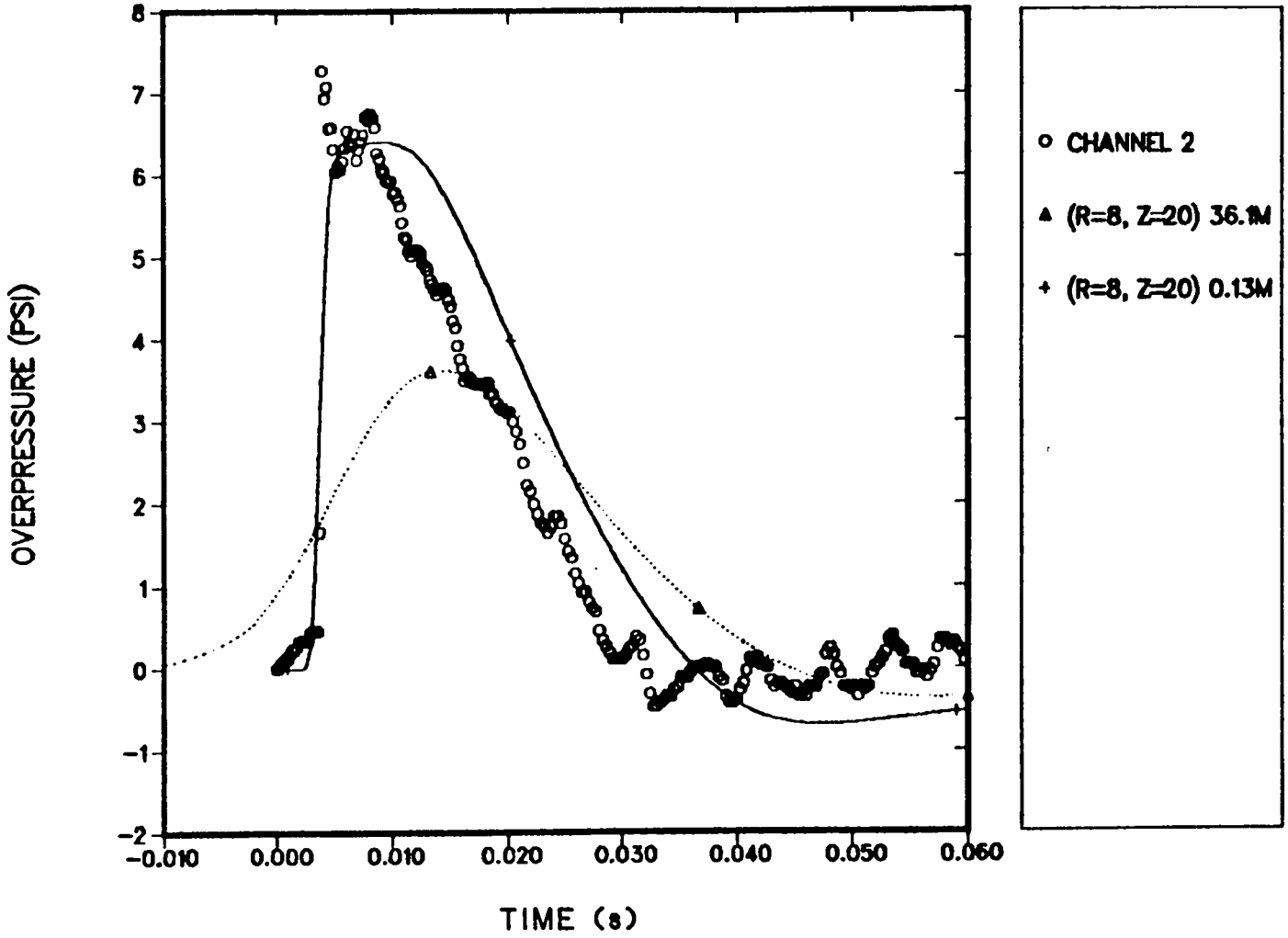

Fig. D-4 (cont).
Shock transmission test with 21.8-kPa (3.163-psi) shock overpressure.

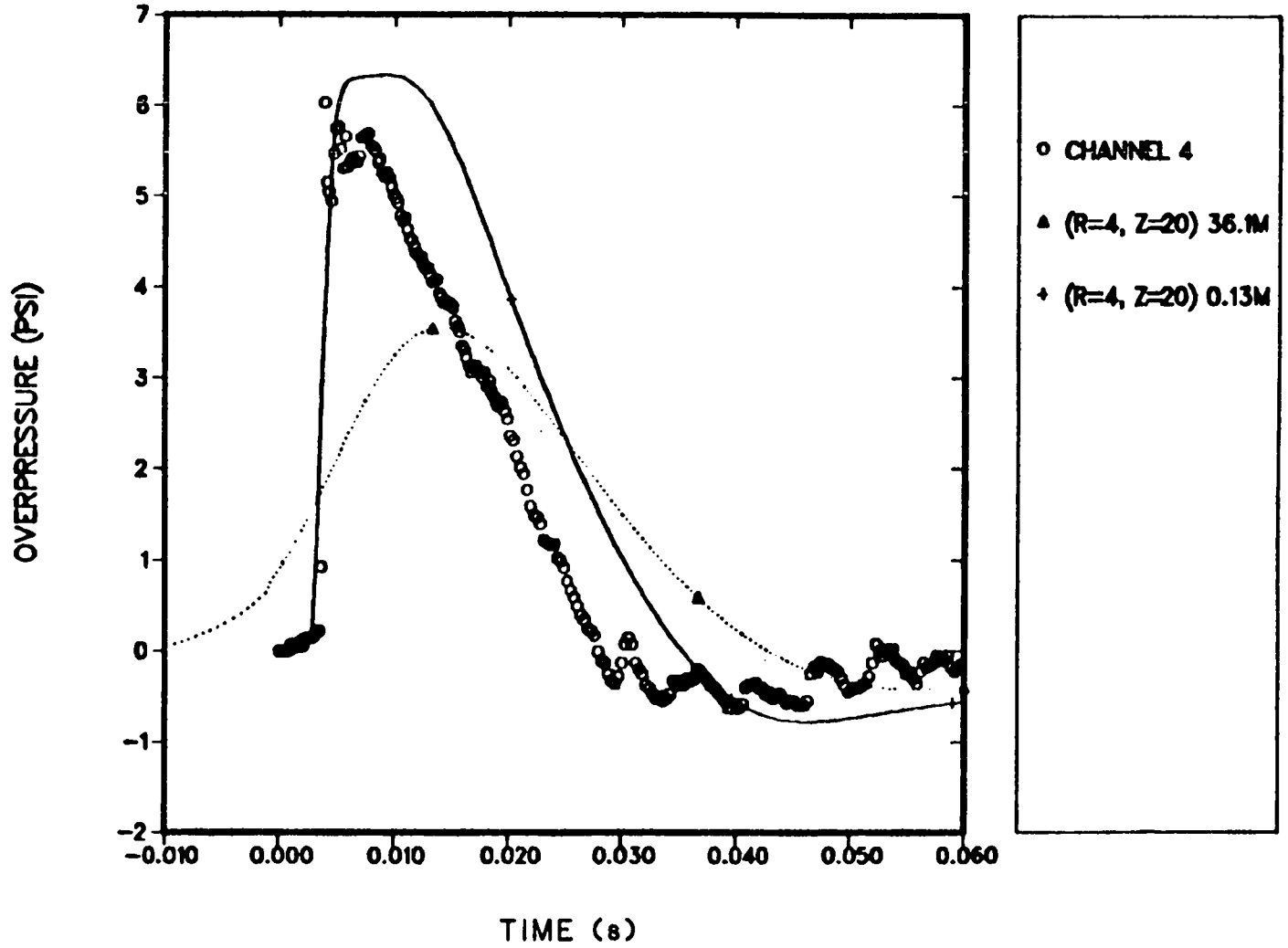

Fig. D-4 (cont).
Shock transmission test with 21.8-kPa (3.163-psi) shock overpressure.

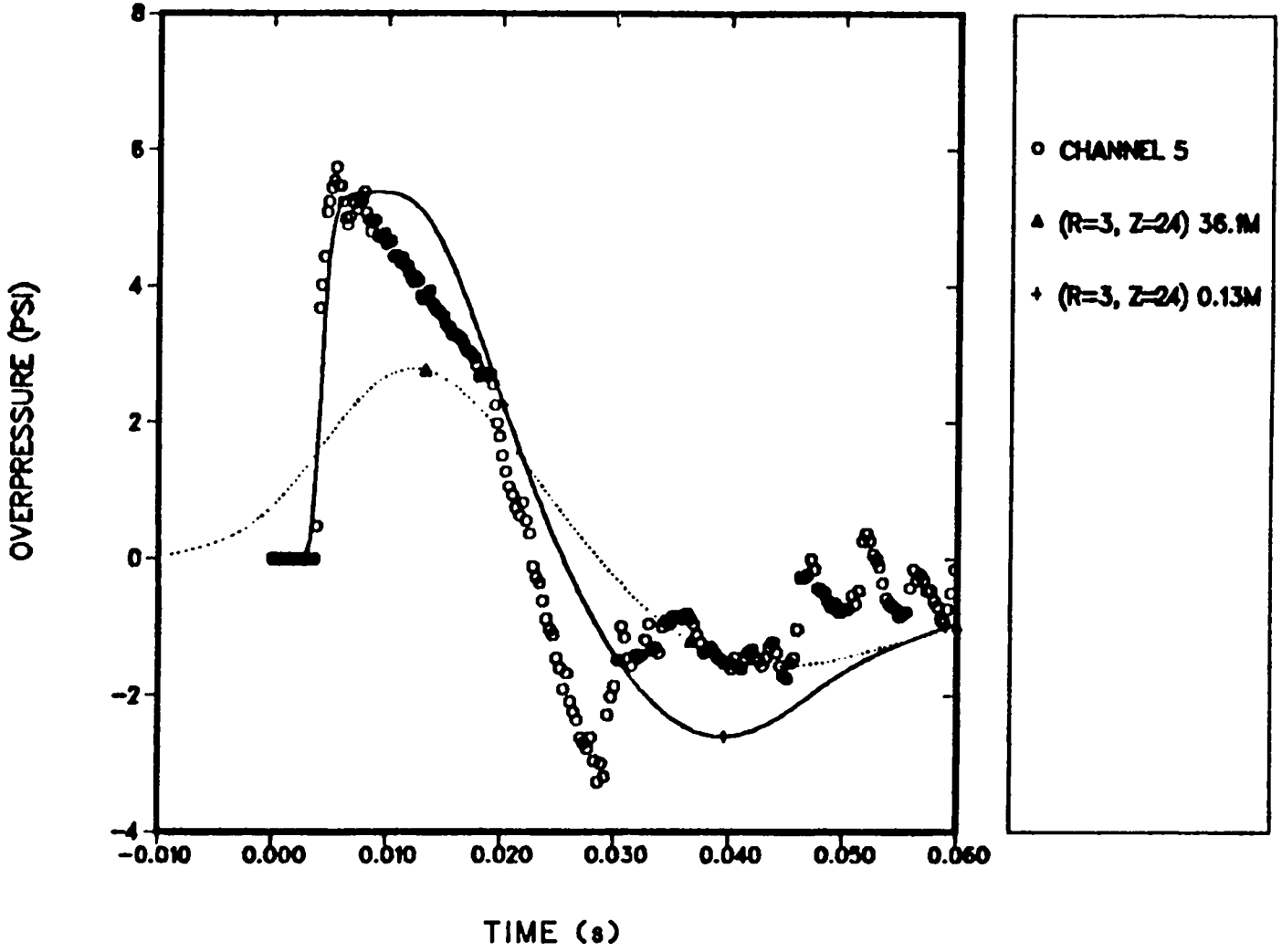

Fig. D-4 (cont).
Shock transmission test with 21.8-kPa (3.163-psi) shock overpressure.

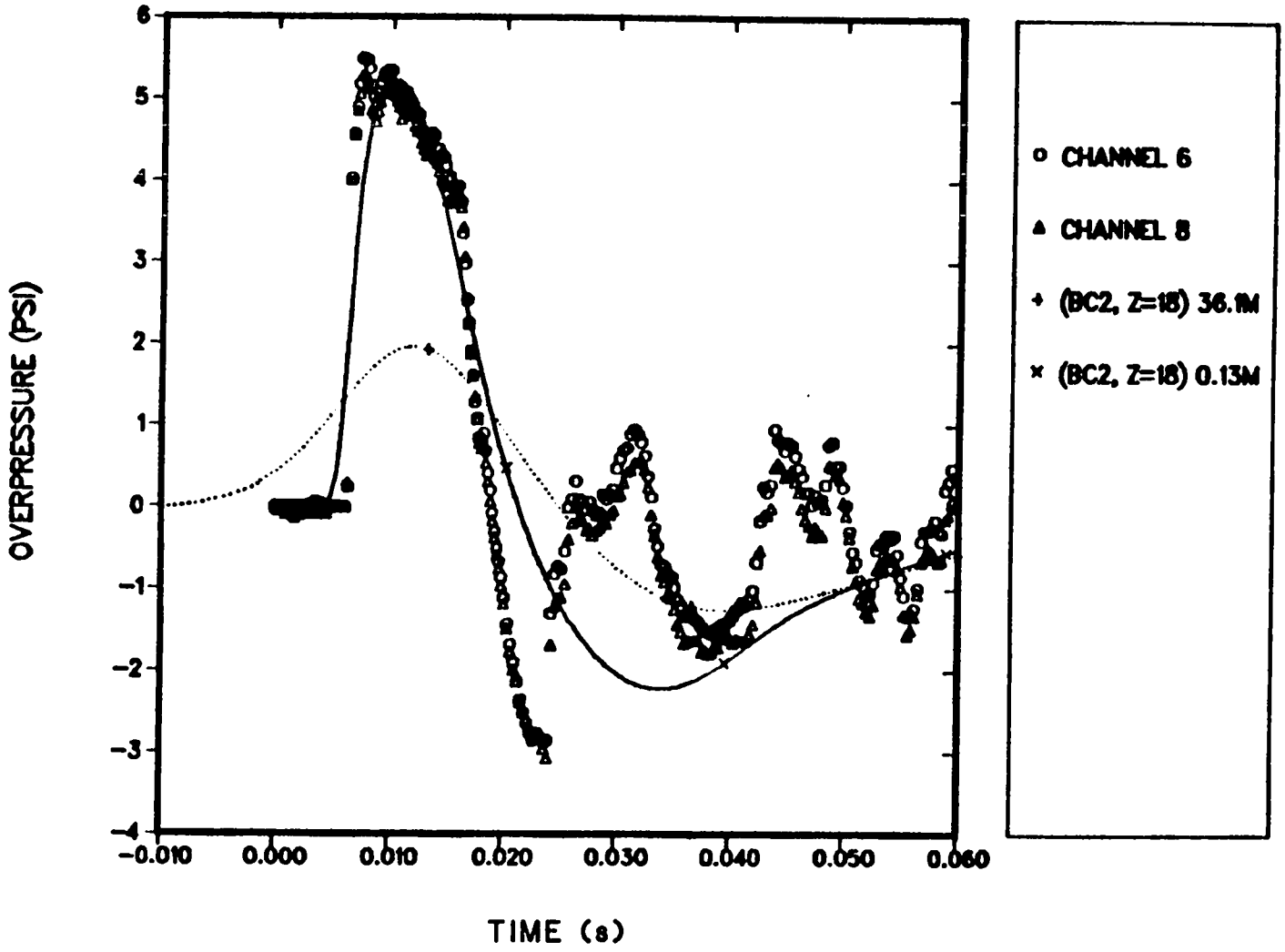

Fig. D-4 (cont).
Shock transmission test with 21.8-kPa (3.163-psi) shock overpressure.

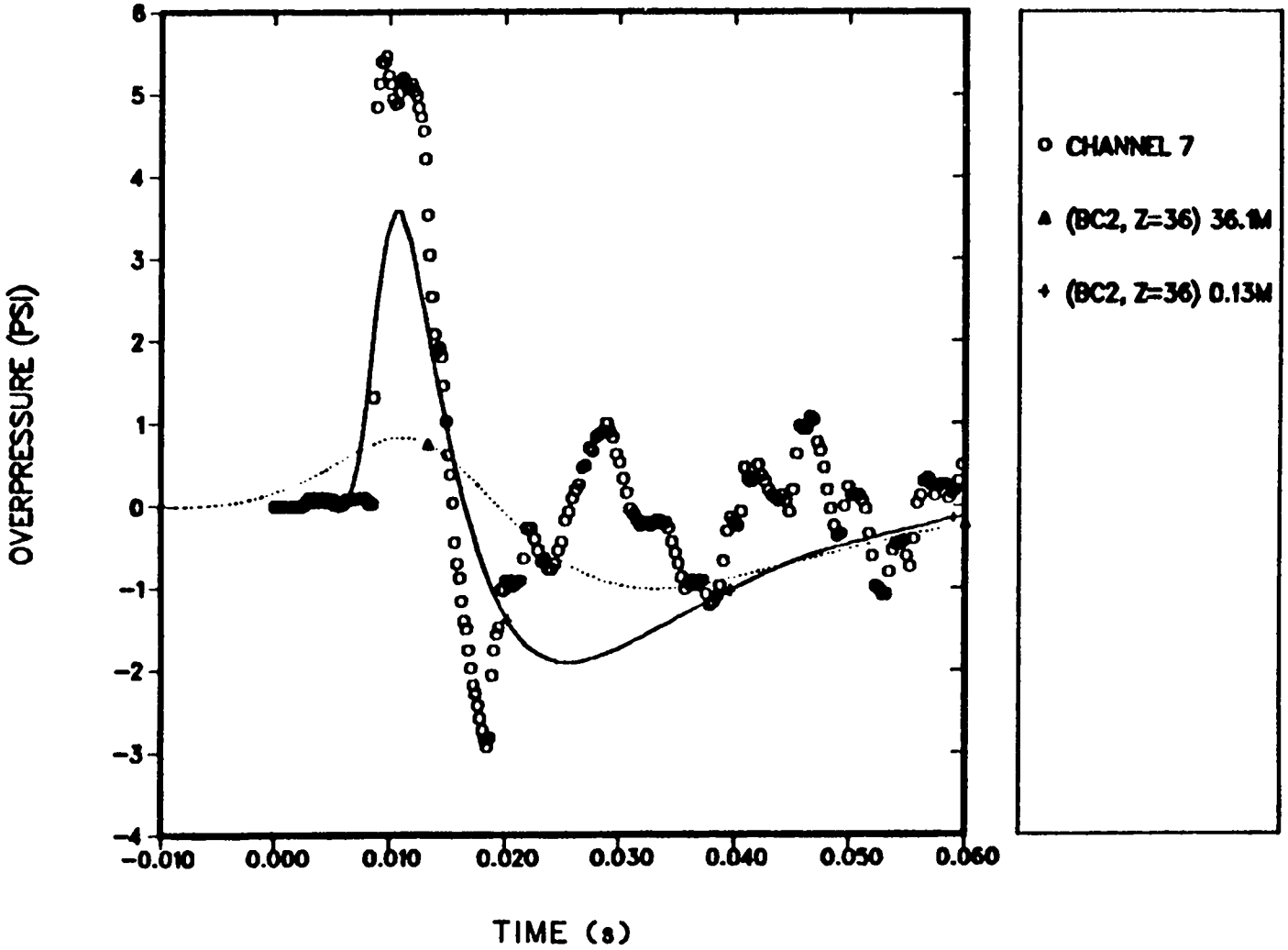

Fig. D-4 (cont).
Shock transmission test with 21.8-kPa (3.163-psi) shock overpressure.

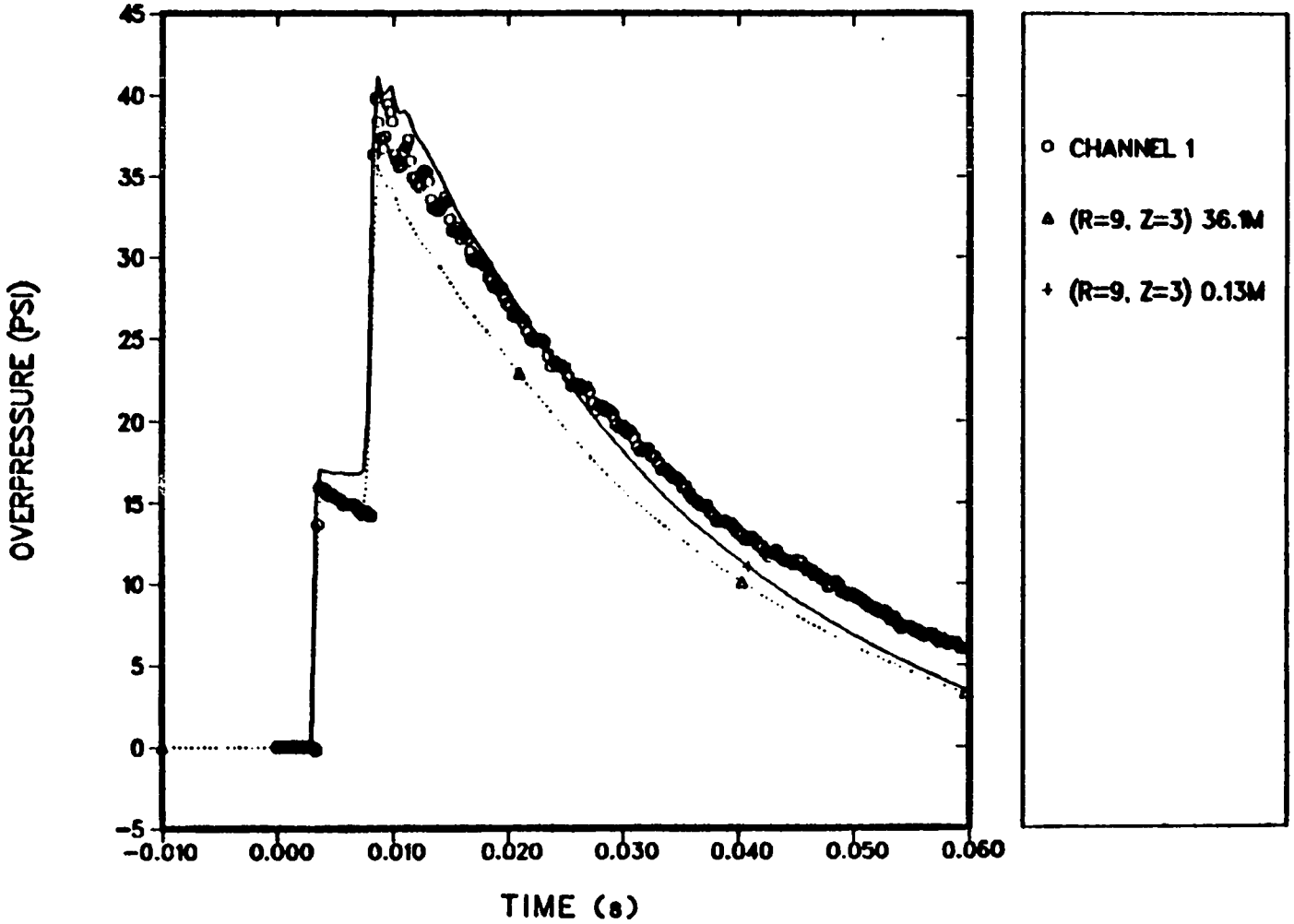

Fig. D-5.
Shock transmission test with 110.3-kPa (16.012-psi) shock overpressure.

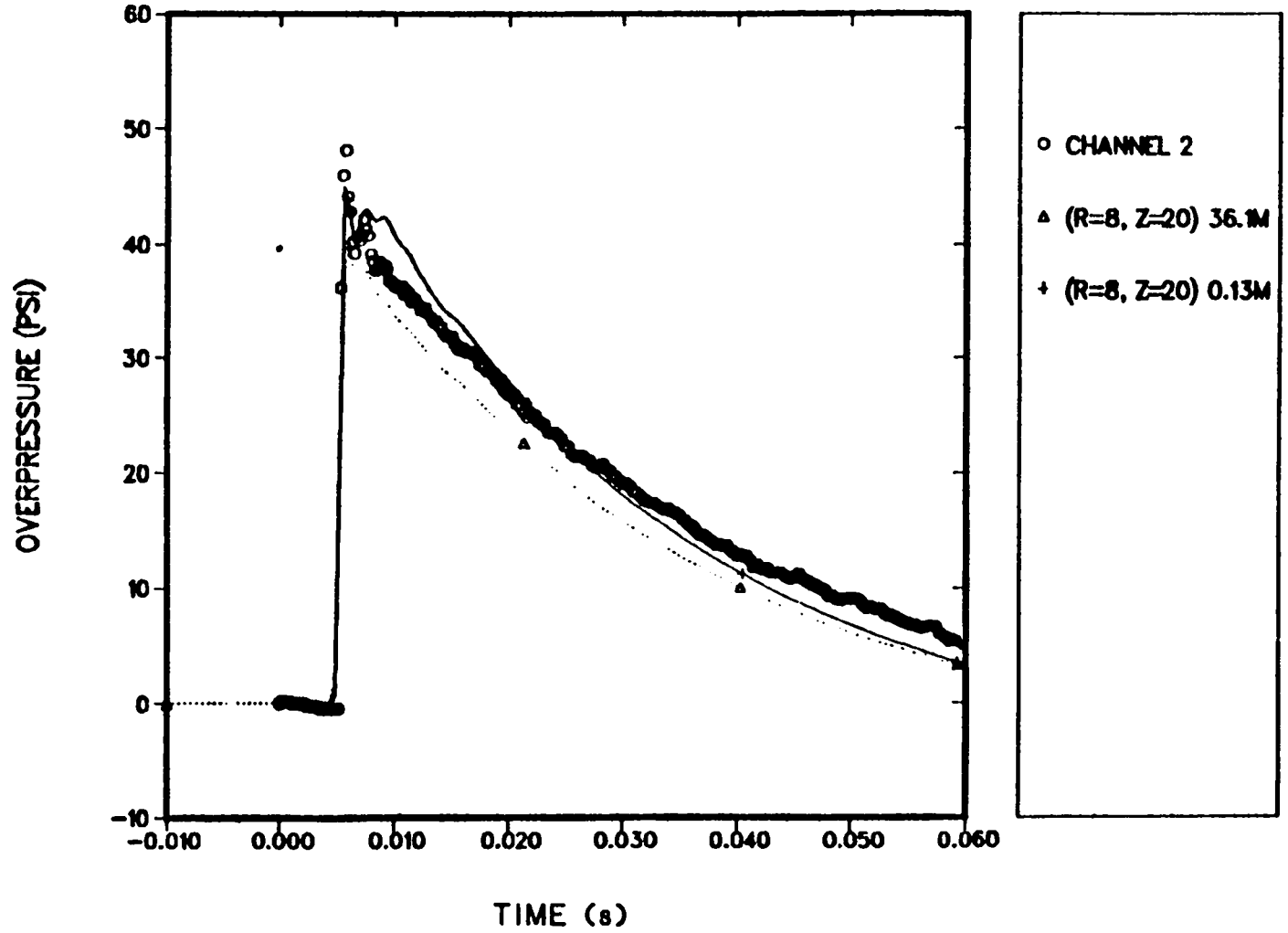

Fig. D-5 (cont).
Shock transmission test with 110.3-kPa (16.012-psi) shock overpressure.

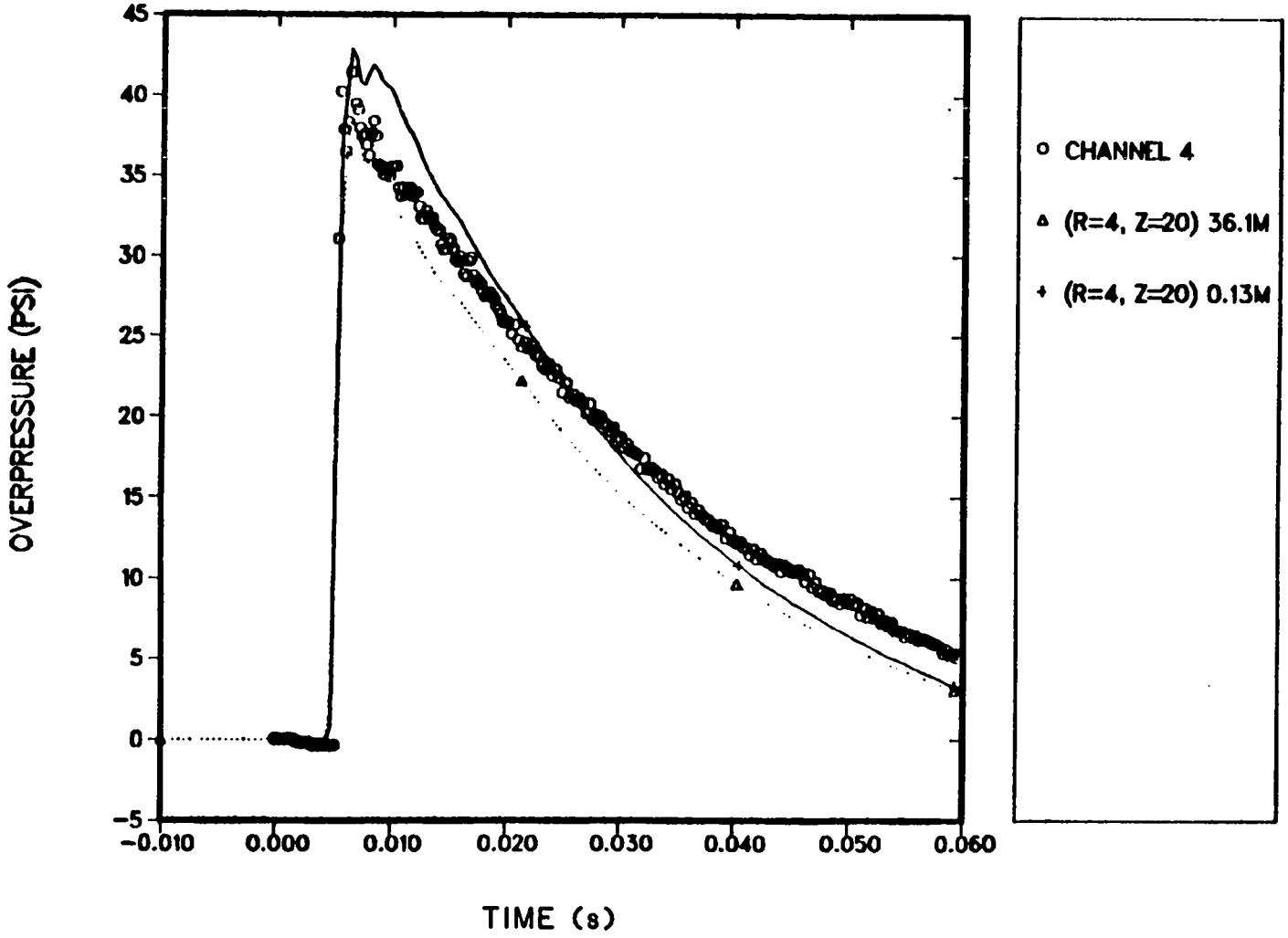

Fig. D-5 (cont).
Shock transmission test with 110.3-kPa (16.012-psi) shock overpressure.

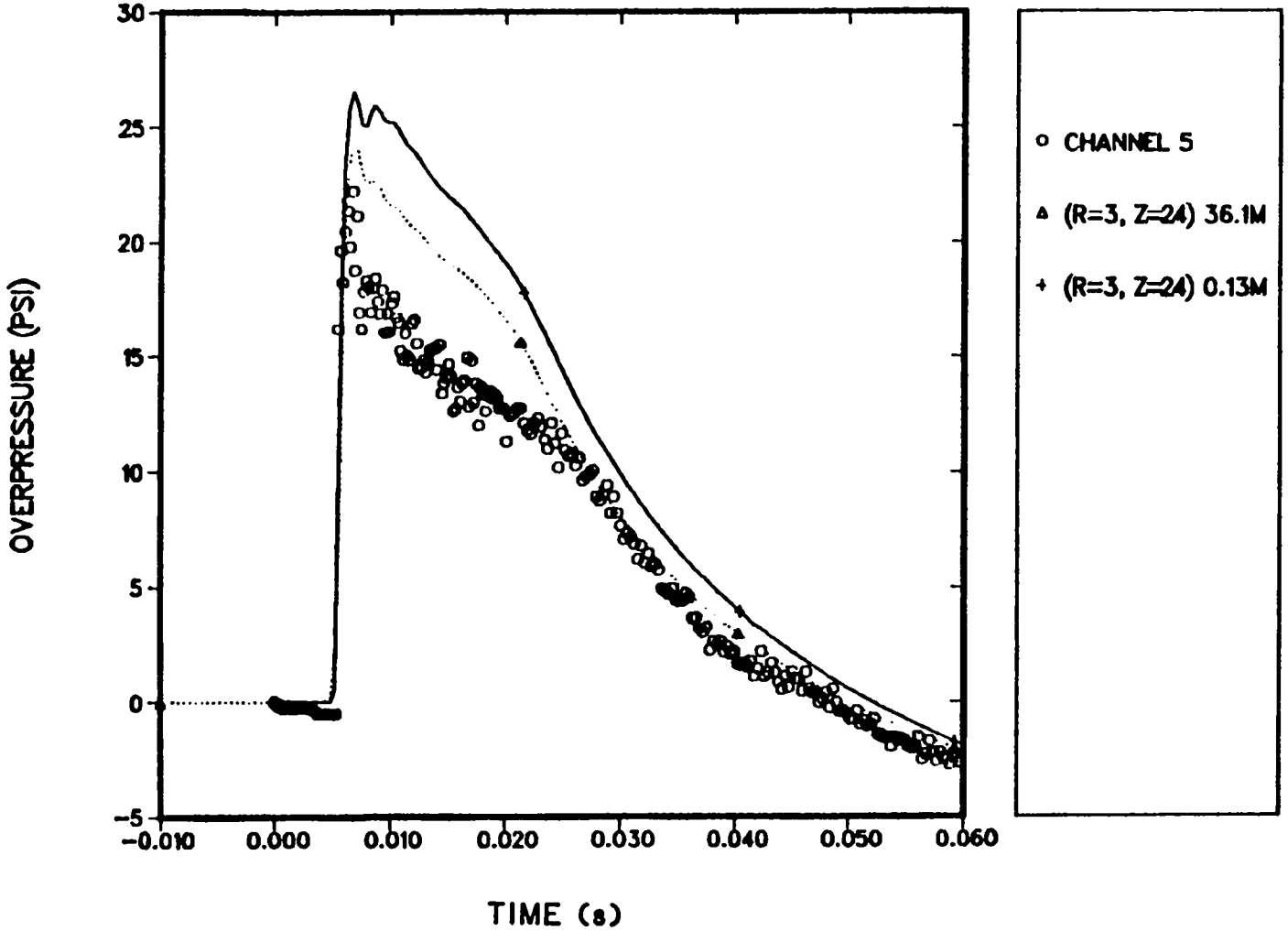

Fig. D-5 (cont).
Shock transmission test with 110.3-kPa (16.012-psi) shock overpressure.

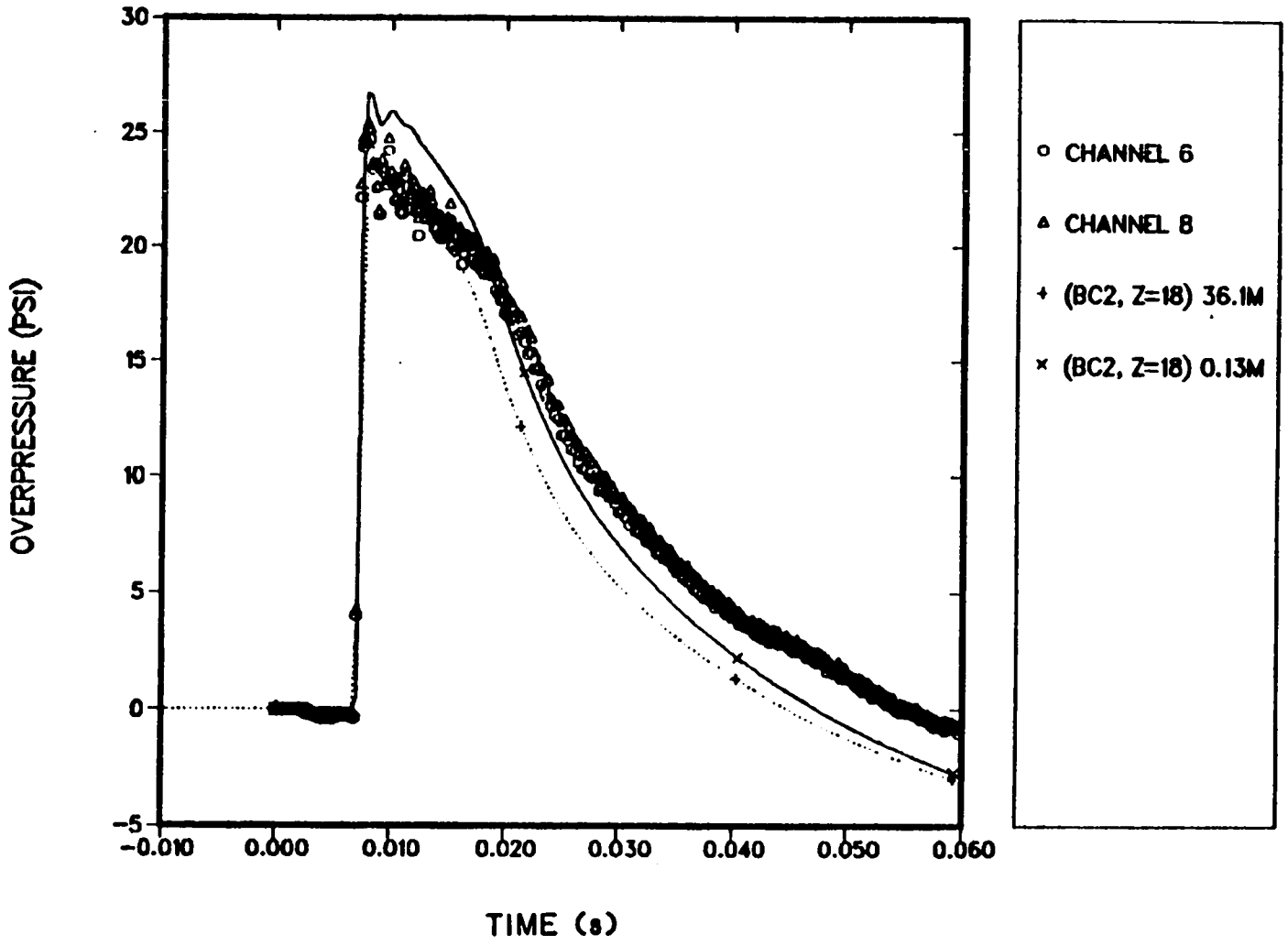

Fig. D-5 (cont).
Shock transmission test with 110.3-kPa (16.012-psi) shock overpressure.

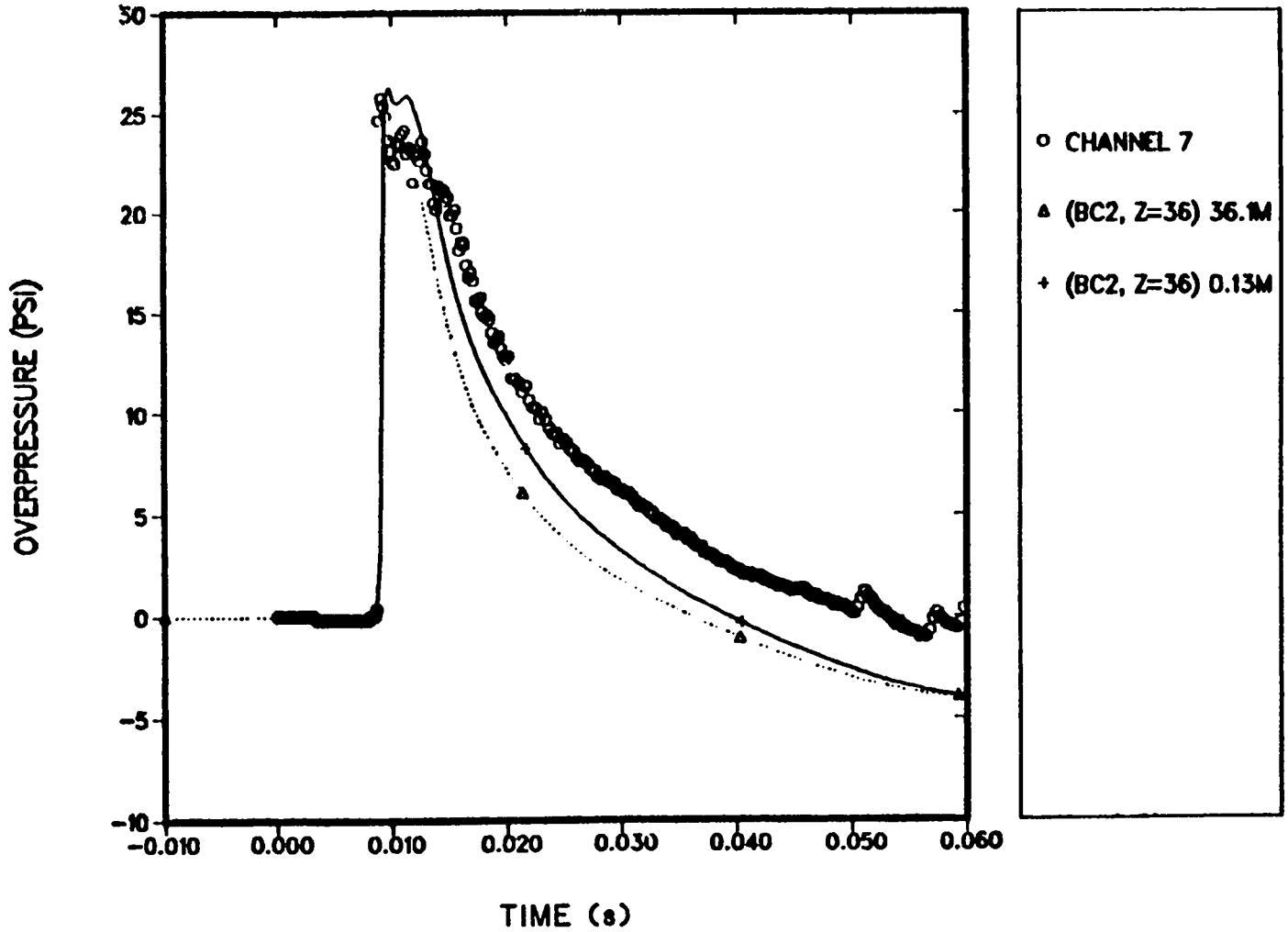

Fig. D-5 (cont).
Shock transmission test with 110.3-kPa (16.012-psi) shock overpressure.

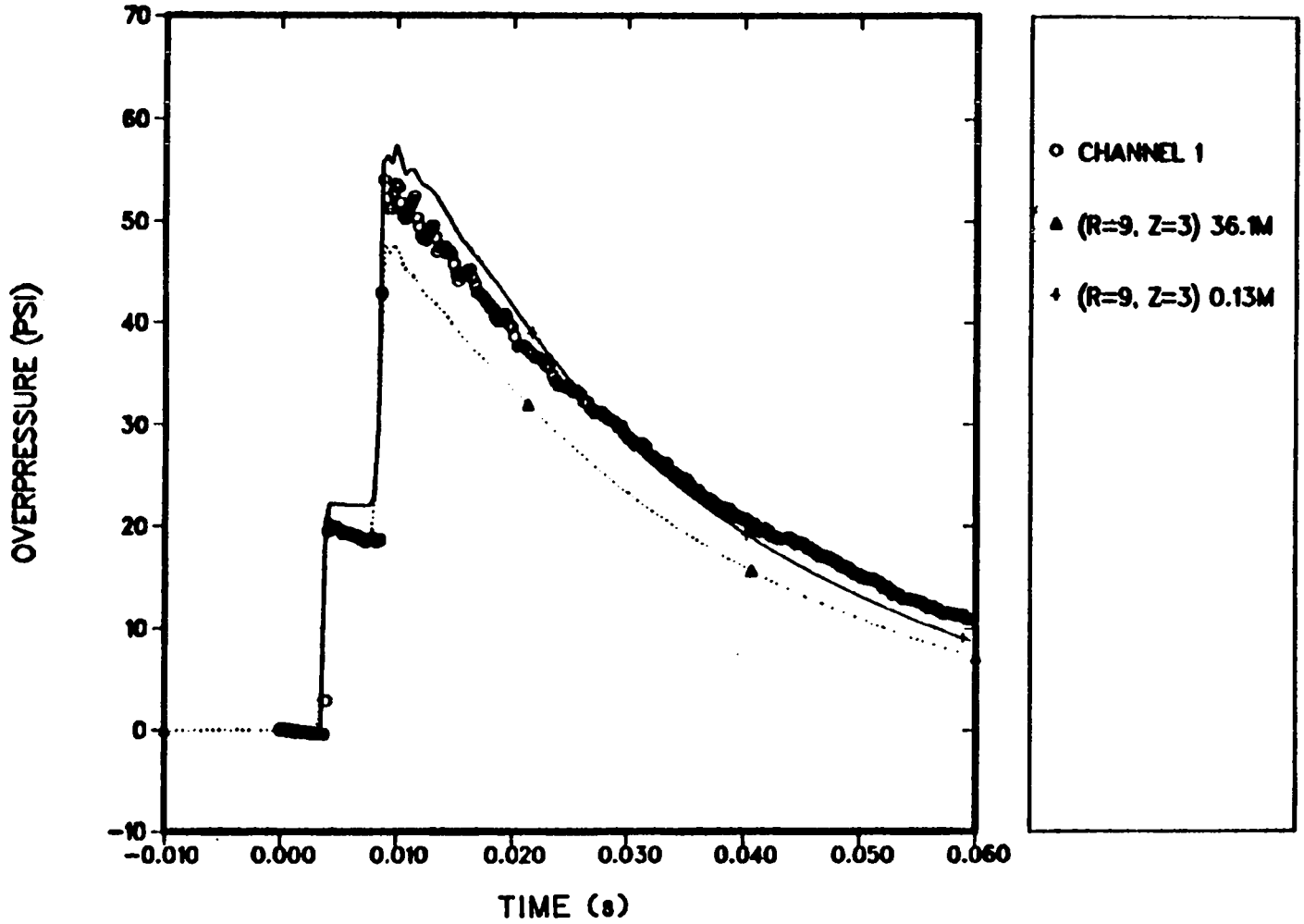

Fig. D-6.
Shock transmission test with 141.5-kPa (20.547-psi) shock overpressure.

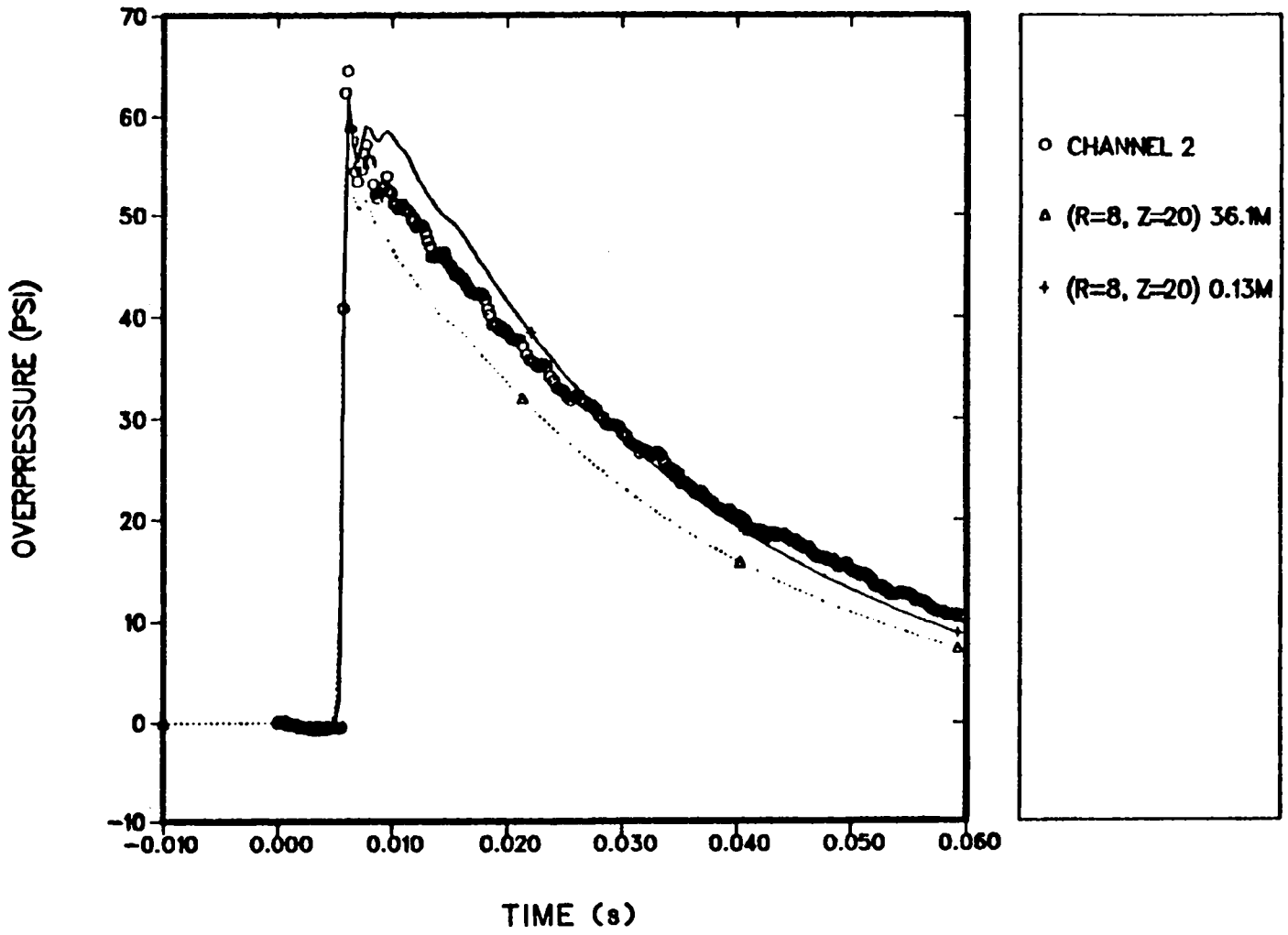

Fig. D-6 (cont).
Shock transmission test with 141.5-kPa (20.547-psi) shock overpressure.

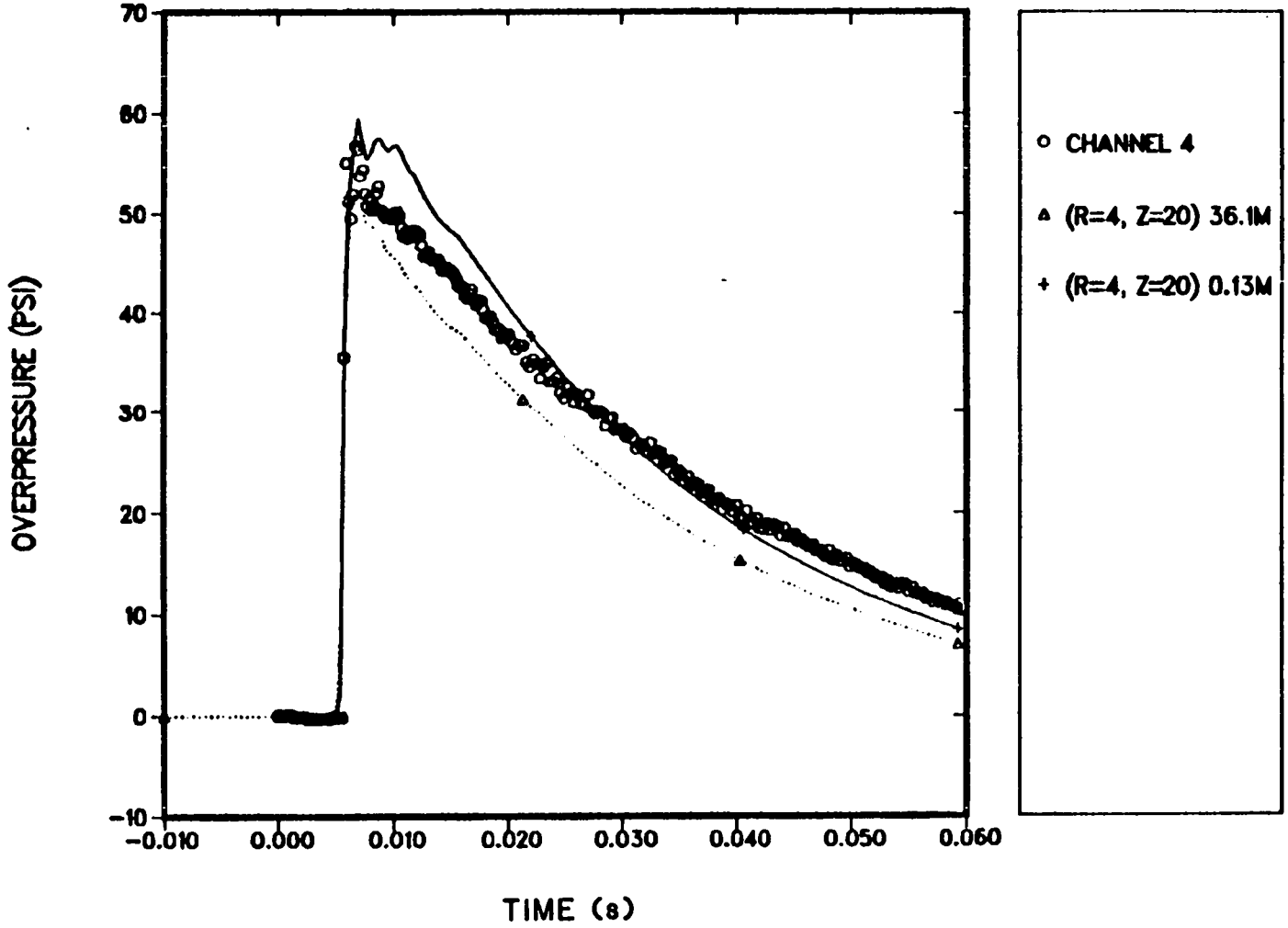

Fig. D-6 (cont).
Shock transmission test with 141.5-kPa (20.547-psi) shock overpressure.

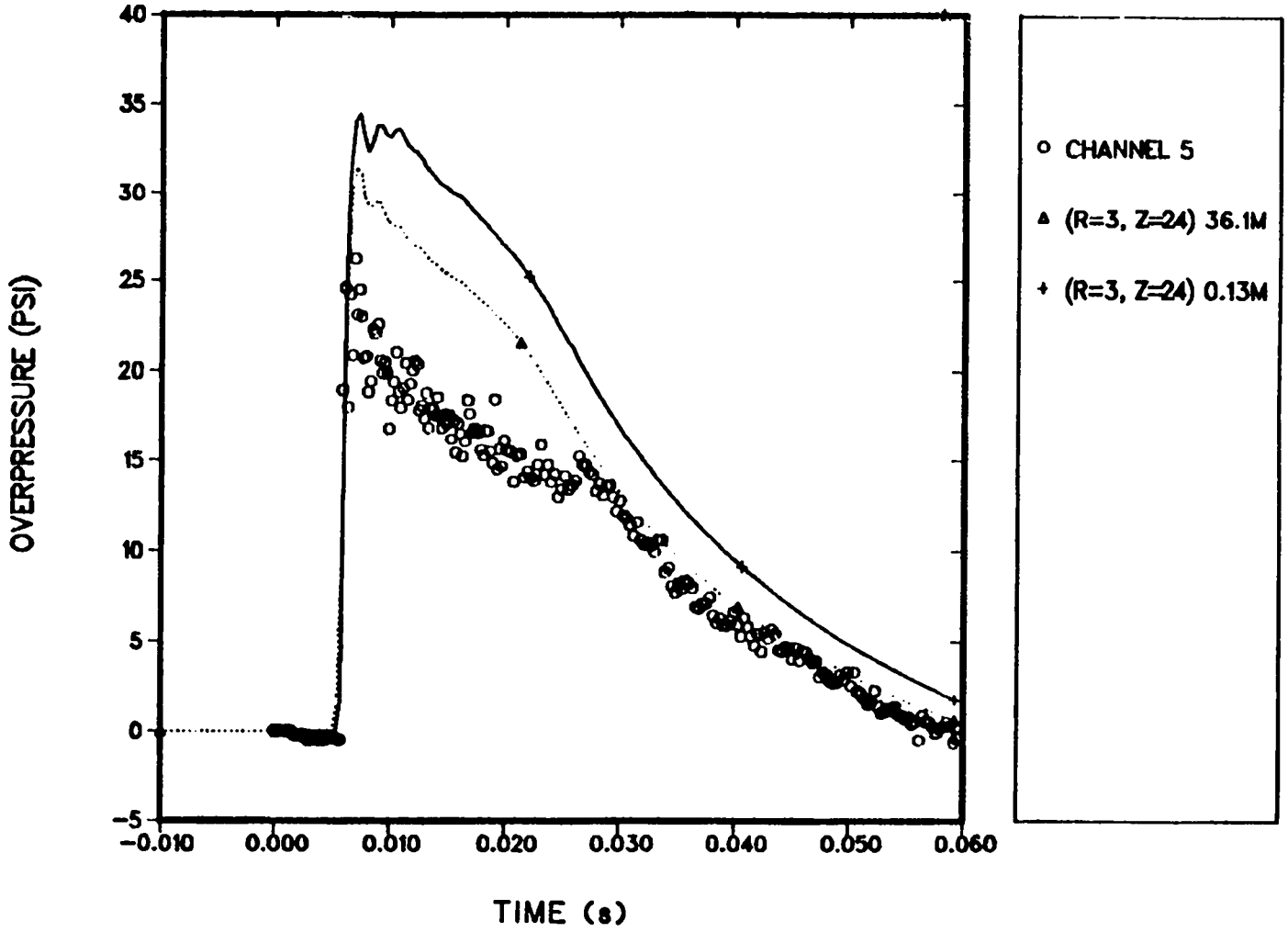

Fig. D-6 (cont).
Shock transmission test with 141.5-kPa (20.547-psi) shock overpressure.

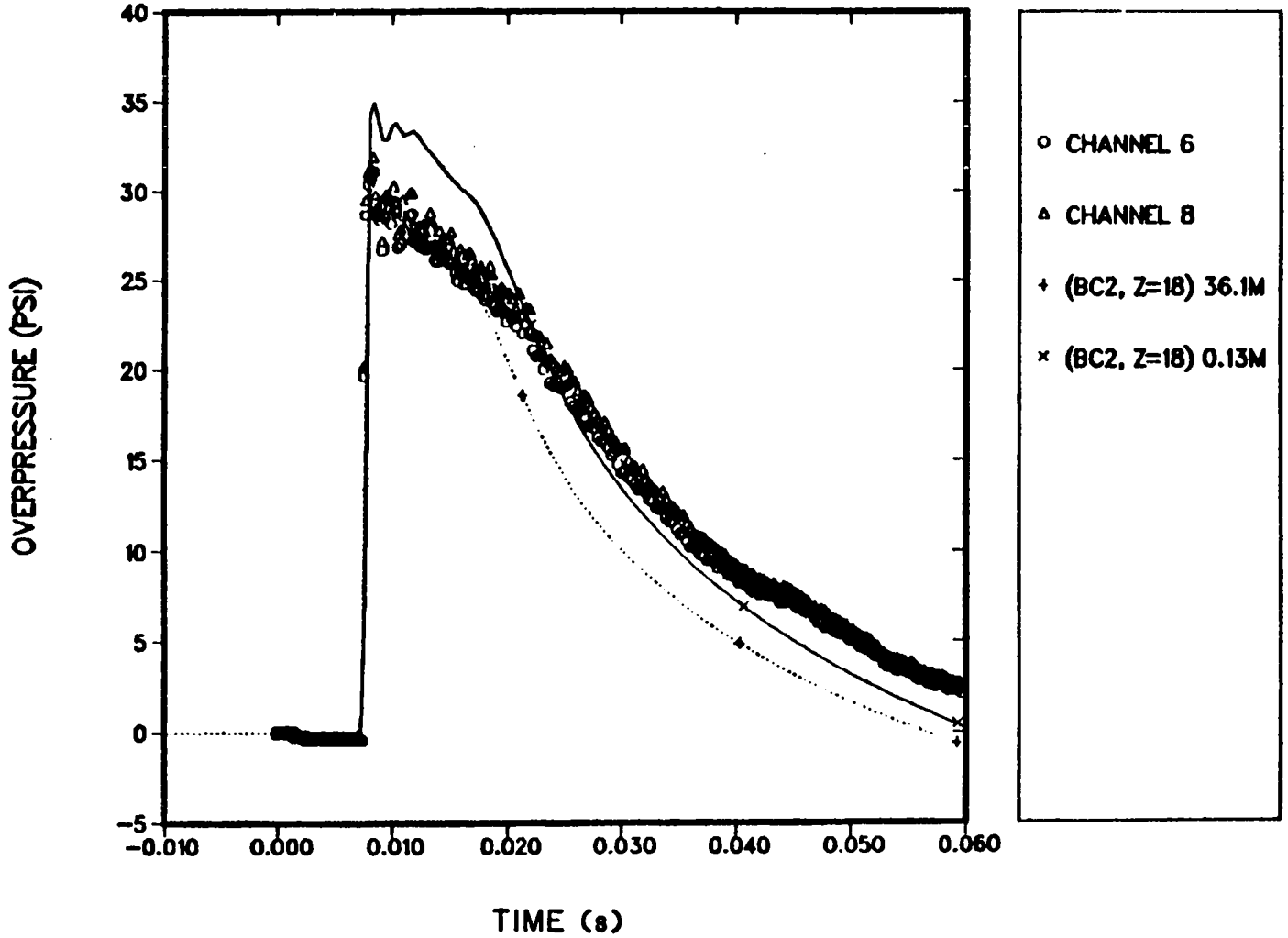

Fig. D-6 (cont).
Shock transmission test with 141.5-kPa (20.547-psi) shock overpressure.

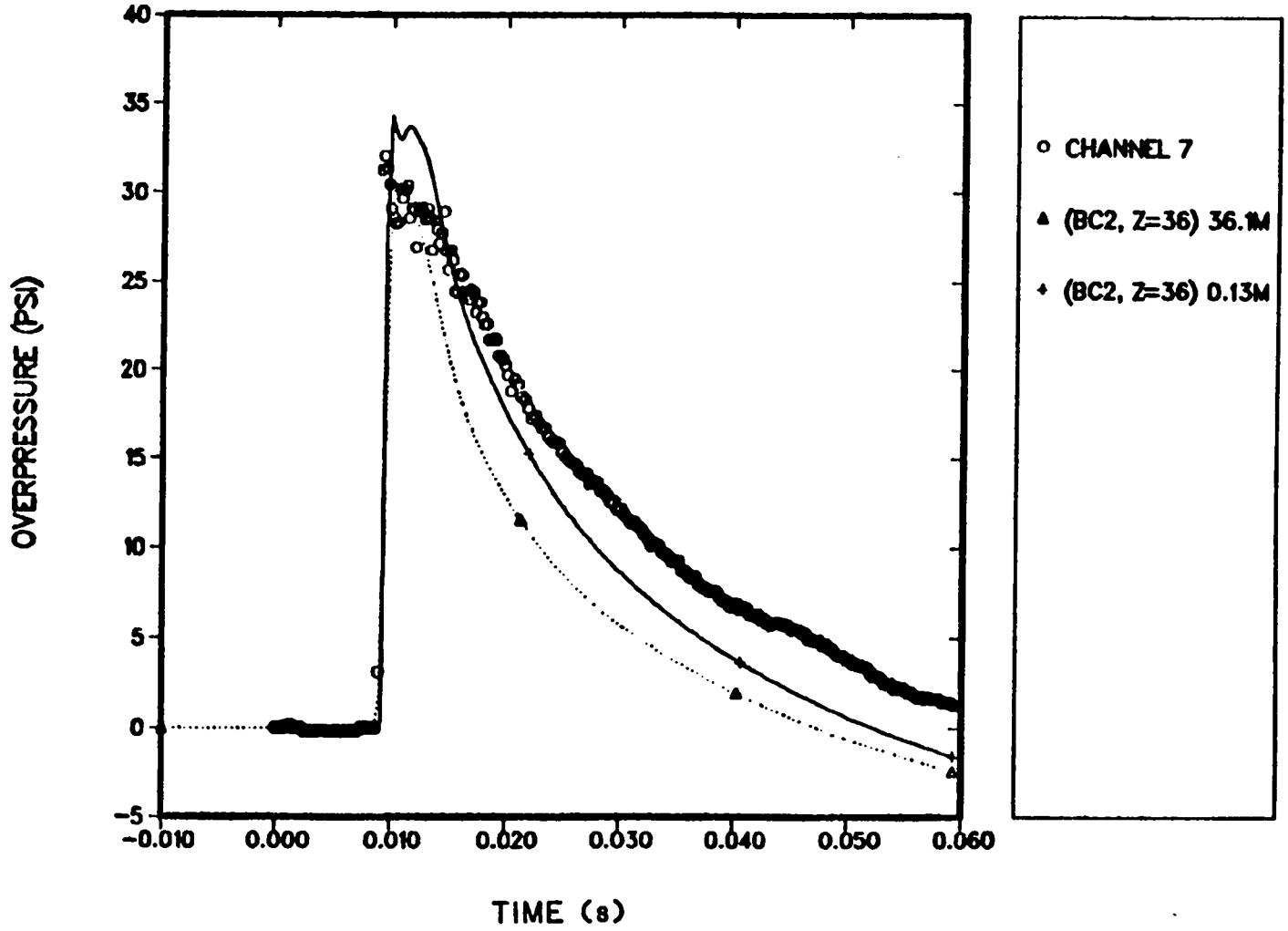

Fig. D-6 (cont).
Shock transmission test with 141.5-kPa (20.547-psi) shock overpressure.

In Figure D-4, we see that spatial smearing error is excessive for the 20.7-kPa (3-psi) shock-front overpressure test calculations. Backward smearing of the shock-wave front and forward smearing of the expansion-wave front result in their overlapping and diminishing the amplitude of the pulse. Starting from the shock-front pulse analytic solution 0.13 m before channel 1, the solid-curve solution initially has very little spatial smearing and is in reasonable agreement with the measurements. However, after 0.020 s, spatially dependent effects begin to be smeared out in space and in time, also at a fixed location because of convection. Note the reduction in amplitude of the pressure pulse at the channel 7 location in even the solid curve because of the shock and expansion wave overlapping-effect error.

The calculative results in Figs. D-5 and D-6 show almost no spatial-smearing error in the shock-wave front. Forward spatial smearing of the expansion-wave front diminishes the amplitude of the shock pulse (evidenced by the dotted curve lying below the solid curve), but the error is small. We see the calculated pressures decreasing faster in time than the measured pressures because of spatial smearing of the expansion wave. All in all, the calculated pressures are in reasonable agreement with their experimental measurements.

The lack of numerical spatial smearing of the shock-wave front for overpressures greater than 103.35 kPa (15 psi) is important to recognize. A first-order, donor-cell convection technique as used by NF85 can calculate spatially sharp shock fronts even after long transmission distances and multiple reflections. It is felt that this is a result of the physical phenomenon of sonic waves piling up behind a shock-wave front acting in an opposite way to numerical diffusion to eliminate spatial smearing of the shock front. Larger shock-front overpressures appear to have enough of this effect to override numerical-diffusion error.

REFERENCES

1. R. Courant and K. Friedricks, "Supersonic Flow and Shock Waves," Applied Math. Sc. 21, 152-4 (1976).

2. R. A. Martin and T. L. Wilson, "EVENT84 User's Manual, A Computer Code for Analyzing Explosion-Induced Gas-Dynamics Transients in Flow Networks," Los Alamos National Laboratory report LA-10312-M (December 1984).

3. J. H. Mahaffy, "A Stability Enhancing Two-Step Method for One-Dimensional Two-Phase Flow," Los Alamos Scientific Laboratory report LA-7951-MS, NUREG/CR-0971 (1979).

4. J. H. Mahaffy, "A Stability-Enhancing Two-Step Method for Fluid Flow Calculations," J. Comput. Phys. 46, 329 (1982).

5. F. H. Harlow and A. A. Amsden, "Fluid Dynamics," Los Alamos Scientific Laboratory report LA-4700, UC-34 (1971), p. 27.

6. R. B. Bird, W. E. Stewart, and E. N. Lightfoot, Transport Phenomena (New York, John Wiley & Sons, 1963), pp. 182-187.

7. TRAC Code Development Group, "TRAC-PF1/MOD1, An Advanced Best-Estimate Computer Program for Pressurized Water Reactor Thermal-Hydraulic Analysis," Los Alamos National Laboratory report LA-10157-MS, NUREG/CR-3858 (1985), pp. 455-463.

8. J. Jones and G. Hawkins, Engineering Thermodynamics (New York, John Wiley and Sons, 1960), Table 13.3, p. 456.

9. M. R. Turner, "TRAP User's Manual," Los Alamos National Laboratory unnumbered internal document (1984).

10. P. R. Smith and W. S. Gregory, "Structural Response of HEPA Filters to Shock Waves," Shock and Vibration Bulletin 52, 43 (1982).

*U.S. GOVERNMENT PRINTING OFFICE: 1987-0-573-034/80005

Printed in the United States of America
Available from
National Technical Information Service
US Department of Commerce
5285 Port Royal Road
Springfield, VA 22161

Microfiche (A01)

Page Range	NTIS Price Code	Page Range	NTIS Price Code	Page Range	NTIS Price Code	Page Range	NTIS Price Code
001-025	A02	151-175	A08	301-325	A14	451-475	A20
026-050	A03	176-200	A09	326-350	A15	476-500	A21
051-075	A04	201-225	A10	351-375	A16	501-525	A22
076-100	A05	226-250	A11	376-400	A17	526-550	A23
101-125	A06	251-275	A12	401-425	A18	551-575	A24
126-150	A07	276-300	A13	426-450	A19	576-600	A25
						601-up*	A99

*Contact NTIS for a price quote.

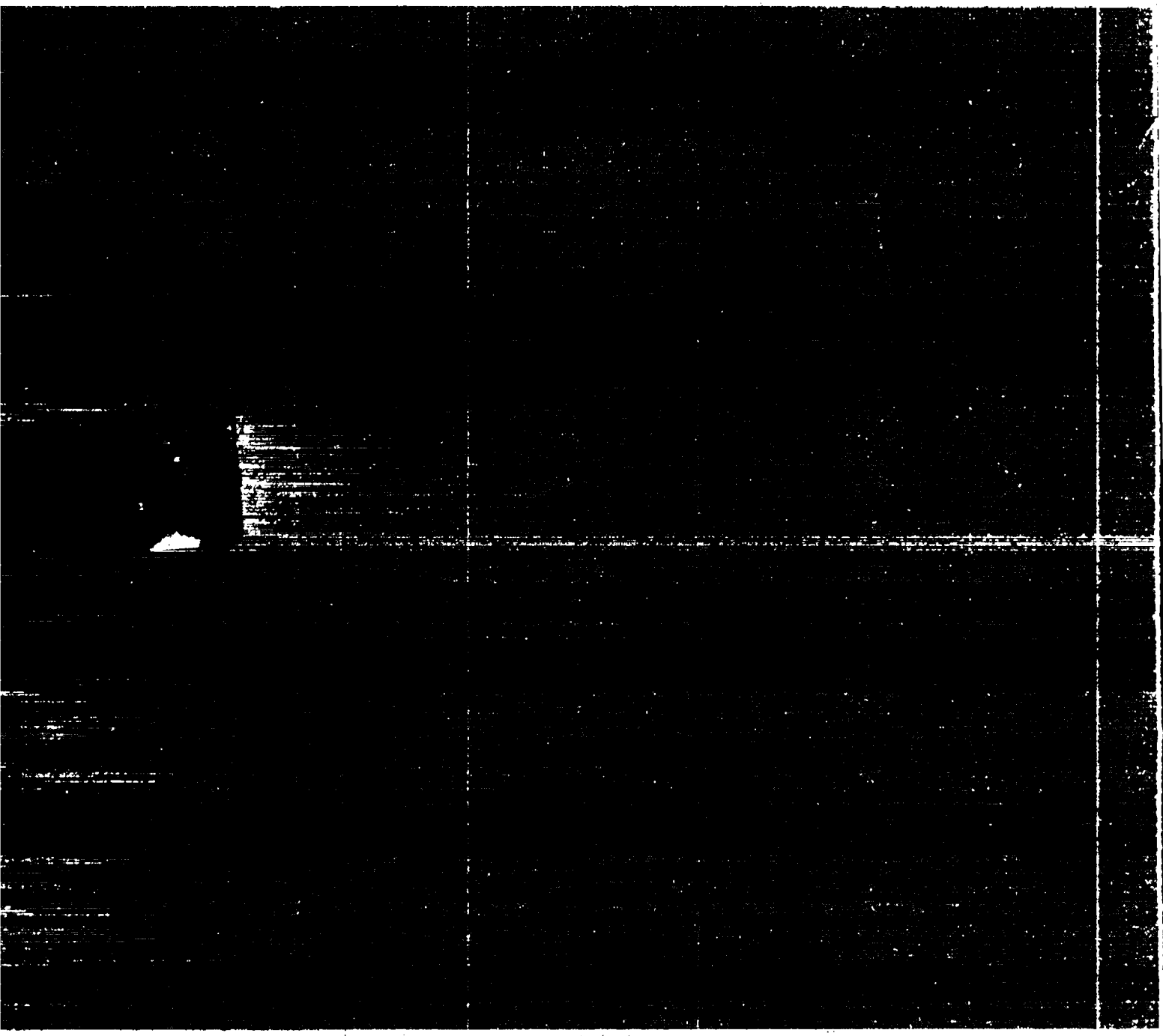

Los Alamos